Intertwining the elemental cycles of iron and carbon: Iron's influence on the fate and dynamics of organic carbon in the environment

Karine Lalonde

A thesis in

The department of

Chemistry and Biochemistry

Presented in partial fulfillment of the requirements

for the degree of Doctor of Philosophy at

Concordia University

Montreal, Quebec, Canada

May 14th 2014

CONCORDIA UNIVERSITY
SCHOOL OF GRADUATE STUDIES

This is to certify that the thesis prepared

By: Karine Lalonde

Entitled: Intertwining the elemental cycles of iron and carbon: Iron's Influence on the fate and dynamics of organic carbon in the environment

and submitted in partial fulfillment of the requirements for the degree of

Doctor of Philosophy (Chemistry)

complies with the regulations of the University and meets the accepted standards with respect to originality and quality.

Signed by the final examining committee:

_____ Chair
Dr. E. Despland

_____ External Examiner
Dr. D. Burdige

_____ External to Program
Dr. D. Walsh

_____ Examiner
Dr. C. Skinner

_____ Examiner
Dr. X. Ottenwaelder

_____ Thesis Supervisor
Dr. Y. Gélinas

_____ Thesis Supervisor
Dr. A. Mucci

Approved by: _____
Dr. H. Muchall, Graduate Program Director

May 5, 2014 _____
Interim Dean J. Locke, Faculty of Arts and Science

Abstract

From respiration and DNA synthesis to superparamagnetic nanoparticles, magnetotactic bacteria and old rusty cars, iron is everywhere. Our understanding of iron geochemistry is central to the study of carbon and vice versa as it is nearly impossible to find an environment where these two elements are not conjoined. Iron has a profound effect on the carbon that cycles on geological time scales—in sedimentary rocks, in coal and petroleum deposits, the balance between carbon preservation and remineralization is in part modulated by iron. Approximately 20% of the organic carbon buried in sediments is protected by reducible iron phases, well below the oxic-anoxic limit of the sediment where they are no longer thermodynamically stable. Iron represents a globally important sink for sedimentary organic matter (OM), contributing to maintaining the delicate balance of O_2 and CO_2 in the atmosphere.

Iron also impacts the carbon cycling in active oceanic, atmospheric and lithospheric reservoirs, for example by linking continental erosion to carbon deposition in sediments, and iron-rich riverine discharge and dust deposition to phytoplankton blooms in the middle of the ocean. The association of iron and OM also influences the photoreactivity (Zepp, 2003) and bioavailability (Mackay and Zirino, 1994; Raiswell and Canfield, 2012a), of both elements in aquatic systems.

In spite of its significance to high-turnover and refractory carbon, the exact mechanism of interaction between iron and OM is not yet known. We postulate the formation of inner-sphere complexes or coagulates at oxic-anoxic interfaces. We observe preferential sheltering of organic molecules with low C:N atomic ratios and enriched isotopic signatures ($\delta^{13}C$). A novel method, coupling a total organic carbon (TOC) analyzer to an isotope ratio mass spectrometer, was developed to determine the $\delta^{13}C$ of the dissolved organic matter that is retained by iron and

other minerals. We find that iron phases increase the affinity and adhesion of ^{13}C-enriched dissolved molecules to particulate phases – which has been reported to slow bacterial degradation. Further elucidation of the mechanism of interaction between the 2 elements could be achieved through novel instrumental methods, including TEM microscopy and EXAFS spectroscopy which are used to determine the macrostructural arrangement of iron and OM and the chemical environment surrounding iron atoms in sediments.

Acknowledgements

A PhD is no feat of superhuman intelligence but rather an exercise in persistence, discipline and self-motivation. These have been hard, humbling, trying but amazing years in which I have learned more about myself than I have about sediments, iron or organic matter combined. I could not have gone into this alone and come out the other end without help from a number of people. I would firstly like to thank Yves, my supervisor, who has watched me make every mistake without judgement or repercussion and who has trusted me to take the reins from the very beginning, but has always giving me counsel when I needed it. I would also like to thank Andrew Barber, who once upon a time was my mentee and became a great science partner and a fantastic springboard for ideas. I would also like to thank my present and past lab members whose ebb and flow in the lab maintained an interesting and fun place to work throughout the years: thank you Alex Ouellet, Rob Panetta, Mina Ibrahim, Anja Moritz, Amanda Gabriel and Francis Haley. Thank you Al Mucci for giving me the unconstrained red pen treatment and making me a better writer for it.

I would also like to thank friends and family who have supported me in this extended stay in University. Thank you mom, dad, Sukhy and Mark for a place to stay and write, believing in me and pushing me to finally finish. Thank you Rob for emotional support and calling me a “killer” even when I felt defeated.

Contribution of Authors

This section lists the contributions of each of the authors included on peer-reviewed (or soon to be peer-reviewed) manuscripts.

In Chapter 2, Yves Gélinas formulated the hypothesis that iron-OM interactions in sediments promoted the preservation of organic matter. I optimized the main method used in this work and carried out all the analyses. I have also written the first draft of the paper, which was then reviewed by my co-supervisors, Dr. Alfonso Mucci (McGill University, 3rd author) and Yves Gélinas (Concordia, last author). Alexandre Ouellet conducted some scouting electrochemical experiments. This manuscript was published in March 2012.

For Chapter 3, Andrew Barber and I designed and built (with the help of the machine shop personnel) the experimental setup as well as sampled and accumulated data over a 250 day period. Andrew Barber and I together wrote the manuscript. The division of labour between Andrew and I was necessary given the complexity and duration of the incubation experiment. Yves Gélinas and Alfonso Mucci edited the manuscript for style and scientific content. The manuscript is now in press in Marine Chemistry.

Lab experiments reported in Chapter 4 were done by me, with some valuable advice from an expert in IRMS, Paul Middlestead from the University of Ottawa. Paul designed the carbon trap used in this work, did some groundwork experiments and proposed the drafting of the manuscript. Paul also ran a few DOC-IRMS analyses to allow comparing similar set-ups in two different labs, and a few EA-IRMS analyses to allow comparing the accuracy of DOC-IRMS analyses. I wrote the manuscript, that Paul and my supervisor, Yves Gélinas reviewed. The manuscript has just been submitted to Limnology and Oceanography: Methods.

Chapter 4 results from an international sampling effort launched by Dr. Anssi Vähätalo, at the University of Helsinki. St. Lawrence River samples were collected during a cruise on which Dr. Gélinas was the chief scientific officer. These and samples from 9 other major rivers were shipped to Dr. Vähätalo. Dr. Vähätalo and his students carried out the photobleaching and microbial degradation experiments before shipping back all the samples to me for DOC-IRMS analysis. I ran all the analyses and wrote the manuscript, which was then reviewed by Dr. Vähätalo and Gélinas. The manuscript is currently being reviewed for re-submission to Biogeosciences.

Table of Contents

List of Figures

List of Tables

List of Acronyms

DOC: Dissolved Organic Carbon

DOC-IRMS: Dissolved Organic Carbon analyzer – Isotope Ratio Mass Spectrometer

DOM: Dissolved Organic Matter

Fe-OM: Iron Associated Organic Matter

Irr-DOC: Irradiated Dissolved Organic Carbon

L-DOC: Labile Dissolved Organic Carbon

DON: Dissolved Organic Nitrogen

MUC: Molecularly Uncharacterizable Carbon

NL-DOC: Non-Labile Dissolved Organic Carbon

OC: Organic Carbon

OM: Organic Matter

R-DOC: Recalcitrant Dissolved Organic Carbon

TDN: Total Dissolved Nitrogen

TN: Total Nitrogen

δ^{13}C-DOC: δ^{13}C signature of Dissolved Organic Matter

Chapter 1: General introduction

Our planet's oxic atmosphere was manufactured from biogeochemical processes in deep ocean sediments. These smelly anoxic muds laid out at the bottom of the ocean, kilometers away from air, are perhaps not the most obvious birthplace of atmospheric oxygen. It actually takes thousands of years for gaseous molecules dissolved in ocean surface waters to be transported by currents to the sediment bed and back again (Williams and Druffel, 1987).

On a molecular basis, atmospheric oxygen is extracted from carbon dioxide. As early as 3.5 billion years ago, photosynthetic organisms started to fix CO_2 into organic matter (OM) and generated oxygen gas as a by-product. Photosynthesized organic molecules are however not irreversibly formed as they are a source of energy for bacteria and other heterotrophs. The heterotrophic consumption of OM is coupled to the utilization of oxygen - whether directly from oxygen gas or from other oxidizing molecules such as nitrates and sulfates - reversing photosynthesis and negating the possible buildup of atmospheric oxygen gas (Berner, 2003; Berner and Canfield, 1989).

A small fraction of the OM formed every year from photosynthesis is not available to bacteria, either because it is structurally indigestible or because it is in some other way, protected from bacterial degradation. Marine sediments are the only long-term reservoir for preserved, recalcitrant organic molecules, which are never reoxidized to CO_2, therefore rendering sediment muds into an indirect source of oxygen gas on the planet. Over the billions of years of OM accumulation in sediments, the Earth's redox balance completely changed. Photosynthetic oxygen first reacted with rocks on land through oxidative weathering, forming oxidized species such as iron oxides and soluble sulfates (Canfield et al., 2000). Oxygen concentrations eventually reached the tipping point at which dissolved iron(II) in the world's oceans was no longer stable,

resulting in the precipitation of layers of iron oxides to the sea floor which produced sedimentary rocks known as the banded iron formations. Eventually all the mineral oxygen sinks on Earth became saturated, atmospheric oxygen concentrations started to build-up and rose to the concentrations that we observe today. The quantity of preserved organic material that was required for this to occur represents $15{,}000 \times 10^{18}$ grams of OC of organic carbon, which accumulated in 800,000,000 cubic kilometers of sediments (Hart, 1969) over billions of years (Hedges and Keil, 1995).

Sediment structure

Sediments are mainly composed of eroded sand, silt and clay particles, carried by currents, deposited kilometers away from land and stacked up in layers. Accumulation rates vary from ≈1cm/yr near river mouths and coastal zones, to a few mm/kyr in the deep ocean basins (Henrichs, 1992). The interstitial spaces between sediment particles are saturated with water. These porewaters can occupy up to 85% of the sediment volume at the seabed, decreasing progressively with sediment depth due to compaction (Berner, 1980).

We can study different time periods by separating sediment cores into layers deposited at different times during Earth's history. Piston corers can extract sediment cores longer than 20 meters (Hollister et al., 1973), which can go as far back as the Paleocene, 65 million years ago (Silva et al., 1976). Organic carbon is generally a minor component, only making up about 1% of sediment dry weight, however, out of all other elements, OM is the most structurally complex and therefore could potentially hold stockpiles of information or untapped paleo-proxies that could recount the evolution of oceanic temperatures, redox conditions, alkalinity and early living organisms (Hedges and Keil, 1995).

Organic matter degradability

OM found in contemporary sediments has already undergone extensive degradation and is likely similar to the OM that was originally sequestered into the million year-old deposits that made possible the build-up of oxygen in the atmosphere. These molecules, leftover after the near complete decomposition of freshly produced OM, are indigestible to bacteria and represent less than 1% of the total photosynthetic carbon produced each year. The molecules that makeup this small fraction are so unusual that bacteria, throughout their billions of years of history on Earth, never evolved the biochemical pathways required to break them down and use their energy (Hedges and Keil, 1995). Whether in the search for the perfect formation conditions for fossil fuel deposits or simply out of academic interest, organic geochemists have long tried to understand where these molecules came from and what depositional conditions or structural alterations imparted them with geological longevity. Nevertheless, despite decades of research, the mechanisms by which OM is stabilized and sequestered in aquatic sediments are only fragmentarily understood, hindering our ability to develop robust theories of carbon burial (Eglinton, 2012).

The OM in marine sediments comes from both land and sea. Decaying vascular plant material on continents is temporarily stored in soils, soil litters or peats and carried to the ocean by rivers, through surface runoffs, continental erosion and groundwater seeps. Algae growing in the sunlit surface waters of the ocean can also sink to the bottom of the water column, but often require transportation to the seabed from mineral ballasts or dense zooplankton fecal pellets (Fowler and Knauer, 1986). Sinking particles are further degraded during their transit in the oceanic water column which may take several weeks (Emerson and Hedges, 1988). Before it even reaches the sediments, bacteria (in terrestrial systems or in the oceanic water column) have

therefore already had the chance to nibble at the OM, removing the most labile, energy-rich pieces and leaving behind the portions that are more recalcitrant.

Transmission electron microscopy shows that the structure of sinking organic-rich particles changes drastically upon arrival at the seafloor, from a collection of discrete organic debris (bioclasts, diatom tests and bacteria) loosely associated to inorganic particles, to intricate organo-clay assemblages and microaggregates (Ransom et al., 1998b). It was therefore suggested that prior to final deposition and burial, loose OM assemblages somehow disaggregate and recombine with eroded detrital material near or at the seafloor. The size/reactivity model outlined by Burdige (1998) largely explains these observations. Particulate OM sinking through the water column to the sediment bed is initially mainly composed of high molecular weight, relatively labile biopolymers. Oxidases, hydrolases and reactive oxygen species are used to break these down into smaller edible pieces that can be incorporated into the bacterial biomass (Arnosti, 2011). During this partial breakdown, less bioavailable polymeric low molecular weight (1000-4000 Da) pieces are broken off and released into the interstitial waters. These dissolved pieces can remain indefinitely in porewaters, escape the sediment to the overlying water column or become attached to particles (Burdige and Gardner, 1998). The irreversible binding of dissolved organic matter (DOM) to clays during degradation explains the microscopic and spectroscopic changes observed upon OM deposition and burial in sediments. The degradation and diagenesis of OM in sediment is depicted in Figure 1-1.

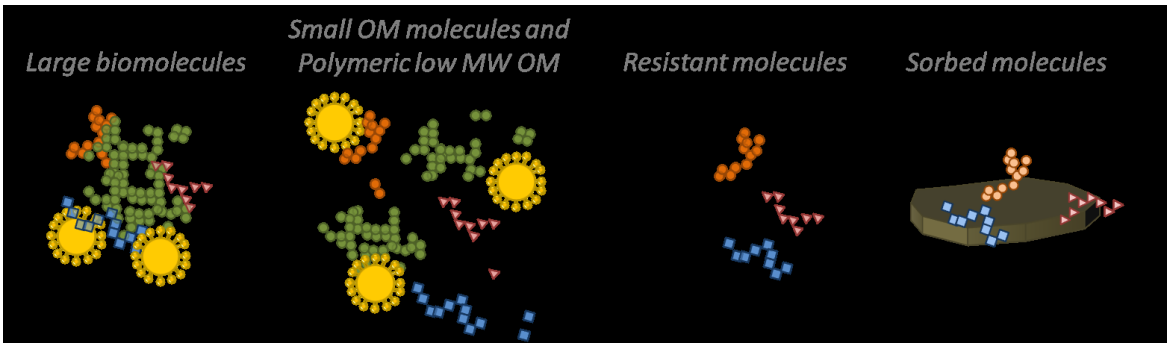

Figure 1-1: Degradation of OM in sediments from large biopolymers to smaller more soluble pieces and CO_2 through bacterial hydrolysis and consumption (bacterial are shown in yellow). The final step shows the adsorption of organic molecules to the sediment matrix. Modified from (Hedges John et al., 1999).

Whether structurally recalcitrant or labile, it should be emphasized that OM is not stable in the presence of oxygen and given enough exposure time, OM is completely remineralized to CO_2. This is illustrated by the very low levels of OM in oxic deep-sea sediments and oxidized turbidites (Buckley and Cranston, 1988; Gélinas et al., 2001). Nevertheless, as sediment particles accumulate and new particles settle to the sediment surface, porewater oxygen concentration decreases with depth because oxygen cannot diffuse into the sediment fast enough to compensate for its bacterial utilization (Berner, 1980). In the absence of oxygen, other electron acceptors (including nitrates, manganese oxides, iron oxides and sulfates, in order of decreasing Gibb's free energy production) are used to decompose OM (Burdige, 1993; Burdige, 2006). Sulfate is normally either the first or the second most important (after oxygen) electron acceptor because of its abundance in seawater. Anoxic bacteria are not as efficient as oxic bacteria at consuming OM and a consortium of bacterial communities typically works symbiotically to breakdown the OM (Bastviken et al., 2004). Sulfate reducers, for example, consume the bi-products of fermenters, like propionate or acetate (Berner, 1980). Typically the breakdown of complex organic molecules is very slow or non-existent in anoxic deposits, as the non-discriminate bond breakage of peroxidases, oxidases and reactive oxygen species does not occur in the absence of oxygen.

Preservation mechanisms

OM degradability is arguably related mainly to chemical structure. Molecular size, elemental composition and functional groups/linkages are all important. Bacteria not only require substrates to be degraded to a size of approximately 600 Da before they can actively transport them across porins in their cell walls (Weiss et al., 1991) but also necessitate the biochemical pathways to breakdown specific chemical bonds (e. g. to hydrolyze sugars and proteins, bacteria require the genetic coding for hydrolase enzymes) (Arnosti, 2011). If a molecule is not consumable by bacteria, it is more likely to be preserved. This is the molecular basis for persistence in sediments and is termed “selective preservation” (Hedges and Keil, 1995; Zonneveld et al., 2010).

The selective preservation of organic compounds is supported empirically by the elemental and structural composition of sedimentary OM which is dramatically different from that of the precursor autotrophic organisms. Whereas carbohydrates, proteins and lipids make up 90% of the biomass of marine algae, the combination of these 3 major biochemicals accounts for less than 10% of the organic carbon in sediments. The remaining 90% falls under an “uncharacterizable” fraction, which is a mixture of molecularly complex and refractory molecules, fondly referred to as MUC or molecularly uncharacterizable carbon (Hedges et al., 2000). It is possible for bits and pieces of MUC, such as amino acid sidechains, peptide bonds or long hydrophobic carbon chains, to resemble the chemical structure of the parent biomolecules but these molecular clues are generally only visible using bulk spectroscopic methods (e.g. by infrared spectroscopy or solid-state nuclear magnetic resonance spectroscopy). Molecular-level information, predominantly derived from selective extraction methods which work well for freshly produced organic substances, only provide a narrow window into a small fraction of the

total sediment OM, as the bulk of the OM in sediments cannot be extracted using these methods (Hedges et al., 2000).

Biopolymers such as algaenan or lignin from the cell walls of algae or woody vascular plants as well as some aliphatic compounds are some of the only structurally-resistant molecules that are directly produced by photosynthesizers (Zonneveld et al., 2010). “Refractorization” by chemical modifications of organic substances may also occur during passage through the microbial loop, bacterial defunctionalisation and rearrangements, or abiotic inter or intramolecular reactions. Condensation reactions to produce melanoidins (or Maillard condensation products) from simple sugars and amino acids, are a commonly given example of chemical refractorization. Because amine and amide linkages are difficult to form abiotically at low temperatures, it is controversial to postulate that their presence in the non-living OM of contemporary sediments can be supported or even supplemented by condensation reactions (Hedges et al., 2000). In ancient sediments however, temperature and pressure increase with burial and up to 40% of the nitrogen can be contained in pyridinic and pyrrolic heterocyclic structures (in contrast to living organisms where nitrogen is almost entirely found in proteinaceous and nucleic materials) potentially formed from the Maillard-type incorporation of nitrogen from amino acids or ammonia into pre-existing molecules via reactions with degradation products of carbohydrates or phenolic groups in humic-like substances (Baxby et al., 1994).

The molecular basis for preservation of OM does not discount the possibility that sedimentary OM is also physically protected. In most sediments, over 99% of OM is found to be inseparable from inorganic particles (Hedges and Keil, 1995), since the majority of the OM deposited in sediments quickly becomes intimately associated to the mineral matrix. The bioavailability of organic molecules and their propensity toward biodegradation by microbes is reduced through

strong organic-inorganic bonds, possibly because inorganic particles sterically inhibit or hinder enzymatic attack (Jones and Edwards, 1998). The preservation of labile molecules such as peptides and carbohydrates can only be explained by physical protection, because unsheltered, they are quickly consumed by bacteria.

Encapsulation of OM in the interlayer structure of expandable clays (Kennedy and Wagner, 2011), in mesopores of clay materials (Ingalls et al., 2003) or in biological inorganic materials such as diatom tests can provide a sheltering and preservative effect (Arnarson and Keil, 2007). Simple adsorption onto particulate surfaces is the primary physical protection mechanism (Mayer, 1994; Mayer, 1995), and only gains in importance after lengthy exposure to oxygen since the OM in these structures have the highest longevity (Arnarson and Keil, 2007). Adsorbed sediment OM is found as amorphous blobs strongly bound to particles, and covering about 20% of the mineral surfaces (Mayer, 1999; Ransom et al., 1997). The location of these blobs was proposed to be related to the surface chemistry of sedimentary particles (Ransom et al., 1998a).

A new mechanism of physical protection was discovered in our laboratory. We showed that 20% of the organic compounds in sediments are associated to reducible metal oxides, such as iron and manganese oxides (Chapter 2, Lalonde et al., 2012). The preservation potential of organic molecules associated to these metals was previously believed to be reserved for oxic environments such as soils (Kaiser and Guggenberger, 2000) since metal oxides can be reductively dissolved under the anoxic conditions of marine deposits. In natural sediments however, iron oxides are metastable over thousands of years, and OM bound these oxides seems to exhibit marked stability and prolonged resistance to microbial attack.

Iron chemistry and possible mechanisms of interaction with OM in sediments

Accounting for almost one third of the mass of the Earth (Morgan and Anders, 1980), you would be hard pressed to find a process or an environment in which iron does not participate. From old rusty cars to respiration, DNA synthesis and bird brains, iron is everywhere. It is a constituent of rocks and soils, and an essential nutrient for plants and heterotrophs (Navrotsky et al., 2008). Our understanding of iron geochemistry is central to our understanding of carbon and vice versa as complexation constants as high as 10^{12} M^{-1} tightly fasten iron to OM through electronegative functional groups (Rue and Bruland, 1995). The chemistry of iron is shaped by its interactions with OM, intertwining the elemental cycles of iron to those carbon, nitrogen, phosphorous, oxygen and sulfur. Co-variation between iron and OC reflect the natural draw of iron to OM and vice-versa. Soils, for example are teeming with both iron oxides and OM, which together act as a mortar that cements particle aggregates (Hedges and Oades, 1997; Kaiser and Guggenberger, 2000). The retention and preservation of soil OM is expressly affected by the presence of iron oxides. Dissolved iron concentrations in lakes (Ouellet et al., 2012), sediment porewaters (Deflandre et al., 2002), rivers and oceanic waters (Johnson et al., 1997) are also controlled by organic ligands that increase iron solubility and modulate bioavailability (Mackay and Zirino, 1994; Raiswell and Canfield, 2012a).

As early as the 1970s, organic carbon and iron concentrations have also been shown to co-vary in sediments (Berner, 1970) though, until recently, it remained ambiguous whether iron and OM where truly chemically bound or whether the co-variations were caused by each element having a high affinity for the same particle surfaces. It has now been shown that a large percentage of OM is directly bound to reducible iron phases (Lalonde et al., 2012) but the exact mechanism of interaction remains ambiguous, in part because iron's chemistry is complicated by the changing

redox conditions near the sediment-water interface (Burdige, 1993). Enough oxygen from the water column permeates through the uppermost layers of the sediment to ensure that iron(III) which is typically found as nano-crystals of hydrated oxides, such as goethite, lepidocrocite or ferrihydrite (Van der Zee et al., 2003), is thermodynamically stable. The small particle size of iron oxides in sediments suggests a high level of diagenetic activity, caused by repeated dissolution and re-precipitation upon changes in redox conditions (Burdige, 2006). Alternatively, OM covering oxide particles may prevent crystal growth beyond a few nanometers by inactivating or poisoning surfaces (Schwertmann, 1966). TEM images focused on iron in lake sediments show iron oxides nanoparticles (3 to 10 nm across) to be surrounded by a veil of OM (Tipping et al., 1981). The mechanism by which OM binds to iron oxide particles likely takes place through a ligand-exchange mechanism in which electronegative functional groups in OM replace hydroxyl groups that line the surface of iron oxide particles (Gu et al., 1995). When sediments become anoxic, some iron is reductively dissolved to soluble iron(II) (Figure 1-2, #1) which can precipitate as iron sulfides (Figure 1-2, #2) or diffuse upwards towards the oxic zone to be reoxidized (Figure 1-2, #3) and precipitated. Fe(III) reduction can occur either abiotically or as a result of dissimilatory iron reduction, involving the microbial reduction and utilization of iron oxides as electron acceptors (Burdige, 2006). Nevertheless, as much as a third of the iron oxides deposited in the uppermost sediment layers are buried in deep, aged sediment deposits due to a high level of metastability (Figure 1-2, #4) (Hease et al., 1997). The kinetic stability of iron oxides, the fast oxidation of iron(II) and the low solubility of iron(III) in oxic waters ensures that iron is trapped in the sediment as long as the water column contains dissolved oxygen (Katsev et al., 2007). Lateral migration of small iron oxide particles swept up from surface sediments by oceanic currents is however possible (Figure 1-2 # 5).

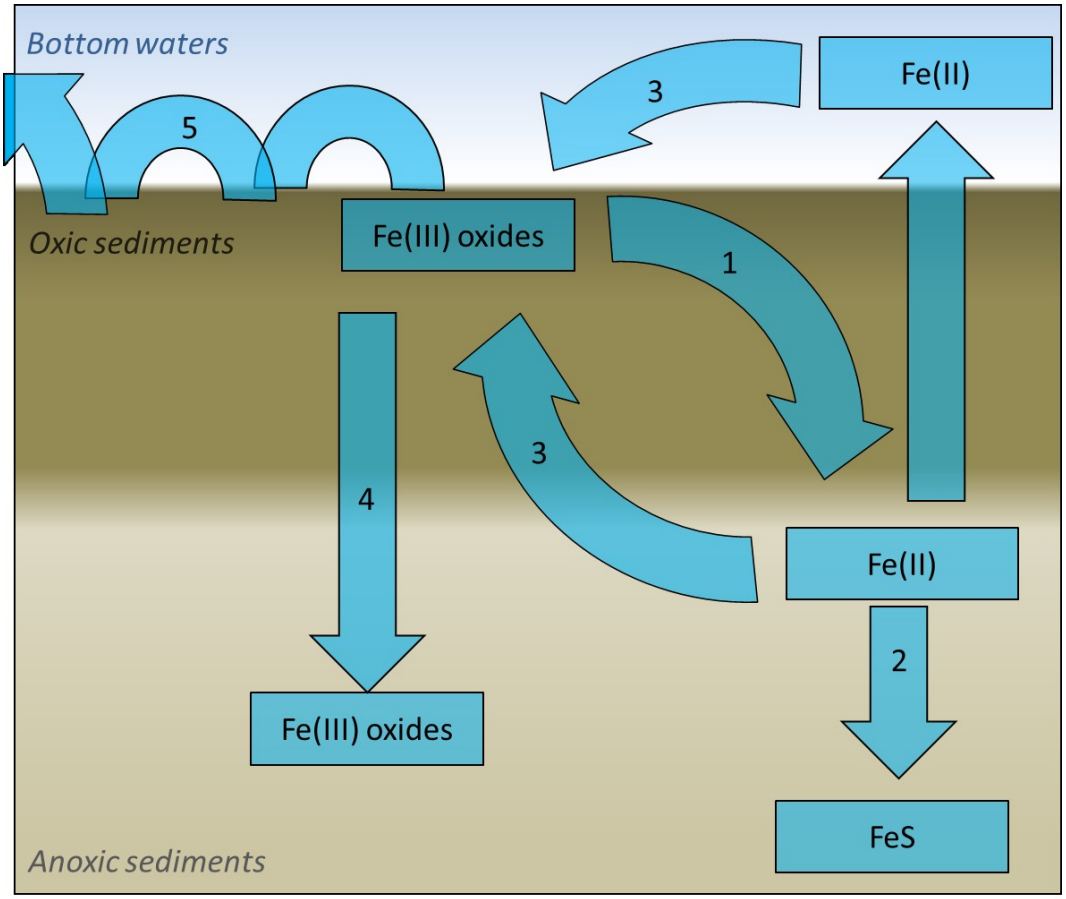

Figure 1-2: Diagenesis of iron in oxic/anoxic sediments and in the water column. Diagenetic processes include 1. Oxidation of iron(II) to iron(III) oxides, 2. Reduction of iron(III) oxides to iron(II), 3. Diffusion, 4. FeS formation from the reaction of iron(II) with sulfides and 5. Burial of iron(III) oxides.

The interaction between iron(III) and OM are likely formed in oxic sediments where OM is most prone to degradation (Figure 1-3). *In-vitro* studies have demonstrated that OM bound to iron oxides or iron(III) have decreased degradation rates compared to solitary organic compounds (Boudot et al., 1989; Jones and Edwards, 1998). The timescale over which iron's protection continues is highly dependent upon the rate of desorption or decomplexation (Henrichs, 1995). If iron-OM associations are not quickly dismantled and if binding to iron slows down sufficiently the breakdown of OM in sediments, iron-OM complexes may survive long enough to be buried into anoxic deposits where OM degradation rates are much lower (Figure 1-3). If iron oxides are reduced, the weak bonds between iron(II) and OM imparts no preservative effect, but if bound

to other mineral components, OM can remain safe from degradation in anoxic sediments. In this case, we view the role of iron as an OM shuttle, from the oxic surficial sediments to anoxic deposits, where preservation is possible. After diagenetic recycling and redeposition in oxic sediments, iron(III) can repeat the shuttling process with newly bound/coagulated OM.

The exact mechanism of interactions between iron and OM form in sediments remains speculative. What environmental conditions facilitate the interaction? Which molecules and what functional groups are most prone to bind iron? Are covalent bonding and ligand-exchange truly the most prevalent binding modes? New computer models, experiments and analytical techniques and instrumentation, are continuously being developed to tackle these difficult geochemical problems.

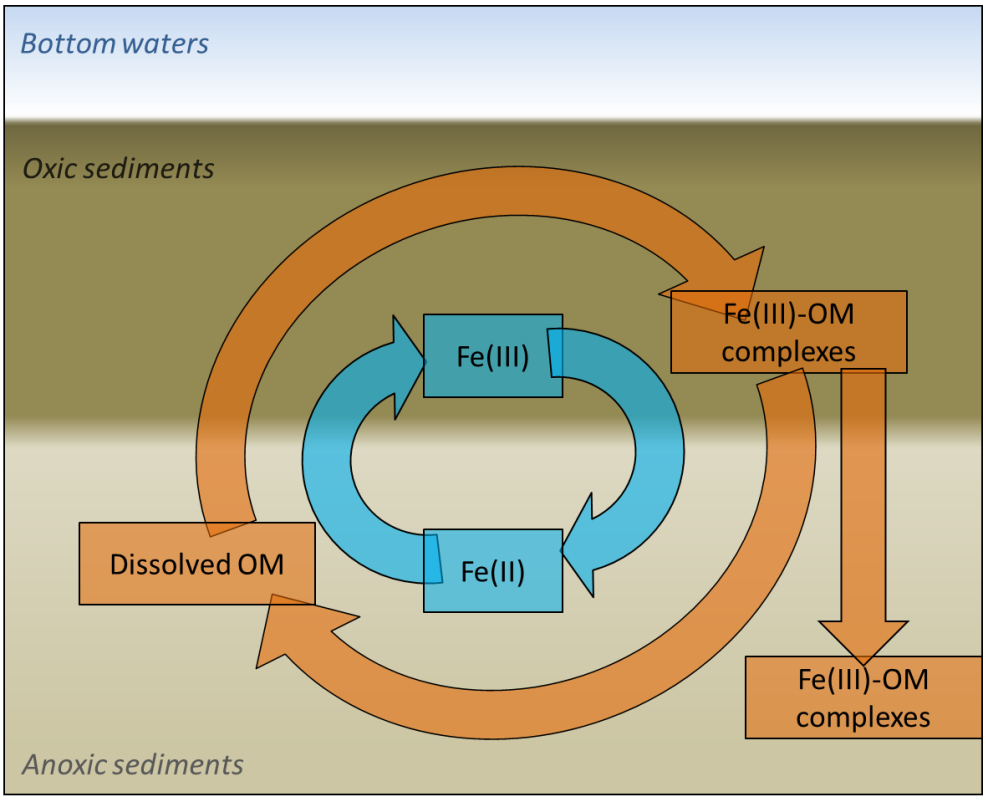

Figure 1-3: Possible coupling of iron's redox cycle to organic matter in sediments through the formation of Fe(III)-OM complexes or through adsorption of DOM onto iron oxide particles.

Iron's influence on fast cycling OM

The chemistry of iron in the environment has a profound effect on the carbon that cycles on geological time scales—in sedimentary rocks, in coal and petroleum deposits, the balance between carbon preservation and remineralization is in part modulated by iron. Nevertheless iron also influences the carbon that cycles in active surface reservoirs, whether in the ocean, in the atmosphere, or on land, linking continental erosion of detrital iron minerals to carbon deposition in sediments, and iron-rich dust deposition to phytoplankton blooms in the middle of the ocean (Burdige, 2006).

The fluidized mud beds of the Amazon River that quickly transition between oxic and anoxic conditions are an interesting locale to study the link between iron's redox chemistry to organic carbon in fast cycling reservoirs (Aller et al., 1996). Contrary to "normal" depositional settings, iron accelerates OM degradation rates in these mud belts. Quick redox cycling causes the spontaneous reoxidation of iron(II) which generates peroxide through the decomposition of superoxide radicals. Iron(II) may combine with peroxide to form Fenton's reagent, a powerful oxidant that can cleave a wide range of bonds non-specifically within OM structures (Hedges and Keil, 1995). A similar mechanism is used to increase oxidation efficiency of DOM in sewage treatment facilities which generate free radicals from the combination of iron salts and UV radiation (Trovo et al., 2008). Iron also appears to significantly enhance the photooxidation of DOM in coastal rivers through direct photoreactions involving ligand to metal charge transfer. As terrestrially-derived organic molecules and iron in coastal waters are both mainly drawn from the continents, the fast removal of riverine DOM almost immediately after its discharge into oceanic waters may in part be explained by iron-accelerated photooxidation (Zepp, 2003).

A special combination of conditions also creates particularly interesting interactions between iron and OM at oxic-anoxic interfaces, which are ubiquitous in marine and terrestrial settings, residing not only in surface sediments, but also in salt marshes, soils, peats, fens and wetlands. The transitioning redox conditions of these systems enriches these interfaces with reactive iron oxides that precipitate from dissolved iron(II) diffusing from the underlying anoxic zones (Burdige, 1993). Precipitation of iron oxides in the oxic surface layer of the sediment removes a large fraction of DOM by coagulation. Mass spectrometry has recently shown the preferential attachment of aromatic and pyrogenic compounds to iron at redox interfaces of peat bogs while carboxyl-rich aliphatic acids remain in solution (Riedel et al., 2012). Iron oxides also alter the surface chemistry of clay particles at redox interfaces, increasing the affinity of particles for DOM, trace metals and phosphates and limiting the mobility of solutes between the solutions and particles (Couture et al., 2008; Sundby et al., 1992). Iron-rich redox interfaces may therefore impact the flow of elements and organic matter, both dissolved and particulate, between sediments and bottom waters, soils and groundwaters and salt marshes/tidal flats and tidal waters.

Increased understanding of iron-OM interactions has prompted geoengineering remediation projects, in which these concepts are implemented to intentionally alter the environment. In an endeavour to restore the balance of natural systems, geoengineers have used iron to remediate a fraction of the anthropogenic carbon emissions produced annually. Two hundred thousand pounds of iron sulfate was dumped into the North Pacific Ocean off the western coast of Canada in July 2012. This experiment was conducted by the Haida Salmon Restoration Corporation, under the direction of businessman Russ George. The growth of phytoplankton in these waters is limited by iron, therefore introducing dissolved iron triggered a massive phytoplankton bloom, which absorbed carbon into their biomass and eventually sunk to the deep ocean waters. On

the time scale of a few hundred years, the carbon is sequestered, purposefully reversing a small quantity of man-made carbon emissions. Though interesting in its applicability to climate change, critics note that "the possible side effects of large-scale iron fertilization are not yet known; and that sufficient research has not yet been done. Significant, unknown, unforeseen, and unforeseeable risks may be involved if iron fertilization is performed on the scale needed to truly affect global CO_2 levels" (Rickels et al., 2011).

Many smaller scale geoengineering applications can be evaluated in experimental lakes in northern Ontario, which were cordoned off for scientific testing (Schindler, 1974). The use of these lakes is crucial since remediation projects, meant to improve environmental conditions, can cause important negative repercussions that are difficult to predict in natural systems affected by hundreds of chemical and ecological variables. Some lakes experiencing harmful algal blooms have been remediated using iron oxides. After their addition to the sunlit surface waters of lakes, iron oxides sink to the bottom of lakes, simultaneously binding and taking down phosphorus, which fertilizes algal growth in these systems. Phosphorous therefore remains trapped under a cap of iron oxides in the lake sediments (Liu et al., 2009). These iron additions help restore the natural ecosystem of these lakes whilst phosphorous waste removal procedures and the use of phosphorus containing household products such as lawn fertilizers, water softeners and laundry detergents are re-evaluated.

Whether it is a prerequisite for natural environmental processes or a key ingredient in some geoengineering project, iron is currently at the forefront of geosciences. Recently developed methods and instruments may help tackle complex biogeochemical problems and help unravel the mechanism(s) of interaction between iron and OM. Soft X-ray absorption techniques, for example, have clearly demonstrated that organic-rich nano-pockets are co-localized to iron with

preferential association of oxygen-rich functionalities in soils (Solomon et al., 2012). Though the lower concentration of organic carbon in sediments would equate to reduced sensitivity, it is possible that X-ray techniques could similarly establish co-localization of iron and OM, and what type of binding, whether covalent or electrostatic, exists between the two. Recent developments in high-resolution mass spectrometry have also greatly expanded our "analytical window" constraining and resolving thousands of individual organic formulas (including N and S compounds) based on precise molecular mass determinations for organic components of highly complex mixtures. This technique has allowed us to identify the types of molecules that are preferentially bound to iron at oxic-anoxic interfaces. It may also be possible to target the molecules that are released from the sediment matrix upon reductive dissolution of iron oxides in soils and sediments (Riedel, pers. comm.). The realization of iron's importance in organic geochemistry has roused questions that are yet to be answered and has evoked iron as a possible culprit in a number of carbon production, degradation and sequestration mechanisms on Earth.

Isotopes and OM

The richness of information stored in buried OM is accessed by targeted instrumental and experimental methods. Bulk characterization of sediment OM using spectroscopic methods generates rather imprecise information as sediment OM is a complex mixture of molecules occupying a continuum of molecular masses, with subtly different chemical structures and elemental compositions, which generate broad, undefined peaks.

Natural abundance stable carbon isotope analysis is a staple for understanding geochemical OM and carbon dynamics. Isotopic analyses using IRMS can detect very small differences in the isotopic ratios of carbon 12 and 13 that occur at the third and fourth decimal place of the ratios

and are highlighted by the delta notation that relates a ‰ difference of a sample and an isotopic reference that is standardized in labs around the world:

$$\partial^{13}C = \left(\frac{\frac{^{13}C}{^{12}C}sample - \frac{^{13}C}{^{12}C}reference}{\frac{^{13}C}{^{12}C}reference} \right) \text{x } 1000$$

Small variations in the $^{13}C/^{12}C$ of photosynthesized OM can indicate the terrestrial or marine provenance of OM, since marine plants use dissolved inorganic carbon as their source of carbon ($\delta^{13}C$ = 0‰) and terrestrial plants use carbon dioxide ($\delta^{13}C$ = -7‰), a difference ensues in the final isotopic signature of the bulk photosynthesized OM (marine = -20‰ and terrestrial = -27‰). Alternatively, terrestrial plants using the less common C4 carbon fixation pathway to generate OM with signatures around -14‰ (Farquar et al., 1989). Within one photosynthetic organism, there are also differences in the signatures of different biochemicals; proteins and sugars being more enriched in $\delta^{13}C$ (ratio is less negative) than the lipids, lignins and non-acid-soluble OM for example (Wang et al., 1998).

The use of stable isotopes in environmental studies therefore allows us to track carbon from different sources in marine sediments as well as aquatic systems such as lakes, rivers, estuaries, coasts and oceans. For example, going seaward from the mouth of a river, where dissolved OM is comprised mainly of continentally-derived material ($\delta^{13}C$ -27‰), isotopic signatures of particulate and dissolved organic matter become progressively more enriched, reaching a value of -20‰ as a result of degradation and dilution of terrestrially-derived material and addition of marine-derived DOC through primary productivity. Monitoring the change in organic matter

concentrations and $\delta^{13}C$ as a function of the change in salinity also potentially makes possible the identification of OM fractionation processes as the preferential degradation of certain biochemicals or coagulation/co-precipitation of specific moieties in dissolved molecules with iron or calcium in the water column may alter the $\delta^{13}C$ signature of the residual dissolved organic matter pool.

Stable isotope analyses of solid samples and carbonates (DIC) are routine methods carried out by coupling an elemental analyzer to an IRMS. Measurements of the isotopic composition of dissolved organic matter are uncommon and have a limited environmental coverage likely due to the difficulty of the analyses. In order to analyse the stable carbon isotope ratio of DOC, a novel method was developed, coupling a total organic carbon (TOC) analyser to an isotope ratio mass spectrometer.

Organization of the thesis

The bulk of this thesis is based on four manuscripts that have either been published, accepted for publication or submitted to refereed journals. Rather than having connecting paragraphs, the relationship between chapters is described in this subsection. The publications chosen for these chapters cover a diverse set of fields of study whose associations include the Nature Publishing Group (Nature), American Society for Limnology and Oceanography (Limnology and Oceanography: Methods), Elsevier (Marine Chemistry) and the European geoscience union (Biogeosciences) and as such connections between the chapters may not be obvious. All chapters are formatted in the same manner with Figures and Tables inserted in the text, and numbered according to Chapter (i.e., Figure 2-1 means Figure 1 of Chapter 2). Sections published as "Supporting Information" are appendices placed at the end of the document with

an "A" preceding the number (i.e., "Appendix A2" corresponds to the appendix of Chapter 2, and "Figure A2-1" corresponds to Figure 1 of Appendix 2).

Chapter 2 ("Preservation of organic matter in sediments promoted by iron" in Nature 483, 198–200) demonstrates through a relatively simple chemical extraction that there is an intimate association between organic matter and reactive iron oxide species in sediments. Specifically, more than 20% of the organic carbon in aquatic sediments from a wide range of depositional environments — which vary in salinity, proximity to land, water depth, organic carbon content and oxygen availability — is associated with reactive iron phases. Detailed methodological information is given in Appendix A2. Though the main conclusion of this paper had a fairly wide-ranging impact on theories of carbon burial in marine sediments, the exact mechanism of interaction still remains speculative. Chapter 3 ("The role of iron in the diagenesis of organic carbon and nitrogen in sediments: A long-term incubation experiment" accepted for publication in Marine Chemistry) attempts to further elucidate the preservative role of iron on OM in sediments through an incubation experiment. One necessary analytical technique used in Chapter 3 is developed and optimized in Chapter 4 ("Automation of $^{13}C/^{12}C$ ratio measurement for freshwater and seawater DOC using high temperature combustion" to be submitted in Limnology and Oceanography: Methods) which describes the development of a novel technique to measure the stable carbon isotope ratio of dissolved organic carbon in saltwater and freshwater samples. This technique allows us to monitor the isotopic composition of dissolved organic matter in sediment porewaters during our incubation experiment and to demonstrate increased solid-solution partitioning upon addition of iron oxides to sediment particles. Though useful for sediment porewaters, chapter 4 covers method development and validation for application to a wide-range of natural samples. Chapter 5 ("Revisiting the disappearance of terrestrial dissolved organic matter in the ocean: a $\delta^{13}C$ study" submitted to Biogeosciences)

also uses the DOC-IRMS technique to monitor the isotopic composition of riverine waters during photooxidation with simulated UV light. Though not directly related to the iron axis of this thesis, photooxidation of dissolved organic matter was shown to be in part modulated by iron chemistry through the generation of free radicals.

Chapter 2: Iron promotes the preservation of organic matter in sediments

The biogeochemical cycles of iron and organic carbon are strongly interlinked. In oceanic waters organic ligands have been shown to control the concentration of dissolved iron (Johnson et al., 1997). In soils, solid iron phases provide a sheltering and preservative effect for organic carbon (Kaiser and Guggenberger, 2000), but the role of iron in the preservation of organic matter in sediments has not been clearly established. Here, we determine the amount of organic carbon, associated with reactive iron phases in sediments of various mineralogies collected from a wide range of depositional environments, using an iron reduction method previously applied to soils (Wagai and Mayer, 2006). Our findings suggest that 21.5 ± 8.6 per cent of the organic carbon in sediments is directly bound to reactive iron phases, representing a global mass of 19 to 45 x 10^{15} g of organic carbon in surface marine sediments (Hedges and Keil, 1995). We propose that these organic carbon-iron associations, formed primarily through co-precipitation and/or direct chelation, promote the preservation of organic carbon in sediments. Since reactive iron phases are metastable over geological timescales, they serve as an efficient “rusty sink” for OC, a key factor in the long-term storage of organic carbon and thus contributing to the global cycles of carbon, oxygen and sulphur (Berner, 2003).

Evidence of interactions between Fe and OC in marine sediments was reported nearly 40 years ago, where concentrations of Fe and OC were found to co-vary (Berner, 1970). Since both Fe and OC are commonly associated with clay mineral surfaces, it was simply stated that "where there is more deposited fine-grained material with high surface area for adsorption, we find more organic matter and more Fe"(Berner, 1970). It is still not clear whether this correlation stems from the strong affinity of both species for solid surfaces or if it reflects enhanced OC preservation by Fe. Iron's preservative effect on organic matter was previously demonstrated in laboratory studies (Boudot et al., 1989; Jones and Edwards, 1998), which report that the presence of iron-rich solid substrates or the formation of organo-ferric complexes hampers microbial degradation of simple organic compounds. Iron also imparts a protective effect to OC in soil systems (Kaiser and Guggenberger, 2000), but this preservation mechanism has never been explored in sediments.

In modern sediments, reactive Fe phases (operationally defined here as the solid iron phases that are reductively dissolved by sodium dithionite) are typically found as nano-spheres of goethite of <10 nm in diameter (Poulton and Raiswell, 2005; Van der Zee et al., 2003). These phases accumulate or are formed within the oxic sediment layer through oxidation and precipitation of dissolved Fe(II) produced during weathering and diagenetic recycling within the sediment (Canfield, 1997). Over time, reactive Fe phases become more crystalline, resulting in reduced surface reactivity/area and solubility. Crystallization is, however, hindered by the active diagenetic recycling of iron (Burdige, 2006), and by organic matter coating of Fe phases (Schwertmann, 1966). Accordingly, reactive Fe phases have been shown to survive in sediments for hundreds of thousands of years (Hease et al., 1997).

We examined sediments collected from a wide range of environments, including freshwaters, estuaries, river deltas, continental margins and the deep-sea, encompassing various depositional environments and mineralogies. These samples include OC-rich sulphidic Black Sea sediments and OC-rich sediments from O_2-deficient zones along the Indian and Mexican (Stn. 306) margins. Also included are sediments from the Arabian Sea, the Saanish Inlet and a boreal lake (Lake Brock) which exhibit a productivity-driven seasonal pattern of O_2-deficient waters. Estuarine, deltaic and margin deposits accumulating below well-oxygenated waters of the Arctic margin, the St. Lawrence Estuary and Gulf, the Mexican margin (Stns. 303-305), the Eel River Basin and the Washington coast and adjacent Columbia River delta are also examined along with pelagic sediments from the Southern Ocean, the Santa Barbara Basin (Stn. M) and Equatorial Pacific Ocean. This sample set comprises freshwater, estuarine and marine clastic sediments, carbonate and siliceous oozes, as well as pelagic red clay sediments. We focused on determining the amount of OC associated with reactive Fe phases by applying the citrate-dithionite iron reduction method of Mehra and Jackson (Mehra and Jackson, 1960), which simultaneously dissolves all solid reactive Fe phases and the OC associated to these phases (OC-Fe) from the sediment matrix. The reduction reaction is conducted at circumneutral pH using sodium bicarbonate as a buffer, thus preventing the hydrolysis of organic matter as well as its protonation and readsorption onto sediment particles which occur under acidic conditions. Whereas the extraction of the same samples with artificial seawater released a negligible fraction of the total OC (less than 3%; results not shown), samples treated under the same experimental conditions after substituting trisodium citrate (complexing agent) and sodium dithionite (reducing agent) for sodium chloride (equivalent ionic strength) released on average 7.2 ± 5.4% of the total OC (Appendix A2 Table 8-2). Because the OC released in these control experiments is not associated with Fe, results of individual control experiments were subtracted

from the amount of OC released from the dithionite extractions (see Appendix A2 for results and discussion on contamination and specificity for the OC-Fe fraction).

We determined that for all sediments tested, an average of 20.5 ± 7.8% of the total OC is directly associated to Fe, with the highest OC-Fe concentrations in the uppermost sediment layers where most of the reactive Fe phases accumulate (Figure 2-1). Considering OC burial within different depositional settings - deltaic and continental margin sediments account, respectively, for 44% and 45% of global OC burial, while pelagic sediments and high productivity zones, including anoxic basins, account for 5% and 6%, respectively[17] - we estimate that the global pool of OC specifically associated to Fe corresponds to 21.5 ± 8.6% of the total sedimentary OC or 19 to 45 × 10^{15} g of OC. Even in mature sediments (1000 to 1500 yrs old), 23-27% of the total OC remains bound to reactive Fe oxide phases, suggesting that the strong association between Fe and OC may inhibit microbial OC degradation and enhance OC preservation.

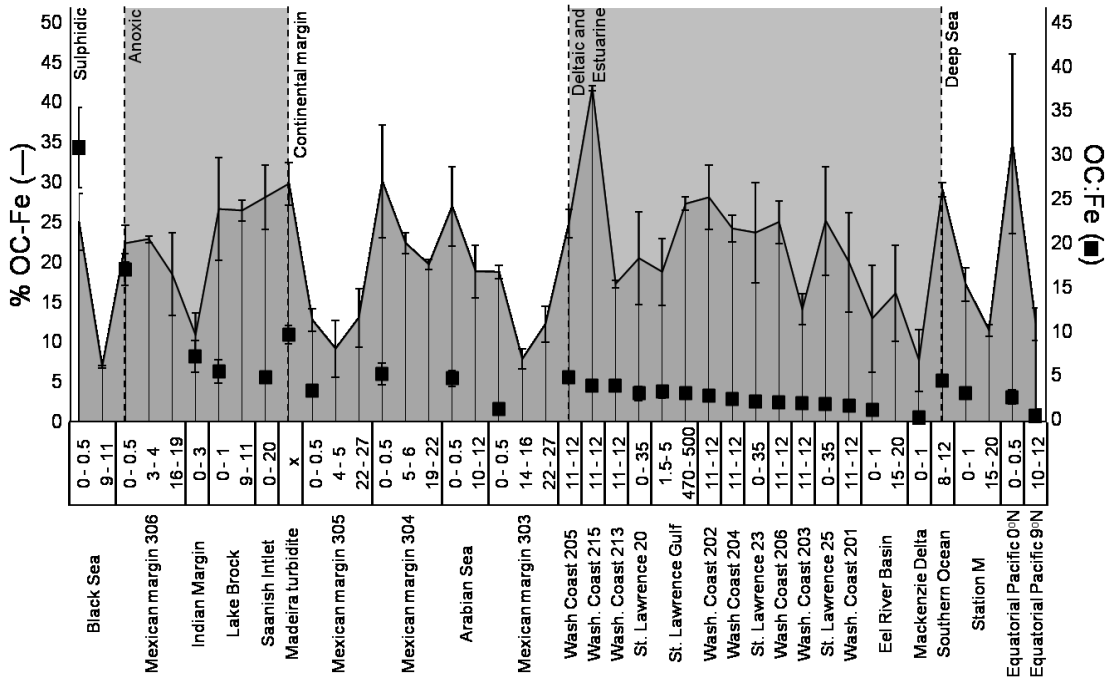

Figure 2-1: Control-corrected percentage of the total sediment organic carbon (OC) bound to reactive iron phases, i.e., dislodged from the sediment during the reductive dissolution of reactive iron oxides. Depth intervals (cm) and sample names are indicated below the x-axis. Molar OC:Fe ratios of the uppermost surface sediment layer are also shown (black squares). The iron reduction was carried out following the method of Mehra and Jackson (1960) without adding agents that promote flocculation of the dissolved organic matter after the reduction step. Error bars show s.d. (n = 12-15 for the St. Lawrence samples, and n = 3 for all the others).

In agreement with Wagai and Mayer's calculations (Wagai and Mayer, 2006), our measurements reveal that reactive Fe phases do not provide sufficient surface area (<5% of the total surface area of sediments; Appendix A2, Table 8-3) for adsorption of the entire OC-Fe pool onto Fe oxides. Alternatively, we propose the existence of largely organic OC-Fe macromolecular structures that are dissolved and dislodged from the sediment during iron reduction. Transmission electron microscopy studies describe sedimentary organic matter as "discrete, discontinuous blebs" that adhere to the surface of sediment clay particles (Ransom et al., 1997). These "blebs" are consistent with our proposed structure of OC-Fe, as are the findings of Mayer (Mayer, 1999), who reported that sedimentary organic matter is not spread evenly over clay

particles but covers only about 15% of particle surfaces. We believe that Fe or Fe oxides are critical in providing cohesion to these macromolecular structures, possibly fixing them to clay particles through strong covalent bonds.

Calculations by Wagai and Mayer (Wagai and Mayer, 2006) indicate that simple sorption of OM on reactive Fe oxide surfaces results in a maximum molar OC:Fe ratio of 1.0 for the co-extracted organic carbon and iron, based on the maximal sorption capacity of reactive iron oxides for natural organic matter. On the other hand, co-precipitation and/or chelation of organic compounds with Fe generates low density, organic-rich structures with OC:Fe ratios between 6 and 10 (Wagai and Mayer, 2006). According to the results of our dithionite extractions, typical continental margin sediments overlain by oxic bottom waters yield an average OC:Fe ratio of 4.0 ± 2.8 (Appendix 2, Table 8-3), greatly exceeding the maximum sorption capacity of Fe oxides but consistent with the formation of OC-Fe chelates. These chelates are predominantly organic structures which likely resemble those depicted by the 'onion model' of Mackay and Zirino (Mackay and Zirino, 1994), where organic molecules are 'glued' together by Fe ions or nanophases of Fe oxides. The formation of such chelates from solution is possible when the molar porewater OC to Fe ratio is approximately 10 (Baas Becking and Moore, 1959; Guggenberger and Kaiser, 2003). This molar ratio is typically observed in anoxic sediment porewaters such as in the St. Lawrence Estuary (Lalonde unpubl. data) and in the nearby Saguenay Fjord (Deflandre et al., 2002). The diffusion of dissolved Fe(II) from anoxic to surficial oxic sediments would trigger the oxidation of Fe(II) to Fe(III) and the formation of very stable organic complexes ($K \approx 10^{14}$ M^{-1} for natural dissolved OC to 10^{52} M^{-1} for siderophores) (Kraemer, 2004; Rue and Bruland, 1995).

Sediments bathed by oxygen-depleted bottom waters, such as in the Black Sea, the Mexican margin (Stn. 306) and the Indian margin, host high OC:Fe ratio structures (7 to 32). These organo-metallic structures appear to be particularly stable under anaerobic conditions and survive degradation. In contrast, in oxic environments, the organic lining of these structures is progressively degraded, reducing the OC:Fe ratio to levels observed in typical continental margin sediments Figure 2-1. Long periods of exposure to oxic conditions increase the fraction of the total sedimentary OC pool that is tightly adsorbed to particle surfaces (Arnarson and Keil, 2007), owing to the preferential degradation of organic structures that are more loosely attached to the clay mineral matrix, such as the OC-Fe chelates. Very long exposure to oxic conditions results in the very low OC:Fe observed at the deep-sea Equatorial Pacific site (0.36; Figure 2-1).

We also analyzed the isotopic ($\delta^{13}C$ and $\delta^{15}N$) and elemental composition (C:N molar ratio) of the bulk OM and the Fe-associated OC fractions of all sediment samples. In most cases, we find that the OC-Fe is enriched in ^{13}C ($\delta^{13}C$ increases by 1.7 ± 2.8‰) (Figure 2-2) and nitrogen (C/N decreases by 1.7 ± 2.8) relative to the rest of the sedimentary OC pool whereas $\delta^{15}N$ displayed little or no fractionation (Appendix 2, Figure 8-1, Figure 8-2). ^{13}C-rich natural organic compounds include proteins and carbohydrates (Wang et al., 1998), which are rich in nitrogen and/or oxygen functionalities that favour the formation of inner-sphere complexes with Fe. The preferential binding of such highly labile organic compounds to Fe may explain why reactive organic compounds can be preserved in sediments while other, more recalcitrant molecules, are degraded (Hedges and Keil, 1995).

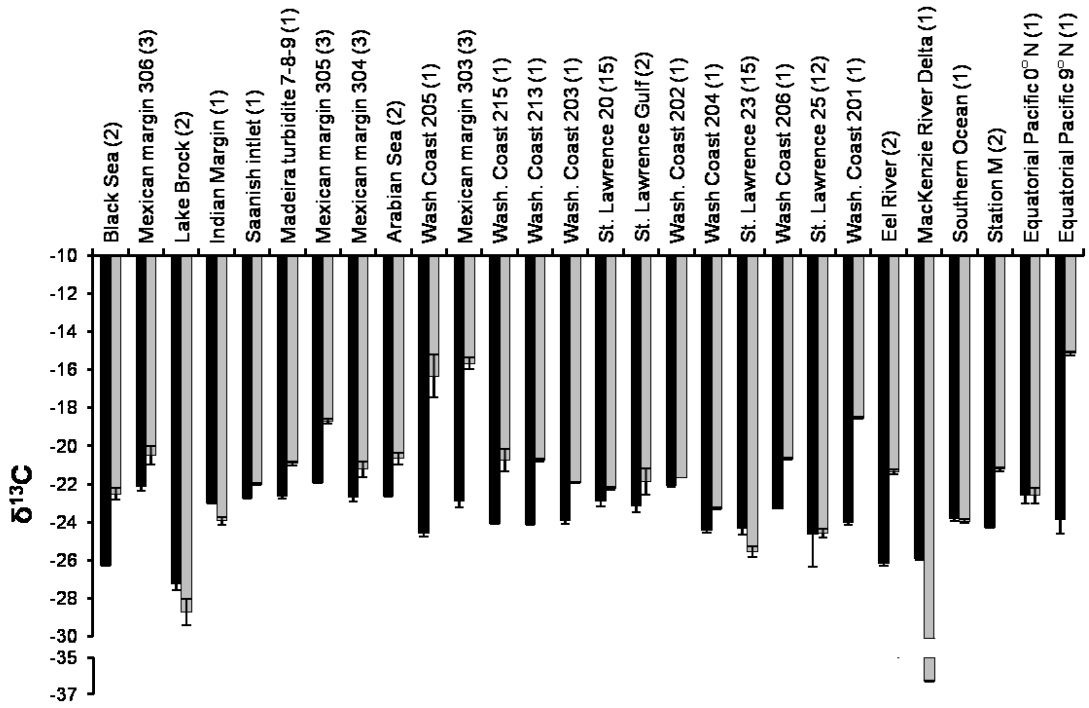

Figure 2-2: Carbon isotopic signatures ($\delta^{13}C$ normalized to VPDB) of non iron-bound organic carbon (OC) (black) and iron-bound OC (grey) for all sediment samples. The samples were depth-integrated whenever possible; the number of depth intervals integrated is indicated in parentheses above the sample name. Error bars show s.d. (n = 12-15 for the St. Lawrence samples, and n = 3 for all the others).

Our findings have far-reaching implications on our understanding of organic matter cycling in sediments. First, the protection mechanism described above, which preferentially shields ^{13}C- and nitrogen-rich organic compounds from microbial degradation, could help explain a phenomenon that has puzzled organic geochemists for decades: the replacement, seaward of river mouths, of terrigenous organic matter from sediments by compounds bearing a more marine isotopic and elemental signature (Hedges et al., 1997). Our data also show that the traditional sorptive stabilization mechanism, which hypothesizes that clay particles have a preservative effect on organic matter through direct adsorption on their surfaces (Hedges and Keil, 1995; Mayer, 1994; Mayer, 1995), does not describe accurately the mode of stabilization for all organic compounds in sediments. Although more work is needed to elucidate the exact

nature of OC-Fe interactions, our data suggest that direct chelation or co-precipitation of macromolecular OC-Fe structures also plays a significant role. Finally and most importantly, our results reveal that 21.5 ± 8.6% of the OC buried in surface marine sediments (150×10^{15} g of OC) (Hedges and Keil, 1995), or a global mass of 19 to 45×10^{15} g of OC, is preserved as a result of its intimate association with reactive Fe phases. Assuming that our estimate also applies to OC locked in the sedimentary rock reservoir ($15{,}000 \times 10^{18}$ g of OC) (Hedges and Keil, 1995), Fe-associated OC would account for 1900 to 4500×10^{18} g of OC, or roughly 2900 to 6800 times the size of the atmospheric carbon pool. Hence, reactive Fe phases serve as an extremely efficient "rusty sink" for OC, a key factor in the long-term storage of organic carbon and the global cycles of carbon, oxygen and sulphur.

Chapter 3: The role of iron in the diagenesis of organic carbon and nitrogen in sediments - A long-term incubation experiment

Abstract

The burial and preservation of organic matter (OM) in marine sediments is tightly coupled to the diagenetic cycles of iron and manganese. Recently, it has been shown that approximately 20% of the sedimentary organic carbon (OC) may be bound to reducible iron oxides (Lalonde et al., 2012). These strong iron-OC complexes, formed within the oxic layer of the sediment, are transferred to the deeper anoxic sediment layers through sedimentation, physical reworking and bioturbation and are metastable over geological timescales. Using long-term (250-day) incubations under various redox and amendment conditions (Fe(II) and dissolved OM (DOM) additions), we examined the effect of iron on the early diagenetic transformations of OM in marine sediments. The fate of fresh, algal-derived DOM was monitored by tracking its stable carbon isotopic signature ($\delta^{13}C$). We demonstrate the incorporation of the ^{13}C-depleted tracer into the sediment through sorption (adsorption and co-precipitation). In the presence of iron oxides, we observed increased transfer of the dissolved algal material to the solid phase, revealing the role of iron in shuttling DOM from sediment porewaters to sediment particles. Furthermore, we show that the presence of iron has a differential effect on OC and organic nitrogen (ON), with preferential preservation of OC and accelerated degradation of ON in the presence of reactive iron oxide surfaces. Hence, we propose that redox-sensitive metals may regulate the global redox balance through increased carbon preservation as well as exerting a control on the concentration of fixed nitrogen species in marine sediments.

Introduction

The burial and preservation of organic matter (OM) in marine sediments are important factors in modulating the concentration of atmospheric oxygen and carbon dioxide over geological time

(Berner, 1989). Hence, elucidating factors that favor sedimentary OM preservation over its degradation is important. OM can be physically shielded from degradation by adsorption to mineral particles. In fact, over 99% of sedimentary organic carbon (OC) is bound to particle surfaces - the remainder is found as discrete organic debris (Hedges and Keil, 1995; Keil et al., 1994; Ransom et al., 1998a). The surface area of sedimentary mineral particles determines the abundance of OM binding sites and modulates OC-mineral binding, maintaining surface loadings at a near constant and universal value (0.5-1.0 mg OC m^{-2}) on continental shelves and margins (Keil et al., 1994; Mayer, 1994; Mayer, 1995). Organic compounds can also be protected from microbial degradation through encapsulation within diatom tests (Arnarson and Keil, 2007; Ingalls et al., 2003) expandable-clay interlayers (Kennedy and Wagner, 2011), particle mesopores (Mucci et al., 2000), and macromolecular hydrophobic OM (Mariotti et al., 1981). Over the past 20-30 years, the identification of these processes has shaped our understanding of the fate of OM in sedimentary systems, but the exact nature of these preservative interactions as well as the conditions under which they form still remain unclear. Recently, metal oxides have been identified as key players in the physical protection of OM, accounting for the sequestration and preservation of ≈20% of the OC in marine sediments (Lalonde et al., 2012).

Sedimentary nitrogen is essentially affected by the same preservative associations as OC, but the two species display divergent degradation pathways. The production of N_2 through denitrification and anammox in marine sediments is an important component of the global nitrogen cycle, influencing the oceanic inventory of fixed nitrogen (Burdige, 2006). Bacteria mediate the bulk of both OC and ON mineralization to CO_2 and N_2, but unlike OC remineralization, the traditionally accepted mechanisms of bacterial N_2 production are mainly confined to anoxic conditions (Burdige, 2006). A proposed alternative pathway of N_2 production in sediments (Devol, 2008) and soils (Yang et al., 2012) involves the direct oxidation of NH_4^+ by

manganese and iron oxides, a thermodynamically feasible process under both oxic and suboxic conditions (Yang et al., 2012). Balanced equations for these processes are shown here:

$FeOOH + 1/3NH_4^+ + 5/3H^+ \rightarrow 1/6N_2 + Fe^{2+} + 2H_2O$

$MnO_2 + 2/3NH_4^+ + 5/3\ H^+ \rightarrow 1/3N_2 + Mn^{2+} + 2H_20$

Redox-sensitive metals, such as iron and manganese, strongly impact the turnover of both OC and ON in marine sediments, but OM also affects the diagenetic cycling of iron. The growth of authigenic amorphous iron oxide phases is, for example, strongly inhibited by OM bound to their surfaces (Schwertmann, 1966). The reduction of oxides in sediments may also be hampered by organic matter (O'Sullivan et al., 1995). Nanophases of iron oxides are the dominant reactive oxides in both marine and lacustrine sediments (Raiswell and Canfield, 2012b; Van der Zee et al., 2003) and these redox-sensitive phases, when associated to OM, somehow resist reduction after thousands of years of burial in anoxic sediments (Hease et al., 1997).

Elucidating the role of iron and manganese oxides on the degradation/preservation of OC and ON in sediments is impeded by the intrinsic complexity (e.g., spatial and temporal heterogeneity) of these systems. Benthic macrofauna, for example, affect elemental transport and cycling within the uppermost sediment layers and create microenvironments and lateral variability through burrowing and surface feeding (Aller and Aller, 1998; Aller et al., 1996; Boudreau, 1986; Katsev et al., 2007; Michaud et al., 2005). Additional difficulty is imparted by the poorly characterized nature (chemical structure) and wide-ranging reactivity of sedimentary organic matter (LaRowe and Van Cappellen, 2011). Not only are the latter dictated by OM sources, but also by the depositional setting as well as the intensity and frequency of physical, biological and chemical reworking (Aller et al., 1996). Due to the large range of OM reactivities

(half-lives ranging from 10 to 2000 years or longer; Hedges and Keil, 1995), it is difficult to tease out the environmental and depositional factors that control OM preservation and degradation on the timescales of field observations or laboratory experiments.

This paper describes a long-term (250 days) incubation, carried out under different redox and amendment conditions, that assesses the fate of OM (partitioning, degradation, iron oxide association) over a longer timeframe than typical laboratory experiments. We systematically controlled the incubation conditions to more readily identify differences between oxic and anoxic OM degradation rates as well as the preservative interactions between OM and redox-sensitive minerals. A pulse of labile dissolved organic matter (DOM) derived from ^{13}C- and ^{15}N-depleted algae was added to a natural sediment slurry to study its degradation/preservation. Since there is little isotopic fractionation of the stable carbon isotopic signature ($\delta^{13}C$) during physical and biological processing of sedimentary OC and given that the $\delta^{13}C$ signatures of carbon sources are discrete and well constrained, $\delta^{13}C$ is a sensitive source indicator in this system (Bauer, 2002; Middelburg et al., 2000), allowing us to track the fate of the algal OM pulse within the solid and aqueous phases.

Materials and methods:

Sampling

Sediment samples were collected at 325 m depth at station 23 (48°42.419'N, 68°38.387'W) in the Lower St. Lawrence Estuary onboard the *R/V Coriolis II* in May 2011. The first ≈20-25 cm of the grab core sample (fine silt/clay, porosity ≈ 0.85) was homogenized, removing visible living macrofauna, seashells and detritus. The wet sediment was transferred to glass jars and stored on-board and in the laboratory at 4°C for less than 4 months in order to preserve the native microbial communities and chemistry of the sediment. The bulk of the sediment remained

anoxic during storage as only the surface of the sediment within the jar was in contact with the atmosphere.

Fresh algal dissolved organic matter

Algal dissolved organic matter (DOM) was liberated from *Nannochloropsis* algae cells (Reed Mariculture) through cell lysis following repeated freezing in liquid nitrogen and thawing. Lysed cells were diluted with deep Pacific seawater (DOM concentration < 1 mg L^{-1}), centrifuged for 20 minutes at 19,000 g and filtered through a 0.7-µm glass fiber filter to generate a highly concentrated DOM solution. The algal-derived DOM is ^{13}C- and ^{15}N-depleted ($\delta^{13}C$ = -41.34 ± 0.12‰, $\delta^{15}N$ = -5.12 ± 0.26‰) relative to the natural sedimentary material ($\delta^{13}C$ = -24.29 ± 0.10‰, $\delta^{15}N$ = +5.67 ± 0.22‰), making it easy to follow its progressive integration into the sediment and degradation during the incubation. For example, a 6% addition of carbon and a 9% addition of nitrogen through the incorporation of algal DOC and DON, respectively results in a 1‰ depletion in sediment $\delta^{13}C$ and $\delta^{15}N$.

Slurry incubation setup

The incubation setup is illustrated in Figure 3-1. The 24 glass amber 250 mL vials (12 duplicate experimental conditions) were filled with wet homogenized sediment (14.6 g dry weight) in 175 mL of seawater giving a total volume of approximately 200 mL. Each vial was sealed with a custom designed PTFE cap lined with a Viton O-ring. Three ports were machined into the caps to accommodate standard PEEK fittings for gas purging and transfer as well as reagent additions. Three parallel sequences of 8 vials (4 amendment conditions done in duplicate) connected in series by PTFE tubing were incubated at 4°C under different redox conditions using a flow-through gas method (≈30 mL/min). The first two series were maintained either oxic or anoxic

using air or nitrogen gas, respectively. The redox conditions in the third series of incubations alternated monthly between oxic and anoxic conditions for the duration of the experiment.

After one week of redox equilibration, each set of 8 vials was amended with fresh algal DOM (final concentration 36.1 mmol L^{-1}) and/or dissolved ferrous iron ($FeCl_2 \cdot 4H_2O$, final concentration 4.25 mmol L^{-1}), making 4 duplicate experimental scenarios: A. Addition of iron(II) and OM (Fe-OM scenario) B. Addition of iron (II) only (Fe scenario) C. Addition of OM only (OM scenario) and D. Control vials containing only the original sediment and seawater (Control scenario) (Figure 3-1). Algal DOM and dissolved iron were injected as anoxic solutions through the septum port of each vial. Under oxic conditions, Fe(II) is expected to undergo rapid oxidation and precipitation as an iron oxide.

Aliquots (5 or 10 mL) of the well-mixed sediment-seawater slurries were extracted at various time intervals from each vial through the septum port using a syringe (shown in Figure 3-1) and immediately transferred to centrifuge tubes. After centrifugation for 10 minutes (1000 g), the aqueous phase was isolated, acidified to pH < 2 for sample preservation and dissolved organic carbon (DOC) analysis, and stored at 4°C while the solid phase was freeze-dried and stored for later analysis. The overlying water pH at the end of the incubations was measured using an Accumet AB15 pH electrode calibrated using three NIST-traceable buffer solutions (3.95, 7.05 and 10.27 at 5°C).

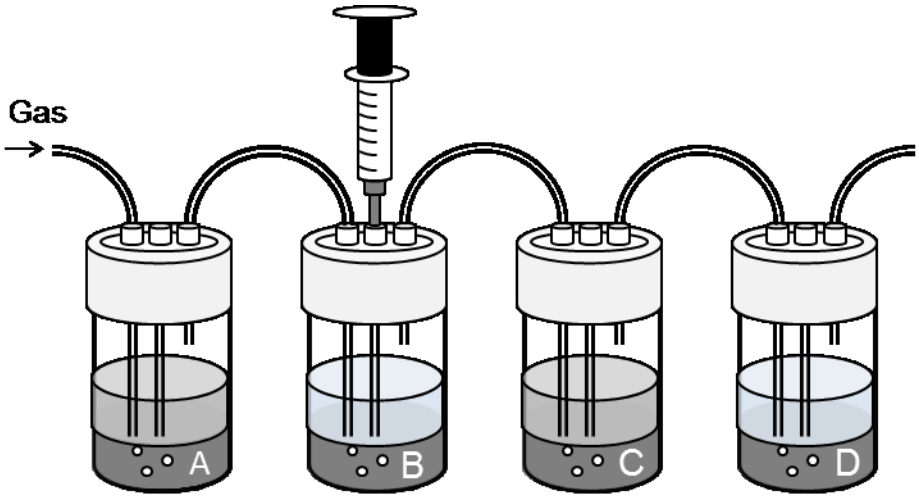

Figure 3-1: Illustration of the incubation setup. Incubations were carried out under 3 different redox conditions (anoxic, oxic, and mixed redox) by purging the overlying water with nitrogen gas, air, or alternating between the two gases. The sediment-seawater incubations were spiked with A) Fe(II) and DOM (Fe-OM scenario), B) Fe(II) only (Fe scenario), C) DOM only (OM scenario) and D) no addition (Control scenario). Note that each vial was duplicated (in series) in this experiment (8 vials per redox condition, 24 vials in total).

Analyses

Solid Phase Measurements

The OC and TN content as well as the $\delta^{13}C_{org}$ and $\delta^{15}N_{tot}$ signatures of the solid phase were measured using a CHN analyzer (EuroVector 3028-HT) coupled to an isotope ratio mass spectrometer (IRMS, Isoprime GV Instruments). Prior to the %OC and $\delta^{13}C_{org}$ analyses, the samples were decarbonated by fumigation with 12 N HCl for 12 hours followed by a 1-hour heating step at 50°C and 6 hours in a desiccator to remove remaining water/acid.

Elemental and isotopic measurements were calibrated to IAEA-C6 sucrose ($\delta^{13}C$ = -10.45 ± 0.03), IAEA-N1 ammonium sulfate ($\delta^{15}N$ = 0.43 ± 0.07‰), and β-alanine (pre-calibrated in-house; $\delta^{13}C$ = -25.98 ± 0.23‰; C = 40.45% and $\delta^{15}N$ = -2.21 ± 0.24‰; N = 15.72%). The reproducibility of replicate measurements was better than 1% for OC and TN (relative error), and better than 0.3 and 0.5‰ for $\delta^{13}C$ and $\delta^{15}N$ signatures (absolute), respectively.

DOC concentrations and isotope analysis

DOC concentrations and $\delta^{13}C_{DOC}$ were measured simultaneously using a modified high-temperature catalytic oxidation TOC analyzer (OI Analytical Model 1010, College Station, TX) coupled to an isotope ratio mass spectrometer (IRMS, Isoprime GV Instruments) after acidification and purging of any dissolved inorganic carbon. The TOC analyzer's PTFE tubing was replaced with PEEK tubing to reduce the atmospheric CO_2 background. Repeated blank injections at 680°C under ultra-high purity O_2 (Praxair) were started 12 hours prior to sample analysis in order to desorb atmospheric CO_2 from the combustion column.

The injection volume was adjusted to 750 µL, producing enough CO_2 for accurate concentration and isotopic measurements, while maintaining efficient combustion. The CO_2 gas, generated from DOC combustion, was routed to a chemical CO_2 trap (Graden Instruments) before being cleaned of oxygen and sent to the IRMS using helium as the carrier gas. The concentration and $\delta^{13}C$ signature of the DOC were determined by calibrating the measured infrared peak area and $\delta^{13}C$ signature to solutions of IAEA-CH-6 certified sucrose and β-alanine. Duplicate sample measurements give a mean error of ±2.15% in DOC concentration (relative) and ±0.15‰ for the $\delta^{13}C$ signature (absolute).

Dissolved iron measurements

Soluble iron was measured spectrophotometrically (Pharmacia Biotech Novaspec II) at 562 nm using a modified version of the ferrozine method (Stookey, 1970). Briefly, each sample was filtered through a 0.2 µm PTFE filter before adding 25 µL of the hydroxylamine hydrochloride reducing agent (1.40 mol L^{-1}), 100 µL of the ferrozine complexing agent (0.01 mol L^{-1}) and 50 µL of a pH 5.5 ammonium acetate buffer (1 mol L^{-1}, to maintain pH between 5 and 7). A solution of bathophenanthroline in isoamyl alcohol (6 mmol L^{-1}) was used to strip off iron contamination in

the hydroxylamine reducing agent and buffer solution using a repeated (3x) solvent-solvent extraction. Using iron-extracted reagents, the limit of detection for this ferrous iron determination method is 0.3 µmol L^{-1} (Viollier et al., 2000) and the precision is better than ± 5%.

Tracking the fate of pulsed algal DOM

The incorporation and degradation of fresh algal DOC in the sediment and overlying water was quantified using a two-component mixing model (Eqn 1).

$$\partial^{13}C_{pooled} = f_{algal}\,\partial^{13}C_{algal} + (1 - f_{algal})\partial^{13}C_{native} \qquad \text{Eqn 1.}$$

where the f_{algal} refers to the fractional contribution of algal OC to the total OC pool. As we have access to both solid phase and aqueous phase OC concentrations and their respective isotopic $\delta^{13}C$ compositions, we can trace the disappearance of the algal OC through decomposition, remineralization and gas phase transfer/escape from the system. This mass balance was done by calculating the fractional contribution of algal carbon in both the solution and solid phase at each sampling interval as a percentage of the initially added algal OC. Isotopic fractionation caused by the mineralization/alteration of components of the algal pool were not accounted for in isotopic mass balances as shifts in $\delta^{13}C$ are typically minimal (± 1‰; Bauer 2002), in comparison to $\delta^{13}C$ differences between the algal tracer and native sediment OC.

Algal DOM partitioning coefficients

Adsorption-desorption isotherms were constructed in order to derive equilibrium partitioning coefficients for algal DOC on oxic and anoxic sediments. Initial algal DOC concentrations of 0, 2, 4, 6, 8 and 10 mg L^{-1} were allowed to equilibrate with oxic surface sediments (0-0.5 cm) and deeper anoxic sediments (10-15 cm) collected from the Lower St. Lawrence Estuary. Final DOC concentrations, after an equilibration period of 18 hours at room temperature (≈ 25 ºC) and

centrifugation (1000 g) of the slurry for 10 minutes, were measured using a high-temperature catalytic oxidation TOC analyzer (Section 2.4.2). Using the slope of the adsorption isotherms, we derived equilibrium partitioning coefficients for the algal DOC (K = adsorbed concentration/dissolved concentration, in L g^{-1} dry weight).

Measurement of nitrogen in solution

Dissolved nitrogen species were determined only on the final centrifuged sample of the time-series incubations owing to water volume constraints. Total dissolved nitrogen (TDN) was measured as nitrate after alkaline persulfate oxidation (0.075 g $K_2S_2O_8$ and 0.015 g NaOH per 10-mL sample) and autoclaving for 90 minutes (Arneel et al., 1993). Nitrate/nitrite and digested TN samples were analyzed by the cadmium reduction method using an automated Alpkem analyzer (Cattaneo and Prairie, 1995). The concentration of dissolved organic nitrogen was determined from the subtraction of the sum of nitrate and nitrite from TDN. Ammonium was not directly measured but is included within the dissolved organic nitrogen pool.

Results

The incubation lasted 250 days and each vial was sub-sampled at irregular intervals with higher frequencies in the starting months. Dark, iron sulfide-rich sediments (pungent sulfidic odor) were produced under anoxic conditions in contrast to oxic and mixed redox sediments, which remained odorless and reddish-brown. The darkest sediment, and presumably the greatest amount of iron sulfide, was precipitated anaerobically when both iron and algal OM were added, as there was no shortage of either labile OM for sulfate reducing bacteria or reactive iron oxides for iron sulfide production. Dissolved iron concentrations were measured to verify that the anoxic redox conditions were properly maintained throughout the incubation and during sampling. In the aerobic scenarios, soluble iron(II) concentrations were below detection limit

within one week of the start of the incubations (all amendment scenarios). In contrast, under the anoxic scenario, there was progressive release of dissolved iron from the unamended, natural sediment (Control scenario), to a concentration slightly above 21 µmol L^{-1} (data not shown). Dissolved iron(II) concentrations decreased from 4250 µmol L^{-1} to about 290 µmol L^{-1} upon the addition of iron(II) chloride (Fe and Fe-OM scenarios) to the reactors maintained under anoxic conditions, demonstrating the strong affinity of iron(II) for sedimentary mineral surfaces (Burdige, 1993), its precipitation as sulfides throughout the incubation, as well as its oxidation to iron(III) by electron acceptors other than oxygen, such as manganese oxides and nitrate, at the start of the incubation (Magen et al., 2011). Dissolved iron profiles for all redox conditions of the control and iron-amended scenarios are available in section 2 of Appendix A3 of this paper.

The pH remained circumneutral throughout the incubation; between 6.5 and 7.9 in the anoxic vials and between 7.3 and 7.9 in the oxic vials, within the range of pH conditions observed in natural sediment porewaters (Burdige, 2006). Under all conditions, the solution pH decreased progressively during the incubation from its initial seawater value (pH ≈ 8) likely due to OM degradation, concomitantly releasing metabolic CO_2 and H^+ to the solution (Burdige, 2006; Mucci et al., 2000). These marginal shifts in pH do not modify the speciation (protonation/deprotonation) of OM functional groups, therefore abiotic processes such as adsorption, co-precipitation and aggregation are not affected (protonation of negatively charged functional groups such as carboxyls (pKa 1.9-4.3) would cause an enhancement in the affinity of DOM for particle surfaces whereas protonation of neutral groups such as histidine (pKa = 6.0) would reduce affinity).

Control and Fe Scenarios

Based on depositional data, the average accumulation age of the incubated sediments is already approximately 20-25 yrs (Smith and Schafer, 1999), therefore the OC and ON native to these sediments was not anticipated to be reactive during the timeframe of this relatively short incubation (250 days). The unreactive nature of the native sediment OM, relative to the timeframe of this incubation experiment, is demonstrated by the unchanging sediment OC and N content in the unamended control scenario (ranging from 1.54 ± 0.01% to 1.58 ± 0.02 % for carbon and 0.163 ± 0.002 to 0.161 ± 0.010% for TN). Also reflecting the refractory nature of the native sediment OM, was the stability of the $\delta^{13}C_{org}$ and $\delta^{15}N_{tot}$ values in the control scenario which remained constant at $\delta^{13}C$ = -24.29 ± 0.10‰ and $\delta^{15}N$ = 5.67 ± 0.22‰ throughout the incubation.

The %OC and $\delta^{13}C$ of organic carbon in the solid phase of sediments supplemented with freshly precipitated iron oxides were statistically equivalent to control sediments throughout the incubation. However, the addition of Fe to the oxic and mixed redox condition caused a significant decrease in the sediment %TN from 0.163 ± 0.002 % initially to 0.142 ± 0.003% under oxic conditions and 0.141 ± 0.007% under the mixed redox conditions, corresponding to a 11.65 ± 4.83% decrease in sediment nitrogen content respectively (Figure 3-2). Removal of the native sediment nitrogen only occurred in the Fe amended scenarios under oxic and mixed redox conditions, and despite this loss of sediment nitrogen, no significant isotopic fractionation was observed ($\delta^{15}N$, p = 0.0443). It is noteworthy that under anoxic conditions and/or upon addition of the algal tracer this N removal process was not detected (Figure 3-2).

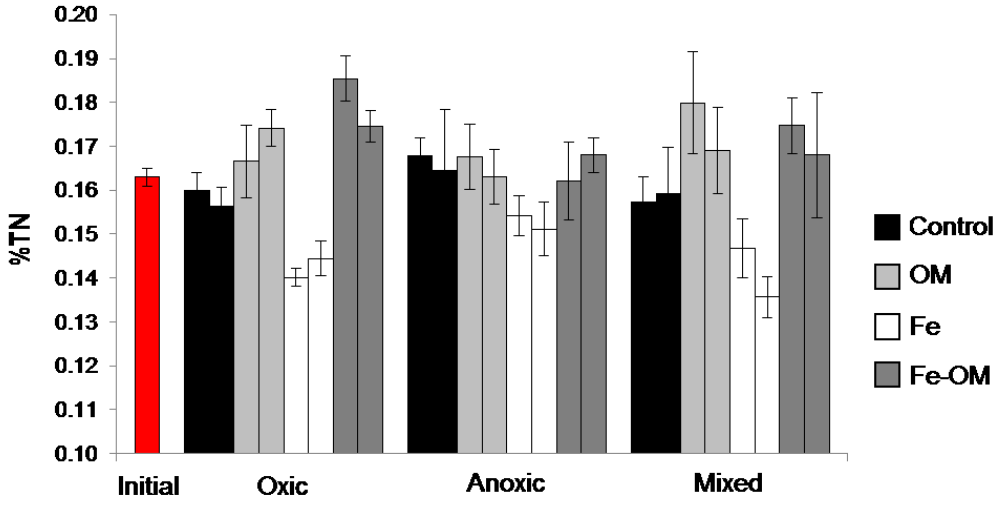

Figure 3-2 Final nitrogen concentration (%TN) of the sediment under different redox conditions for the different amendment scenarios.

In order to better understand the decrease in sediment nitrogen content in the iron amended (oxic and mixed redox) scenarios, the concentration of products formed during typical sediment N removal processes such as nitrite, nitrate and organic nitrogen were measured in the aqueous phase at the end of the incubation (Table 3-1). Nitrite was only detectable in the mixed redox incubation scenario, with the most abundant concentrations found for the Fe and Fe-OM scenarios. The highest nitrate concentration was detected in oxic and mixed redox conditions, but interestingly no nitrate was found in iron amended mixed redox incubation vials. Neither nitrate nor nitrite was detected in the anoxic redox conditions (Table 3-1). Total organic nitrogen, defined here as TDN - (nitrate + nitrite) (total organic nitrogen also includes dissolved ammonium, since ammonium was not measured directly), did not show any obvious relationship to redox condition or amendment.

Table 3-1: Concentrations of dissolved species at the end of the incubations (250 days, asymptotic value) in µmol L^{-1}. Standard deviations are shown in brackets when available.

	Oxic					Mixed					Anoxic				
	DON + NH_4^+	NO_2^-	NO_3^-	DOC		DON + NH_4^+	NO_2^-	NO_3^-	DOC		DON + NH_4^+	NO_2^-	NO_3^-	DOC	
Control	122	*n.d.*	472	829	*(200)*	12	4	1042	1207	*(143)*	732	*n.d.*	*n.d.*	864	*(329)*
Fe	81	*n.d.*	490	557	*(200)*	107	256	*n.d.*	471	*(143)*	674	*n.d.*	*n.d.*	500	*(100)*
OM	388	*n.d.*	346	2214	*(371)*	122	11	821	2257	*(271)*	345	*n.d.*	*n.d.*	2629	*(643)*
Fe-OM	420	*n.d.*	321	921	*(157)*	459	201	843	764	*(57)*	217	*n.d.*	*n.d.*	2014	*(693)*

*n.d. = not detected

We also measured the DOC content of the control and Fe amended scenarios. Although the native sediment OM appears unreactive when looking at the solid phase carbon and nitrogen content, the composition of the slurry water is more sensitive to diagenetic changes with DOC concentrations drifting progressively during the course of the experiment from 233 ± 75 µmol L^{-1} up to 1125 ± 475 µmol L^{-1} across all control scenarios, mirroring the progressive release of OM from sediment particles. The Fe scenario follows a similar trend (climbing from 191 ± 75 µmol L^{-1} to 594 ± 208 µmol L^{-1}) although DOC concentrations remain lower throughout the experiment, possibly showing increased partitioning of DOC onto solid particles. Final DOC concentrations are shown in Table 3-1 and all profiles of DOC concentration and $\delta^{13}C$ are shown in section 1 of Appendix A3.

OM Amended Scenarios

Despite the addition of fresh organic matter, the final sediment %OC in the OM amended incubation scenarios (OM and Fe-OM) are not significantly different from those of unamended scenarios (Control and Fe). However, the large differences in isotopic signature between the native OM ($\delta^{13}C$ = -24.29 ± 0.10‰) and the OM tracer ($\delta^{13}C$ = -41.34 ± 0.12‰) allows the incorporation and retention of the algal OM to be tracked throughout the incubation using $\delta^{13}C$ measurements and isotopic mass balance calculations. For example, the incorporation of about 20% of the added algal tracer would cause an increase in the sediment OC content by 0.09%. This difference would not be detected from OC content measurements alone, as the average precision over the 4 final timepoints (%OC over these timepoints is stable), was ± 0.06%. An equivalent incorporation of the tracer would give rise to a significant drop in the bulk sediment $\delta^{13}C$ signature (1‰) compared to the average precision of the final timepoints for the bulk solid phase $\delta^{13}C$ measurements (± 0.17‰).

From the isotopic mass balance calculations about 50% of the added algal DOC was integrated into the solid phase within the first two hours of the amendment (First timepoint, Figure 3-3). The initial algal OM incorporation was greater for the oxic Fe-OM scenario compared to all other OM amended scenarios and redox conditions (Figure 3-3). The incorporated algal material had a C:N molar ratio of 5.13 ± 1.04, this is slightly richer in nitrogen than the bulk algal C/N (7.58 ± 0.32). The degradation/disappearance of the algal tracer was monitored through the progressive recovery of the bulk $\delta^{13}C$ over the 250 days following amendment, starting at a fairly depleted signature (tracer/native OM mix) to a signature that approaches that of the native sediment. At the end of the incubation the $\delta^{13}C$ signature of the solid phase was -25.08 ± 0.12‰ for all OM amended scenarios (Figure 3-4). This significant depletion in $\delta^{13}C$ compared to

the native sediment OM corresponds to a retention of 10.91 ± 2.49% of the total added algal OC at the end of the incubation (Figure 3-3 and Figure 3-4).

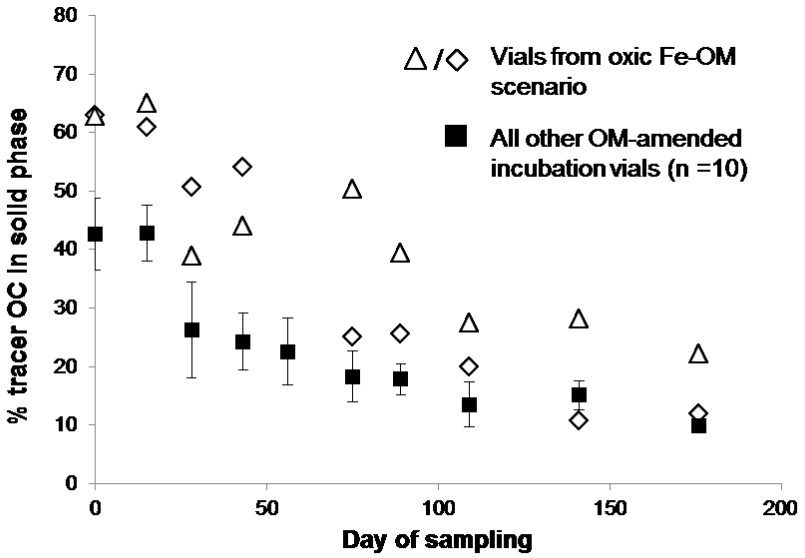

Figure 3-3: Incorporation of the algal tracer in the sediment for OM and Fe-OM scenarios based on carbon isotope mass balance calculations. Black squares show the average incorporation of all redox conditions except the oxic Fe-OM scenario. White diamonds and triangles each represent a duplicate vial of the oxic Fe-OM condition. Error bars represent standard deviation.

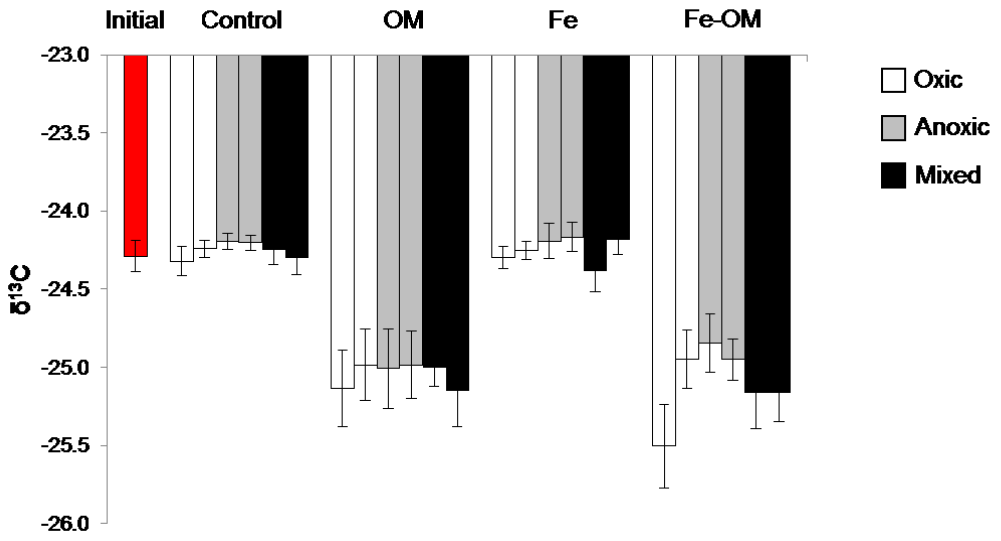

Figure 3-4: Final stable carbon isotope signature ($\delta^{13}C_{org}$) of the sediment (last 4 time points). Error bars represent the standard deviation of the last 4 time points.

The concentration of the algal tracer in solution decreases throughout the incubation, following first order kinetics down to a stable (Figure 3-5, section 1 of Appendix A3), asymptotic value, attained within 30 to 150 days of the start of the incubation, depending on redox condition (Table 3-2). The half-life of DOC is 2 to 3 times shorter under oxic rather than anaerobic conditions. Oscillating redox conditions causes a segmented decrease in DOC concentration with an abrupt increase in DOC consumption following the switch from anoxic to oxic conditions. Rate constants and half-lives corresponding to the mixed redox condition were therefore not included in Table 3-2. The rate of DOC decomposition of the algal tracer is similar to rates reported for porewater DOC from seasonally anoxic shallow sediments (Burdige, 2002) but much faster than the more recalcitrant porewater DOC collected typical coastal sediments (Burdige, 2002; Komada et al., 2013). Despite stable DOC concentrations within the asymptotic segment, $\delta^{13}C$ drifts from the depleted signature of the tracer (-41.34‰ ± 0.12‰) to a more enriched signature (-33.4 ‰ ± 0.53 ‰), demonstrating partial degradation, release and

desorption of soluble material from the native sediment organic matter ($\delta^{13}C$ = -24.29 ± 0.10‰) into solution.

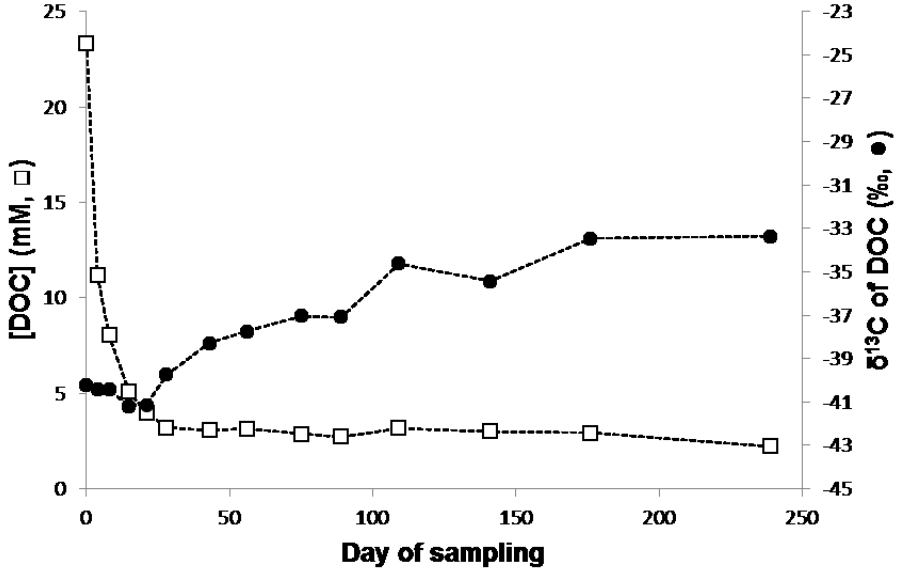

Figure 3-5: Temporal evolution of the DOC concentration and isotopic signature ($\delta^{13}C_{DOC}$) in duplicate incubation vials (OM scenario, oxic conditions).

Table 3-2: Pseudo first-order degradation rate constants and half-lives of DOC in oxic and anoxic incubations. Standard deviations are shown in brackets.

	Oxic				Anoxic			
	Fe-OM		OM		Fe-OM		OM	
Rate constant (d^{-1})	0.061	*(0.0014)*	0.068	*(0.0014)*	0.032	*(0.0058)*	0.019	*(0.0035)*
half-life (d)	11.46	*(0.28)*	10.25	*(0.22)*	21.46	*(3.88)*	37.28	*(7.16)*

Discussion

Role of iron in OM preservation and DOM shuttling

Nearly two decades ago, Keil et al. (1994) and Mayer (1994) hypothesized that sorption of OM to mineral surfaces stabilizes the sorbed molecules, a mechanism that was proposed to account for the enigmatic preservation of intrinsically labile organic compounds in marine sediments, such as those in our algal tracer. This hypothesis was founded on the strong association of sedimentary OM with the mineral matrix. Mechanistically, the process of adsorption implies that the particulate OM reaching the seafloor initially undergoes degradation and is broken into smaller, soluble fragments that readily adsorb to mineral phases (Hedges and Keil, 1995) or can co-precipitate with metal oxides at anoxic/oxic interfaces (Lalonde et al., 2012). Algal DOM, injected into the overlying water of the incubated sediments, was rapidly incorporated into the solid phase, leading to a shift in the sediment's stable carbon isotope signature. Isotopic mass balance calculations reveal that approximately 50% of the added DOC was incorporated within the first two hours (Figure 3-3). The rapid timeframe for this incorporation is consistent with adsorption or co-precipitation (with metal oxides) of the algal DOM into the solid sediment phase (Figure 3-6, pathways 1 & 2), in agreement with previous studies (Arnarson and Keil, 2000; Berner, 1980). Note that the incorporation of the algal tracer was also accompanied by an increase in the day to day scatter as well as the variability in solid phase $\delta^{13}C$ measurements between twin vials (OM and FeOM scenarios: $\sigma = 0.36‰$; versus control and Fe scenarios: $\sigma = 0.093‰$), which could be attributed to the heterogeneous distribution of algal DOC on sediment particles.

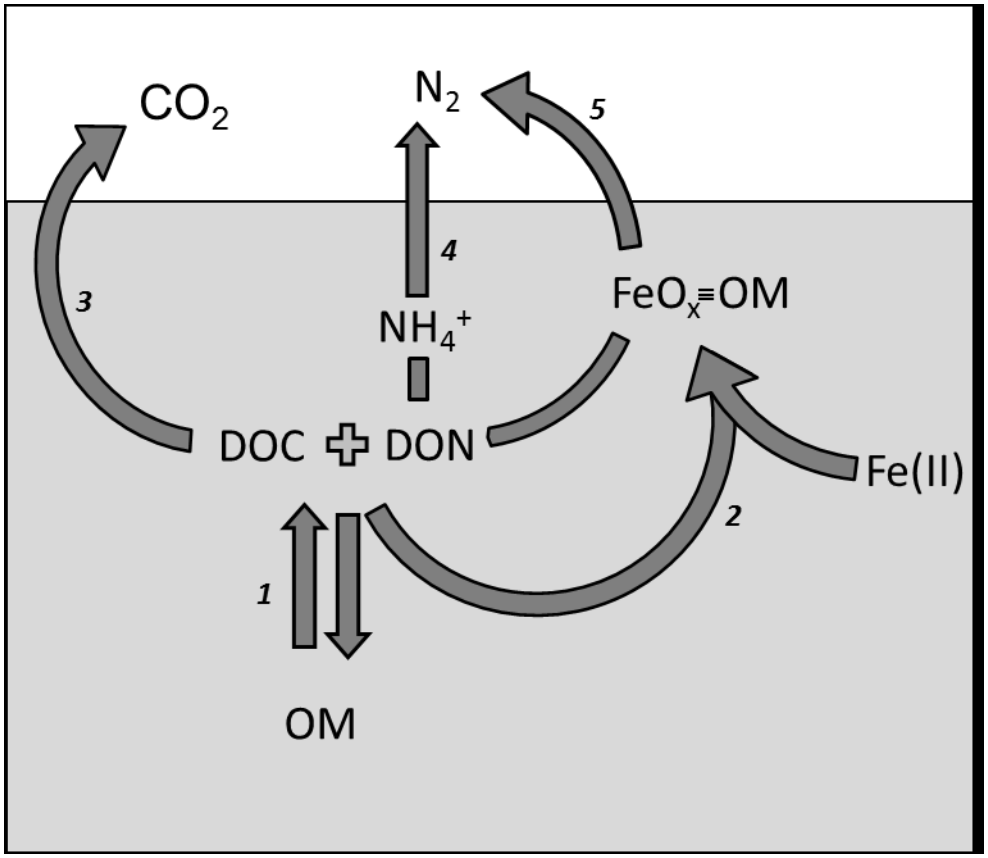

Figure 3-6: Simplified pathways of DOM incorporation (1. Adsorption/Desorption and 2. Co-precipitation during Fe(II) oxidation) 3. Organic carbon remineralization to CO_2, 4. Bacterial denitrification/anammox, and 5. Iron mediated N_2 production) in marine sediments.

Irreversibly mineral-bound molecules are more likely to resist prolonged degradation (>250 days) and thus account for the $\delta^{13}C$ signature of algal OM preserved in the incubated sediment. The final incubation time-series sample (250 days) shows the retention of approximately 10% of the total added algal OC (OM and Fe-OM scenarios) (Equation 1 and Figure 3-4). DOM surface binding is controlled by the availability of sorption sites which is likely a function of sediment particle surface area (Mayer, 1994; Mayer, 1995) as well as mineralogy (Lalonde et al., 2012; Ransom et al., 1998b). Hydroxylated iron and manganese oxides are known to strongly adsorb and retain soluble organic compounds through ligand-exchange and inner-sphere complexation (Gu et al., 1995; Ransom et al., 1998b). These surface interactions favour nitrogen and oxygen-rich organic molecules which typically carry more functional groups that bind covalently to

mineral surfaces (Arnarson and Keil, 2000). This preference of electronegative groups possibly explains why the composition of the preserved OM is different from that of the bulk algal DOM with C:N molar ratio of the fraction of the algal material incorporated into the sediment at 5.13 ± 1.04, which is slightly richer in nitrogen than the bulk algal C/N (7.58 ± 0.32).

To further probe the effect of metal oxides on DOM binding in natural sediments, we derived equilibrium partitioning coefficients (K = adsorbed concentration/dissolved concentration, in L g^{-1} dry weight) for algal DOC adsorbing to iron oxide-rich surficial sediment (0-1 cm depth) and underlying anoxic sediments (10-13 cm depth). K values of surficial sediments (0.038 ± 0.0075 L g^{-1}) exceed those of the underlying anoxic deposits (0.0052 ± 0.00036 L g^{-1}) approximately 8-fold, indicating that authigenically-produced metal oxides greatly increase DOM partitioning onto solid surfaces. Reactive iron oxides, produced in our oxic incubated slurries upon amendment with Fe(II), also promote the transfer of DOC to particle surfaces, lowering DOC concentrations most likely through sorption or co-precipitation of DOM (Table 3-1; the reader should compare Fe to Control scenarios as well as Fe-OM to OM scenarios). The efficacy of solution-solid transfer by metal oxides possibly affects the turnover of carbon and nitrogen in natural sediments through the modification of DOM fluxes through oxide-rich surface sediments and the enhancement of OM preservation (Lalonde et al., 2012). Once sorbed to the solid phase, molecules become more resistant to microbial decay since only DOC is amenable to bacterial uptake (only molecules <600 Da can cross cell membranes through porins) (Arnosti, 2011)and degradation (Figure 3-6, pathway 3). Molecules that are only weakly-bound to the sediment are shuffled between the particulate and aqueous phase, which over time leads to their degradation (Henrichs, 1995) (Figure 3-3and Figure 3-5).

The make-up of porewater DOC is likely altered by re-equilibration with the much larger mineral-bound OC pool (Hedges and Keil, 1995). The relationship between the dissolved and solid OC pools is however seldom obvious and can be further obscured by transport processes that lead to the addition or removal of DOC (diffusion, bioirrigation, remineralization) and particulate OC (sedimentation, burial, bioturbation) (Berner, 1980). The use a ^{13}C-depleted isotopic algal tracer allows us to circumvent some of the intrinsic complexity of the sediment and to demonstrate the sorption of dissolved and colloidal (<0.7 μm) organic molecules onto sediment particles (Figure 3-6, pathways 1 & 2), as well as to track its decomposition and mineralization from both the solid sediment and the aqueous phase.

The degradation of our algal tracer in the aqueous phase (Figure 3-5 and Figure 3-6, pathway 3) follows first-order kinetics down to asymptotic but variable DOC concentrations. These final concentrations vary with redox conditions and amendment scenario (Table 3-1) with the lowest concentrations found in oxic and mixed redox conditions. The final asymptotic concentrations observed in these incubations are analogous to the constant DOC concentrations found at depth in sediment cores which result from (*i*) the production of DOC at these depths being equal to its consumption or (*ii*) the production and consumption of DOC at depth approaches zero, entailing that porewater DOC at depth is effectively unreactive and therefore preserved indefinitely (Burdige, 2002). In this work, we show a gradual substitution of algal DOC by reversibly-bound autochthonous OC through $\delta^{13}C_{DOC}$ measurements (increasing $\delta^{13}C_{DOC}$ signature, implying the release of native OM into sediment porewaters; Figure 3-5). This is the first direct demonstration of a surface exchange between porewater DOM and adsorbed OM and supports a steady-state condition of production/consumption of porewater DOC. Labile algal molecules are more amenable to bacterial decomposition, which allows more recalcitrant native molecules

to become a more important fraction of porewater DOC and leads to an overall decrease in the reactivity of porewater DOM over the timeframe of the incubation.

First order degradation kinetics of the algal marker is consistent with most early diagenetic models (Berner, 1980). All incubation conditions had a pool of DOM that was essentially unreactive during the course of the experiment (corresponding to the final asymptotic DOC concentration, Figure 3-5). As consumption equals production during the asymptotic segment (the overall rate of DOC disappearance is zero), asymptotic/refractory DOC concentrations can be subtracted from rate calculations. We began measuring the kinetics of OM degradation at the second timepoint (day four), excluding microbial degradation of the extremely labile DOM pool (this DOM pool is typically respired in the water column before reaching the sediment and is not representative of typical marine sedimentary OM) as well as adsorption/desorption of DOM (reaching equilibrium within 2-3 hours; Arnarson and Keil, 2000) from rate calculations. These processes are rapid compared to the degradation of the added OM tracer, making them negligible in the degradation rate calculation (Berner, 1976). According to first order kinetic rate laws ($dC/dt = -kC_t$), rate constants (k) and half-lives ($t_{1/2} = \ln(2)/k$) for algal DOC were determined for the different redox and amendment conditions (Table 3-2). The half-life of DOC is 2 to 3 times shorter under oxic rather than anaerobic conditions. This, along with lower asymptotic DOC concentrations measured in the oxic and mixed redox conditions (Table 3-1), likely results from more effective utilization of the DOC produced during mineralization by oxic bacteria (Burdige, 2002). Anaerobic decomposition of DOM is less efficient, requiring a consortium of bacteria; with fermenters, for example, supplying DOM substrates to sulfate reducers (Burdige, 2006).

Results of our incubation experiments demonstrate the preservative effect of iron oxides on sediment-bound organic matter through increased OM retention and reduced microbial degradation likely owing to strong complexation (Lalonde et al., 2012). The highest OM incorporation of the algal tracer occurred as a result of DOM-iron co-precipitation upon amendment with both iron and algal OM under oxic conditions when compared to all other conditions (Figure 3-3, first time points). The incorporation of DOM into the solid phase results in slower decomposition as microbial degradation is inhibited by the formation of strong bonds to the solid phase. Within natural systems, the preservative effect of iron oxides could allow for the transfer of iron-OM complexes to anoxic sediment layers where OM may be sequestered over geological timescales. The overall extent of OM degradation (observed from the loss of the depleted $\delta^{13}C$ signature of the algal tracer) is independent of redox conditions as seen by the converging % tracer OC time series (Figure 3-3, final time points), indicating that even OM strongly bound to iron oxides or other minerals is sensitive to degradation upon continuous exposure to oxygen. Prolonged oxygen exposure is known to lead to the nearly complete degradation of OM, regardless of the extent of physical protection, as seen by the low OC content of turbidites above the oxidation front (Colley et al., 1984; Cowie et al., 1995; Prahl et al., 1997; Thomson et al., 1998).

Accelerated iron-mediated nitrogen removal

At the end of the incubation period, total dissolved nitrogen (TDN) concentrations were lower than 1.5 mmol L^{-1} and therefore can be excluded from mass balance calculations (< 4% of the total mass balance; Table 3-1). No detectable nitrate or nitrite was measured under anoxic conditions demonstrating the absence of nitrification during ON remineralization or the fast consumption of nitrate/nitrite in the absence of oxygen. Nitrate was the predominant dissolved nitrogen species under oxidizing conditions. In contrast to the other redox conditions, both

dissolved nitrate and nitrite were present in the alternating redox system (anoxic at the time of the measurement), with the amended Fe and Fe-OM scenarios having the highest NO_2^- concentrations (Table 3-1).

Without the addition of reactive iron surfaces, solid ON that is native to the sediment is unreactive; no net losses of solid-phase TN were detected in the control incubation under any of the redox conditions. Losses of N as N_2 (sum of all biotic and abiotic denitrification pathways) from the incubation vials can be estimated as the difference between the total initial mass of N (control and amendment scenarios) and the final mass of N (residual solid phase N plus dissolved N species produced upon mineralization of solid-phase organic N, nitrite, nitrate, ammonium and dissolved organic N). The addition of Fe(II) caused the removal of 11.65 ± 4.83% of the original sediment nitrogen (Figure 3-2), with the highest losses occurring under oxic and mixed-redox conditions, where iron(II) is immediately precipitated as reactive iron oxides. Bacteria participating in denitrification/anammox are confined to anoxic environments (under 4 μmol O_2 L^{-1} for denitrification and under 10 μmol O_2 L^{-1} for anammox) (Crowe et al., 2012; Hulth et al., 2005) therefore making these biochemical pathways unlikely in oxygenated incubation vials. Traditional nitrification/denitrification pathways in fact require both oxic (for nitrification) and anoxic conditions (for denitrification) to take place. To account for fixed-N deficit observed in our oxic incubations, an alternative biochemical N degradation pathway is required. Luther et al. (1997) were the first to propose a direct mechanism for N_2 production from NH_4^+ oxidation, coupled to manganese oxide reduction, “short-circuiting” the traditional N intermediates. Though they proposed that this mechanism is also possible using iron oxides as substrates, they did not demonstrate that this reaction occurs. The reason for proposing a link between the N and Mn elemental cycles likely arose from the similarity in the standard reduction potential of NO_3^- and MnO_x (Froelich et al., 1979), (therefore the proximity of nitrate and MnO_x reduction

zones in sediments). However, despite the lower free energy yield (Froelich et al., 1979), there is a 1-2 order of magnitude greater abundance of reactive Fe compared to Mn in the St. Lawrence Estuary and Gulf sediments (Anschutz et al., 2000) and in most other coastal sediments (Mason, 1966). Since the highest abundance of reactive iron oxides is within the oxygen and NO_3^- reduction zones in all coastal sediment cores (Burdige, 1993), we propose that the iron oxide-ammonium redox couple is equally if not more likely to exist than the manganese oxides-ammonium redox couple. Our N mass balances under oxic conditions and the observed losses of native sediment N in the presence of added reactive iron oxides (Figure 3-2 and Figure 3-6, pathway 5,) possibly demonstrate *in-vitro* evidence of Luther's and Yang's proposed aerobic iron-mediated ammonium oxidation pathway.

No significant isotopic fractionation of TN was observed upon nitrogen loss in iron-amended slurries, in contrast to traditional bacterial denitrification pathways that lead to $\delta^{15}N$ enrichment of the residual nitrogen pool (Mariotti et al., 1981), possibly supporting the occurrence of an alternative N_2-production mechanism. Iron oxide-mediated mechanisms of NH_4^+ oxidation have been documented in wetland soils (Clément et al., 2005) and wastewater treatment plants (Sawayama, 2006), but their occurrence in marine sediments have yet to be demonstrated. Proposed mechanisms of NH_4^+ oxidation by Fe(III) (known as Feammox producing either N_2 or NO_2^-) involve (*i*) NH_4^+ oxidation at reactive iron oxide surfaces, and/or (*ii*) NH_4^+ oxidation by O_2 from iron oxide surfaces (Yang et al., 2012). Notably, both of these mechanisms can be mediated by sedimentary iron oxides and can be biotic or abiotically-mediated (Luther III et al., 1997). The high NO_2^- concentrations, observed under our iron amended mixed redox incubations are consistent with the iron oxide-induced oxidation of NH_4^+ to NO_2^- proposed by Yang et al. (2012), although they could also result from the decoupling of NO_2^- production from its consumption in these sediments. More work, involving the monitoring of N_2 gas production in

sediments spiked with ^{15}N labelled nitrogen substrates alongside dissolved Fe is necessary to positively identify Feammox in sediments.

Along with the algal OC, ON was incorporated into the sedimentary phase. However unlike $\delta^{13}C$, $\delta^{15}N$ is sensitive to fractionation during biochemical pathways such as denitrification, and could not be used as a tracer for algal OM degradation. %TN values do however indicate that, in contrast to Fe amendment scenarios, accelerated TN losses were not observed in the Fe-OM amendment scenarios (Figure 3-2). We propose that this occurs from the shielding of iron oxide surfaces by sorbed fresh OM, which is known to poison iron oxide surfaces in natural conditions and inhibit crystal growth (Schwertmann, 1966), therefore blocking the reactive, hydroxylated iron oxide surfaces from binding other species or being used as catalysts for reactions such as Feammox. The active diagenetic recycling of iron oxides in sediments regenerates reactive iron surfaces (Burdige, 2006) that potentially promotes these reactions. This same surface site inhibition might also occur in the unamended sediment incubations (Control scenario), where nitrogen losses were not detected throughout the 250 day incubation, though it is possible that nitrogen removal reactions may be occurring at rates that are too slow to cause detectable losses in the solid phase. In natural sediments, such as the ones used in these incubations, much of the iron oxide surfaces are also bound to organic molecules. If Feammox and other oxide-mediated diagenetic pathways such as dissimilatory iron and manganese reduction require unpoisoned oxide surfaces, it is possible that these reactions might be confined to the oxic-anoxic sediment interface, where fresh metal oxides precipitate.

Conclusions and implications

Organic matter (OC and ON) degradation and preservation are intimately related to other elemental cycles such as those of oxygen, iron and sulfur. Iron plays multiple roles in OM cycling:

ferric iron serves as an electron-acceptor in the respiration of OM (Burdige, 1993), but also increases the preservation potential of sedimentary OC through adsorption/complexation. Iron's preservative effect is twofold, shuttling OM from the dissolved to the solid phase in the sediment and, upon burial, from the oxic sediment surface to the deeper anoxic layers, as well as increasing its resistance to microbial decay through strong iron-OM complexation. In combination, these two processes can account for the preservation of up to 20% of the OC in marine and freshwater sediments, thus contributing significantly to the global redox balance (Lalonde et al., 2012).

Interesting preliminary data demonstrates accelerated removal of fixed nitrogen species in the presence of iron oxides in marine sediments though further work must be undertaken to elucidate the exact chemical/biochemical nature of this process. With denitrification in marine sediments as an important component of the global nitrogen cycle, accounting for about half of the oceanic nitrogen removal (Christensen, 1994), it is intriguing to consider that iron may play a role in regulating the oceanic production of reactive nitrogen species as well as controlling nitrogen removal through generation of N_2, all the while slowing the degradation of OC through the formation of strong Fe-OM complexes. This effective decoupling of the organic carbon and nitrogen elemental cycles is intertwined to the generation of reactive iron oxides, transported to sediments through continental erosion (Burdige, 2006). This experiment also shows the usefulness of a multi-pronged tracer-based incubation approach to study and model coupled elemental cycles with processes occurring over different timescales that involve labile and refractory components.

Chapter 4: Automation of $^{13}C/^{12}C$ ratio measurement for freshwater and seawater DOC using high temperature combustion

Abstract

We provide a detailed description of the hyphenation of an Aurora 1030C high temperature catalytic conversion DOC analyzer, a GD-100 CO_2 trap and a continuous flow IRMS, which has made possible the high-throughput, automated measurements of $^{13}C/^{12}C$ ratios and DOC concentrations for a wide range of aquatic samples. Precision of $^{13}C/^{12}C$ ratios increases exponentially with sample concentration, reaching 0.2‰ or better for high concentration samples (>5 mg L^{-1}), comparable to that obtained in a conventional elemental analyzer-IRMS setup. The system blank contribution is the limiting factor in obtaining maximal performance; optimal system blanks values are on the order of 0.2 µg C with an isotopic signature varying from -20 to -12 ‰ during the lifetime of the combustion column. With appropriate blank correction procedures, accurate analyses (± 0.5‰ or better) can be obtained on concentrations as low as 0.5 mg DOC L^{-1}, representing the lower limit typically observed in aquatic systems. Sample matrix does not affect reproducibility or accuracy; this method is amenable to both freshwater and seawater samples. Although no certified DOC standards exist for $\delta^{13}C$, our two laboratories (Concordia University & University of Ottawa) analyzed a consensus reference material from a deep-ocean environment (CRM Batch 13 Lot # 05-13, Hansell 2013) and found $\delta^{13}C$ values of –19.9 ± 0.5‰ (*n* = 4) and -20.6 ± 0.3‰ (n = 3), which corroborates previously reported values for similar samples (Bouillon et al., 2006; Lang et al., 2007; Panetta et al., 2008) and is consistent with its marine origin.

Introduction

The oceanic dissolved organic carbon (DOC) pool (≈700*10^{15}g) is similar in size to atmospheric carbon dioxide (≈750*10^{15}g), which highlights its importance to the global carbon cycle. At this scale, the remineralization of only 1% of the DOC in the global ocean would be sufficient to

generate a CO_2 flux larger than that annually produced by the combustion of fossil fuels (Hedges, 2002b). Arriving at a good estimate of the size of the ocean DOC pool has however not been straightforward. Falsely large estimates spurred controversy which can be recounted through a series of geochemical and analytical papers (Druffel et al., 1992; Sharp et al., 1993; Sugimura and Suzuki, 1988; Suzuki, 1993). DOC dynamics and fluxes are also difficult to measure and almost impossible to predict accurately, with some DOC sequestered into a millennium old, refractory seawater component and some comprised in a very labile component that turns over within a few hours or days (Benner, 2002). The structural and chemical complexity of DOC surpasses all other substances dissolved in seawater, imparting DOC with the potential to carry information that may eventually allow us to understand where that water has been and what has happened within it over time (Hedges, 2002b).

The information that can be drawn from dissolved organic matter in seawater is now and has always been limited by the availability of analytical methods and instruments that are designed to answer biogeochemical questions. Stable isotopic measurements of DOC (δ^{13}C-DOC) have been done since the 1960s and remain a useful tool for carbon source determination as well as tracking carbon dynamics in rivers, estuaries, coastal and marine systems through physico/chemical transformations, microbial loops and macrofaunal ecosystems. Despite their usefulness, δ^{13}C-DOC measurements for whole seawater samples are still rather uncommon and are far from being simple or routine measurements. The difficulties associated with δ^{13}C-DOC measurements in seawater are largely associated to the sample matrix, which can contain 70,000 times the weight of DOC in salt, which clogs combustion columns, competes for oxidants, minimizes combustion efficiency and causes mass spectrometer ionization/corrosion issues. To circumvent matrix problems, many have turned to DOM isolation methods using resins or

membranes that, although useful in certain instances, can fractionate the total carbon pool (Bauer, 2002).

The first DOC isotopic measurements of whole seawater were done in the 1960s using up to 1.8L of water, powerful UV lamps and took over 3 hours per sample (Williams, 1968; Williams and Gordon, 1970). Low sample throughput is still problematic for UV oxidation - although improved since the 1970s (Beaupré et al., 2007) - but because of its high sample to blank ratio, UV oxidation is accountable for the highest number and perhaps the most reliable seawater δ^{13}C-DOC measurements in the literature (Bauer, 2002). It took over 20 years for new techniques to develop, including sealed-tube oxidation of lyophilised DOC/salt mixture, wet chemical oxidation (WO) and high temperature catalytic (HTC) oxidation. Apart from high blank values, lyophilisation also suffers from being labour and time intensive (Fry et al., 1993). Wet chemical oxidation has more potential for high-throughput analysis (St-Jean, 2003); but salts scavenge the free radicals that are the principal oxidation agents, markedly reducing DOC oxidation efficiency and prolonging oxidation time significantly (Osburn and St-Jean, 2007). In addition, the large quantities of chlorine gas produced as a bi-product of WO in seawater, causes the rapid corrosion of some of the reaction vessel components, the fouling of the halide/sulfide traps, and the rapid exhaustion of reducing agents. As part of a recent inter-comparison study, two different labs, using wet chemical oxidation, measured the δ^{13}C-DOC of a single seawater sample to be -9.3 and -11.0 ‰ (Van Geldern et al., 2013), an 8 to 10‰ δ^{13}C enrichment over values generally reported for seawater DOC (-20.1 to -22.9‰; Bauer, 2002), probably caused by a WO method artifact.

Though high temperature combustion is not as affected as WO by the sample matrix, frequent maintenance is required to remove salt caking in combustion columns and flow lines. Random

ghost peaks generated by the oxidation of carbonaceous species caused by the flaking of salts off the sides of combustion columns have also been observed (Qian and Mopper, 1996). HTC is also infamous for high blanks, which are detrimental to the analysis of very low concentration samples, such as typical deep seawater samples. Even so, HTC methods have the highest potential for high-throughput analysis of seawater samples. Lang et al. (2007), followed by Panetta et al. (2008), developed methods that coupled HTC analyzers to IRMS via cryogenic trapping of CO_2. Earlier DOC analyzers were however limited to small maximum injection volumes (100-150 µL). In the case of Lang et al. (2007), dual inlet IRMS analysis of CO_2 (from one 100-µL injection trapped offline) was necessary to maximize sensitivity. Panetta et al. (2008) successfully used an open-split continuous-flow IRMS, but needed as many as six 150-µL injections of seawater to generate a large enough (> 1µg) carbon cloud for δ^{13}C-DOC measurements.

Here we show the coupling of an OI Aurora 1030C, a late generation HTC analyzer, to a continuous-flow IRMS through a chemical CO_2 trap. This method is amenable to both freshwater and seawater samples. The maximum injection volume of the Aurora 1030C is more than 10 fold that of most other HTC systems (1800 µL) which allows for the IRMS analysis of a single sample injection, greatly reducing the analysis time per sample and the blank to sample ratio. Hyphenation of the DOC analyzer to an IRMS using a chemical trap rather than a cryogenic trap also enables the facile automation of the DOC-IRMS system, increasing sample throughput, reducing user error and improving reproducibility. Higher sample throughput also allows for more thorough calibration of the instrument as well as a better understanding of system capabilities. Sample properties, system blanks and instrument parameters/limitations that might influence sample combustion and measurement accuracy and precision are outlined here.

Methods

Algae extracts

A 2-L unialgal culture of the algae *Nannochloropsis* purchased from the National Center for Marine Algae and Microbiota was grown in filtered deep Pacific seawater (DOM concentration < 1 mg L^{-1}) to which $NaH^{13}CO_3$ had been added (Sigma Aldrich, final concentration 20 mg L^{-1}). Optimal growth was insured by the addition of nutrients, the maintenance of oxic conditions by bubbling air and 12 hours of daily UV-light exposure.

When sufficient algal material was produced, algal cells were harvested by centrifugation and DOC was liberated through cell lysis by repeated freezing in liquid nitrogen and thawing. Lysed cells were diluted with deep Pacific seawater (DOC concentration < 1 mg L^{-1}), centrifuged for 20 minutes at 19,000 g and filtered through a 0.7-µm glass fiber filter to generate a concentrated DOC solution. The algal-derived DOC is ^{13}C- enriched ($\delta^{13}C$ = +11.58 ± 0.13‰). $\delta^{13}C$-depleted ($\delta^{13}C$ = -41.34 ± 0.12‰) algal DOC was also extracted in a similar fashion from unaltered concentrates of N*annochloropsis* (Reed Mariculture Inc.).

Sample treatment

IAEA-CH-6 certified sucrose standard (International Atomic Energy Agency, -10.45 ± 0.03‰), Suwannee River Fulvic Acid standard (SRFA, International Humic Substances Society, -27.6 ± 0.12‰), β-alanine (Sigma-Aldrich, -26.18 ± 0.10‰ standardized in-house against several certified materials by EA-IRMS), Sucrose (Sigma-Aldrich, -11.77 ± 0.09‰, standardized in-house) and Potassium hydrogen phthalate (KHP) (Sigma-Aldrich, -28.16 ± 0.10‰, standardized in-house) were used as reference $\delta^{13}C$-DOC compounds. β-Alanine was typically used as the quantitative DOC standard because of its ease of oxidation since a benchmark compound was needed to assess the efficiency of sample combustion. Standard solutions and blanks were

prepared with TOC-grade water (Sigma-Aldrich) and acidified with one drop of TraceSELECT grade 12N HCl (Sigma-Aldrich). Natural freshwater samples were also acidified with a minimal quantity of 12N HCl. Seawater samples require a 1:1000 12N HCl:water volume ratio (Farmer & Hansell 2007) to lower the pH to < 2.

Analysis of one sample on the DOC-IRMS takes approximately 20 minutes and requires the use of three separate instruments: 1) a modified OI Aurora 1030C instrument for sample oxidation; 2) a molecular sieve trap (Graden Instruments Inc., model GD-100) for CO_2 trapping; and 3) an Isoprime IRMS (Isoprime, Ltd.) and reference gas box injector for isotopic analysis of the CO_2. $\delta^{13}C$ of standard compounds (Table 4-1) and certified deep seawater provided by the Hansell CRM Program (http://yyy.rsmas.miami.edu/groups/biogeochem/CRM.html) were measured by two laboratories (Concordia University and University of Ottawa), using similar instrumental setups except for the IRMS and reference gas box (Finnigan Mat DeltaPlusXP and Conflow IV reference box). The DOC analyzer, CO_2 trap and IRMS are operated by separate software but all three can communicate for automation through closed contact signals sent from the IRMS software to the DOC analyzer and the trap at the start of each run. The electric signal prompts each instrument to begin a sequence of predetermined steps so that the CO_2 peak generated in the DOC analyzer is delivered to, and trapped wholly by the molecular sieve trap, which releases the CO_2 to the IRMS through the reference gas box injector. The system is shown schematically

in Figure 4-1. Each step is described in greater detail below.

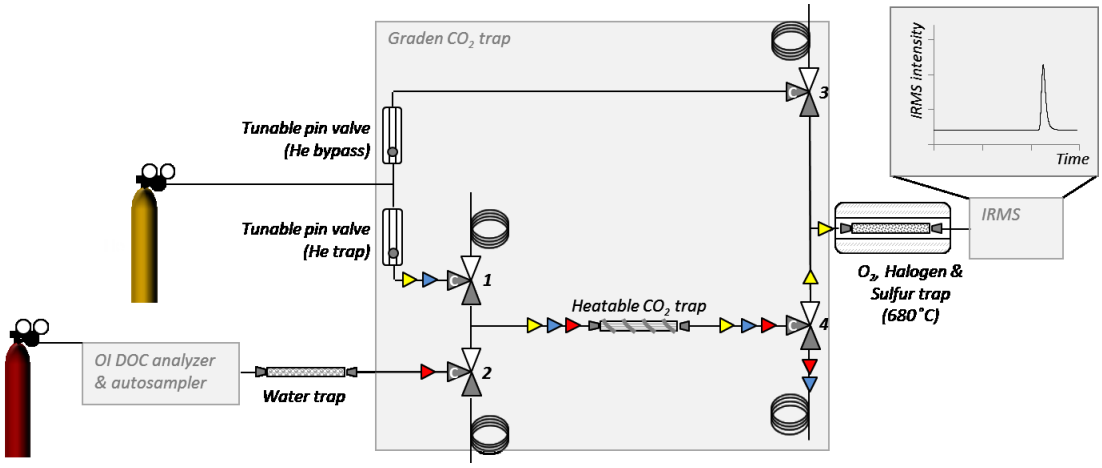

Figure 4-1: Schematic of DOC-IRMS, highlighting flow through the GD-100 CO_2 trap. Electronic three-way valves (1 to 4) are shown in standby configuration, allowing gas flow from the common port (labelled C) through the "normally open" port (filled in grey). Gas is only allowed to flow through the other port (filled in white) when the valves are activated.

Arrowheads show the direction and the origin of the flow through the heatable molecular sieve trap. During trapping mode, valves 1 and 2 are activated allowing O_2 from the DOC analyzer to pass through the molecular sieve and out of the Valve 4 vent outlet (red arrowhead, time: ≈5 min). After trapping, all valves are deactivated to flush the trap with He through the Valve 4 vent outlet (blue arrowhead, time ≈45 sec). The CO_2 peak is sent to the IRMS by heating the molecular sieve to 250°C and activating valves 3 and 4 (yellow arrowhead, time ≈2min). Note that there is always an equal flow of helium going to the IRMS, either from the He bypass or the He trap flow line.

Sample oxidation

All samples were placed in dry-combusted 40-mL EPA vials and placed in the model 1088 rotary autosampler of the OI Aurora 1030C. Beyond this point, sample treatment was handled by the DOC analyzer. Acidified samples, standards and blanks were sparged with high purity O_2 (>99.995%) in the total inorganic carbon chamber heated to 70 °C for rapid removal of inorganic carbon. A volume of sample water (200-1500 µL) was reclaimed and injected onto the head of a heated (680 °C) combustion column purged by a continuous flow of high purity oxygen carrier gas. The OI Aurora 1030C combustion column is U-shaped, requiring samples to pass twice through the hot zone: once upon sample injection and rapid vaporization on a bed of large particle quartz chips (OI 323880) and again when the vaporized sample traverses the opposite

side of the U-tube containing a 5% platinum oxide catalyst (OI 323882) for quantitative conversion to CO_2. Water vapor was sequentially eliminated from the carrier gas stream by condensation in a drain chamber, by a selectively permeable Nafion membrane and finally by drierite indicator chips. The halogen trap (electrolytic copper, OI 265223) was repositioned just upstream from the Nafion membrane (instead of downstream), to minimize membrane corrosion by halogen/sulfur gases. The dried gas stream was then passed through a non-dispersive infrared detector that measures the CO_2 absorption; the detector signal was forwarded to a data gathering system for processing and concentration determination.

As with other systems that were modified for IRMS analysis, (e.g. Peterson et al. 2003; Panetta et al. 2008), we changed the PTFE tubing, which is semi-permeable to atmospheric gases, for PEEK tubing. Diffusion of CO_2 was most significant in the DOC cooling coil, a 1.5-m long portion of tubing positioned right after the combustion column, probably because this tube carries hot carrier gas and water vapor that increases PTFE diffusivity. Other components were tested for microleaks or CO_2 diffusion but were not found to be significant contributors.

After IR detection, the carrier gas was redirected through a magnesium perchlorate trap to remove remaining traces of water, then to the Graden CO_2 trap box where a zeolite molecular sieve efficiently traps CO_2 from the oxygen stream at room temperature. The sieve is encased in a stainless steel tube wrapped in a heatable electric coil that quickly reaches 250 °C (< 45 sec) to quantitatively release the CO_2 gas. The trap flow path and components are illustrated in Figure 4-1. It is equipped with four three-way valves that allowed for (*i*) the CO_2 from the OI to be sent through the molecular sieve for trapping (5 min), (*ii*) O_2 to be rinsed away from the trapped CO_2 with ultrahigh purity helium (45 sec, flow rate between 32-92 mL/min, see discussion), and (*iii*) CO_2 to be redirected to the IRMS for detection upon heating of the trap (1.5 min). Valve

switching and trap heating are run in a sequence dictated by a ladder-logic software that is triggered only once for every sample. At the end of the sequence, the heater is turned off and a fan cools the trap. A bypass flow is used so that a flow of helium is continually sent to the IRMS. The timing and valve activation of one trap cycle is illustrated in Figure 4-1 and described in more detail in the caption.

Before entering the IRMS interface, the CO_2 released from the trap passes through a ¼" quartz tube filled with cobalteous silvered oxide (Isomass B1000) and copper chips (Elementar Americas Inc., 05 000699) maintained at 680°C in order to reduce nitrogen oxides to N_2 and eliminate residual oxygen as well as noxious halogen/sulfide gasses.

Data processing; sample concentration and $\delta^{13}C$ measurement

Sample concentrations were determined from straight line calibrations built from either DOC area or IRMS peak height versus the DOC concentration of standard solutions. Blank areas/heights were determined from the *y*-intercept of these graphs; blank errors were determined from the standard error of the intercept (Skoog et al., 1998). The carbon content of the blank and blank components was determined by dividing the area (DOC) or height (IRMS) of the peaks by the calibration slope (instrument response factor).

Total least squares regression analysis to determine the blank $\delta^{13}C$ signature from measured $\delta^{13}C$ and IRMS height (see discussion) was carried out using MATLAB (R2013a Student Version) to treat both parameters as dependant/error-prone variables. The $\delta^{13}C$ data were corrected for TOC background as described in the following section. $^{13}C/^{12}C$ ratios are expressed as per mil deviations from the international standard Vienna Peedee Belemnite (VPDB): $\delta^{13}C_{sample} = (R_s / R_{st} - 1) \times 1000$ where R_s is the $^{13}C/^{12}C$ of the sample and R_{st} is the ratio of the VPDB standard.

Assessment

Molecular sieve trap and helium flow

Molecular sieves are selective for specific gas molecules, not only on the basis of pore size but also on the basis of molecular polarity and boiling point (Bauer 1992). At atmospheric pressure and room temperature, the sieve has a very high affinity for CO_2 and efficiently focuses 100% of the CO_2 into a very narrow, stationary band independently of the DOC analyzer carrier gas flow rate while O_2 molecules pass freely through the trap. The selectivity of the trapping material for the gas of interest is a notable advantage for molecular sieves over cryogenic collection systems since, at liquid nitrogen temperature, all DOC carrier gases except helium (or helium/oxygen mixtures) condense and clog cryogenic trapping lines (Lang et al., 2007; Panetta et al., 2008). The capacity of the trap for CO_2 has not been measured but is well above the upper limits of the linear dynamic range of the IRMS (22 µg of DOC under the IRMS operation conditions used in this work). The performance of the sieve does not seem to deteriorate significantly with use or time. We have continuously used a single molecular sieve batch for over 36 months with no lessening in trapping efficiency, resulting in significant savings in both cost and maintenance over cryogenic trapping. Sieves are also more amenable to automation, thus reducing user error, enhancing system stability and lengthening feasible sequence times.

In comparison to most other sample oxidation methods, high temperature combustion DOC analyzers work with small sample volumes. While destroying a smaller quantity of sample is normally an advantage over other techniques, it can be detrimental when coupling the DOC analyzer to an IRMS, which suffers from poor reproducibility at very low peak intensities. At the maximum DOC analyzer injection volume (1800 µL), low concentration samples (e.g. deep oceanic samples) generate < 1 µg C, making δ^{13}C-DOC measurements difficult. The height and

width of the IRMS peak was optimized by adjusting the helium flow rate flushing the CO_2 from the trap, into the IRMS. Low flow rates result in longer transit times, but also in lower CO_2 peak dilution, thus increasing IRMS sensitivity and retention time. Nevertheless, the generated peaks were wider and often tailed, making integration more difficult. With ^{13}C-enriched CO_2 held more tightly to the trap material, the measured $\delta^{13}C$ of wide/tailing peaks are prone to isotopic fractionation. In contrast, a higher flow of helium reduces sensitivity and increases operation costs. The optimal helium flow rate is a compromise between maximization of IRMS sensitivity (height of the peak, not the area) and minimization of peak width and tailing. Figure 4-2 shows the width at half height and the peak height as a function of helium flow rate. The highest intensity peaks were recorded at a flow rate of 52 mL/min. Given that peak width is also acceptable (only slightly wider than at 92 mL/min), the helium flow rate was thus set to 52 mL/min for all analyses. This flow rate is amenable to both mass spectrometers (Isoprime and Thermo-Finnigan), used in this work.

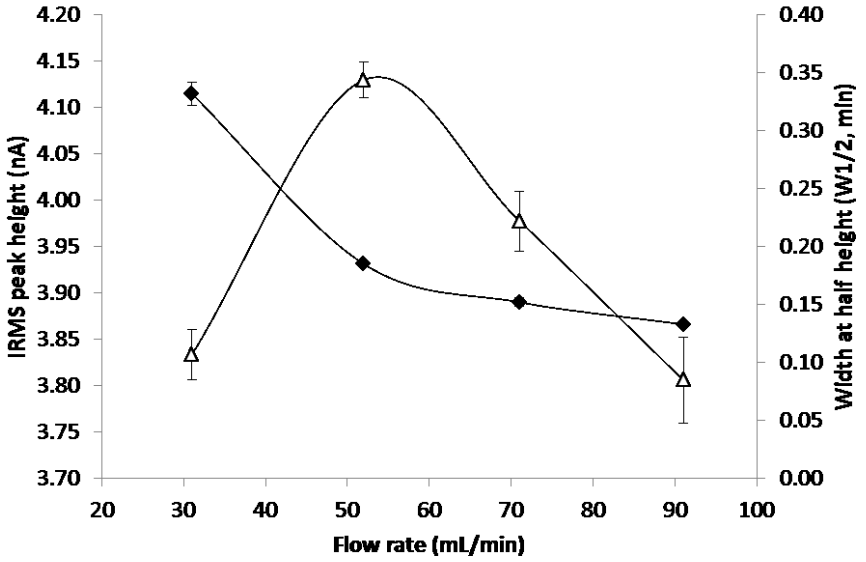

Figure 4-2: Flow rate dependency of IRMS peak intensity (nA) (white diamonds) and peak width at half height ($W_{1/2}$) (black squares).

Effect of pressure and injection volume on combustion efficiency and $\delta^{13}C$ measurements

Combustion efficiency as well as $\delta^{13}C$ accuracy and precision were evaluated for standard compounds (either in-house or certified standards) dissolved in TOC-grade water, with a range of propensities toward thermal oxidation: sucrose, β-alanine, potassium hydrogen phthalate (KHP) and Suwannee River fulvic acid. IRMS response factors (1.70 ± 0.01 nA μg C^{-1}) were statistically identical for all compounds, suggesting complete combustion. Both laboratories (Concordia University and University of Ottawa), operating similar HTC-DOC-IRMS systems, obtained comparable $\delta^{13}C$-DOC values for solutions whose concentrations ranged from 5 to 10 mg C L^{-1}. These values were within error of true $\delta^{13}C$ signatures (Table 4-1). The precision of $\delta^{13}C$-DOC values was only slightly lower than that of elemental analysis-IRMS (EA-IRMS) at these high DOC concentrations. DOC-IRMS and EA-IRMS samples were both run as unknowns; the measured $\delta^{13}C$ values are shown in Table 4-1.

Table 4-1: Comparison of isotopic composition ($\delta^{13}C$) by EA-IRMS and DOC-IRMS for standards and a sample. When available, standard deviations for measurements run in triplicate or quadruplet are shown in brackets.

Sample	true $\delta^{13}C$ values (‰)	EA –IRMS $\delta^{13}C$ (‰)		DOC –IRMS $\delta^{13}C$ LAB 1 (‰)		DOC –IRMS $\delta^{13}C$ LAB 2 (‰)	
Sucrose (In-house)	-11.77	-11.70	(0.03)	-12.1	(NA)	-11.6	(0.2)
KHP*	-28.16	-28.55	(0.03)	-27.8	(NA)	-28.1	(0.2)
β-Alanine	-26.18	-26.11	(0.06)	-25.3	(NA)	-26.1	(0.2)
Suwanee river fulvic acid	-27.60	-27.94	(NA)	-27.4	(NA)	-27.8	(0.2)

Qian and Mopper (1996) showed a relationship between the refractory nature of organic molecules and the width of the DOC peak. Out of all molecules tested, seawater DOC generated the widest peaks indicating that natural samples tend to contain DOC molecules that are more thermally resistant (e.g., dissolved black carbon; Jaffé et al., 2013) than the simple sugars/amino acids and soluble aromatic compounds (e.g. KHP) that are typically used to calibrate DOC instruments. A consensus material should therefore be used regularly, such as deep seawater sample provided by the Hansell CRM Program (Sharp et al., 2002) to monitor day-to-day variability and optimal instrument performance. Environmental samples are also chemically more complex than standard solutions, containing molecules produced from different photosynthetic and biochemical pathways, as well as molecules that have potentially undergone a number of microbial and chemical alterations. Natural DOC molecules thus have a broad distribution of molecular masses, functional groups and reactivities that go alongside varying isotopic signatures. In contrast to a solution containing only one chemical compound, non-quantitative combustion of a natural sample could therefore fractionate the DOC pool and generate CO_2 with an isotopic signature that is not representative of the bulk sample.

We used two complex mixtures to monitor possible combustion inefficiencies under different DOC analyzer pressures and injection volumes. The two mixtures (Mix 1 and Mix 2) are nearly identical in combustibility and composition, having both been made from ≈1:1 carbon equivalents of an algae extract and KHP (KHP $\delta^{13}C$ = -28.7 ± 0.1‰). The algae extracts were derived from two different nannochloropsis stocks: a $\delta^{13}C$-depleted stock (-41.3 ± 0.1‰) was used in Mix 1 whereas a $\delta^{13}C$-enriched stock (+11.6 ± 0.2‰, see methods section) was used in Mix 2. The two mixtures therefore have different overall $\delta^{13}C$ signatures (measured by EA-IRMS), but more importantly, markedly different $\delta^{13}C$ spreads between mixture components (KHP and algae extract): Mix 1 has a $\delta^{13}C$ of -29.7 ± 0.1‰ and a $\delta^{13}C$ spread of 13.2 ± 0.2‰ while

Mix 2 has a $\delta^{13}C$ of -8.3 ± 0.2‰ and a $\delta^{13}C$ spread of 39.7 ± 0.2‰. Incomplete combustion of one component of the mixture would therefore cause isotopic fractionation if the $\delta^{13}C$ of the untrapped/uncombusted carbon (i.e. from peaks tailing beyond trapping period programmed for GD-100 trap or incomplete DOC conversion to CO_2) is significantly different from that of the detected peak. Algae extracts contain a number of biomolecules (proteins, peptides, sugars, carbohydrates, lipids, etc.) but the range of $\delta^{13}C$ values for different compounds within one microorganism does not typically vary more than 5‰ (Wang and Druffel, 2001). Differences in the combustion efficiency of the biomolecules that make up the algae extracts would therefore not be easily detected from measured $\delta^{13}C$. The 13.2‰ or 39.7‰ $\delta^{13}C$ gap between the algae extracts and KHP make the observation of inefficient combustion measurable. With a ± 0.2‰ $\delta^{13}C$ precision, we can detect a 12 and 4 percent difference in the combustion efficiencies of the KHP and the algae extract for Mix 1 and Mix 2, respectively.

The Aurora 1030C DOC analyzer can be operated between pressures of 100 and 240 kPa. We tested the combustion efficiency at 140, 175 and 210 kPa. Higher system pressures require higher carrier gas flow rates which dilute sample CO_2 with oxygen and therefore generate smaller peaks on the DOC analyzer (the area of DOC peaks measured at 210 kPa is approximately 2/3 of those measured at 140 kPa). System pressure also affects the transit time of the sample through the combustion column, possibly influencing combustion efficiency. High system pressures condense the volume of gas generated from the explosive evaporation of water; a 1500 µL injection generates 3.19 liters of gas at 210 kPa compared to 4.78 liters at 140 kPa according to ideal gas laws. We tested the possible effect of pressure on combustion efficiency using 1500 µL injections of ≈5 mg C L^{-1} solutions of Mix 2 and IAEA sucrose (Figure 4-3). The IAEA sucrose solution is used as a benchmark here since its $\delta^{13}C$ signature is close to that of Mix 2 ($\delta^{13}C$ = -10.47 ± 0.03‰) and is not expected to deviate even if sample oxidation is

incomplete. Both the sucrose standard and the complex mixture generated stable IRMS peak intensities and constant $\delta^{13}C$ signatures, indicating that the effect of pressure on combustion efficiency is minimal. The instrument can therefore be used at any pressure, but the lower the DOC analyzer operation pressure, the longer the retention time and the broader the peaks. Wide DOC peaks force the operator to trap for longer time periods, thus increasing the system blank contribution (defined and discussed below). More Gaussian-shaped and easily integrated peaks are obtained when using higher pressures; therefore we recommend the use of 210 kPa.

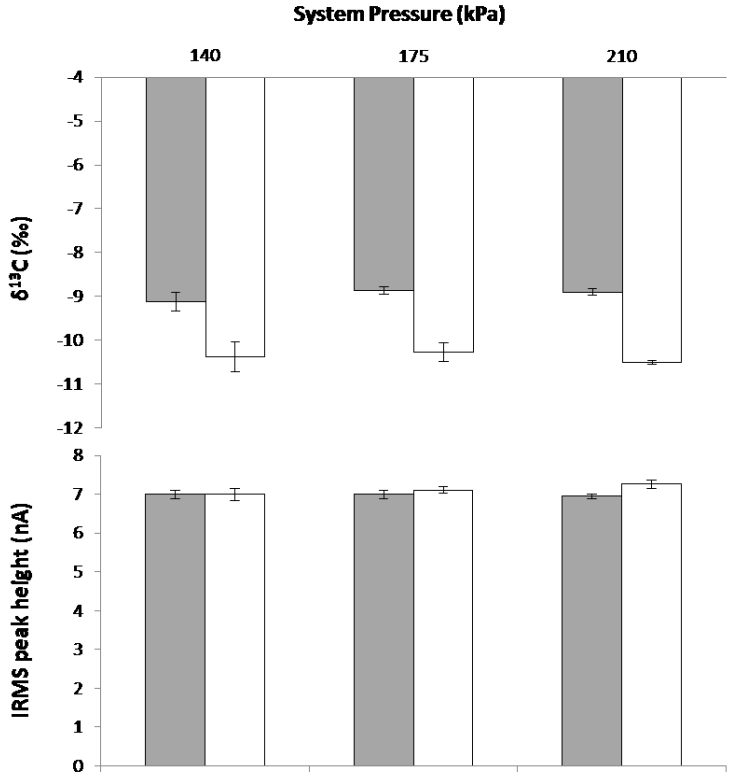

Figure 4-3: IRMS peak intensity (nA) and stable carbon isotopic signature ($\delta^{13}C$, ‰) as a function of system pressure (kPa) for ≈5 mg L^{-1} ^{13}C-enriched algae/KHP mixture (Mix 2, grey bars) and pure IAEA sucrose (white bars).

Similarly, sample combustion was verified at injection volumes ranging from 500 to 1500 µL. For each injection volume tested, we adjusted solution concentrations so that an equal quantity of

carbon was injected (7.5 ± 0.5 µg). At 210 kPa, every 500 µL of water produces about 1 L of gas which is quickly pushed out of the combustion column. Every additional volume increment reduces the average time spent by the sample at high temperature in contact with the catalyst. The oxidation of high volume samples is also potentially hindered by the cooling of the column and quenching of combustion upon water vaporisation. Using Mix 2, we noticed a progressive depletion in the measured $\delta^{13}C$ with increasing injection volumes (Figure 4-4A). A statistically significant isotopic difference of 0.89‰ was observed between the 500 µL and 1500 µL injection volume. In contrast, the $\delta^{13}C$ isotopic signature of the sucrose solution was constant, irrespective of the volume injected. This difference suggests differential combustion efficiency of KHP and the enriched algae extract at high injection volumes; using isotopic mass balance with the two pools of DOC as end-members, we calculate that ≈ 4% of the carbon in the algae extract is not combusted (or not trapped) and measured on the IRMS. This difference is readily detected using isotopes but is within error of the generated DOC peak areas (± 2%, http://www.oico.com) and IRMS peaks heights. Due to the smaller isotopic difference in mixture components (12.8‰ versus 39.7‰), no volume-induced isotopic variations are observable when Mix 1 is used instead of Mix 2 (Figure 4-4B). Indeed, the same difference in combustion efficiency between mixture components would generate a 0.28‰ difference in isotopic signature between low (500 µL) and high (1500 µL) injection volumes; a difference that is not statistically significant since the $\delta^{13}C$ precision at this concentration is about ± 0.15-0.2‰ (Figure 4-5). In this case, β-alanine was chosen as the isotopic benchmark so that the sample $\delta^{13}C$ signatures were close to that of the standard. Though it is important to consider that there is a limitation in DOC combustion efficiency, natural samples typically do not have large inter-compound isotopic differences that would lead to erroneous $\delta^{13}C$ measurements. The largest isotopic differences (>13‰) likely occur from DOC samples originating from mixed

photosynthetic sources (e.g. estuarine waters that contain terrestrial ($\delta^{13}C$ =≈ -27‰) and marine ($\delta^{13}C$ = ≈-20‰) DOC) or photosynthetic pathways (e.g. soil porewaters that have seen a change between C4 ($\delta^{13}C$ ≈-14‰) and C3 vegetation ($\delta^{13}C$ ≈-27‰)) or from systems pervaded by ^{13}C-depleted petrogenic or methanogenic DOC (Ouellet et al., 2012; White et al., 2005). Nevertheless, performance limitations of DOC analyzers are important for samples amended with an enriched compound because of the unusually large $\delta^{13}C$ difference between the spike and natural abundance DOC molecules.

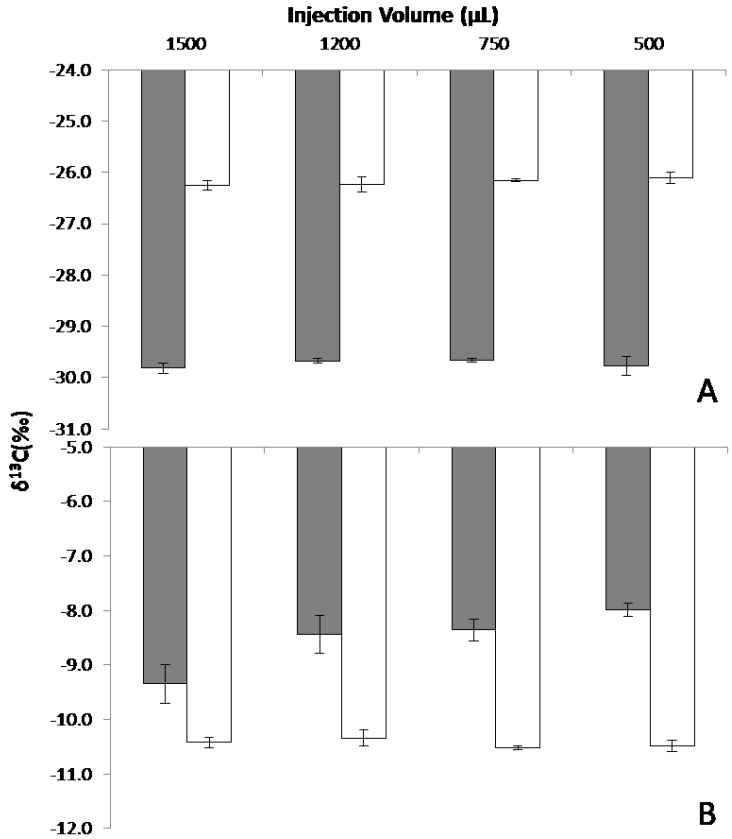

Figure 4-4: Stable carbon isotopic signature ($\delta^{13}C$, ‰) as a function of volume injected (µL) for ^{13}C-enriched algae/KHP mixture (Mix 2, grey) and pure IAEA sucrose (white) in panel A and for ^{13}C-depleted algae/KHP mixture (Mix 1, grey) and β-alanine (white) in panel B. Solution concentrations were adjusted so that a constant ≈7.5 µg of carbon was injected.

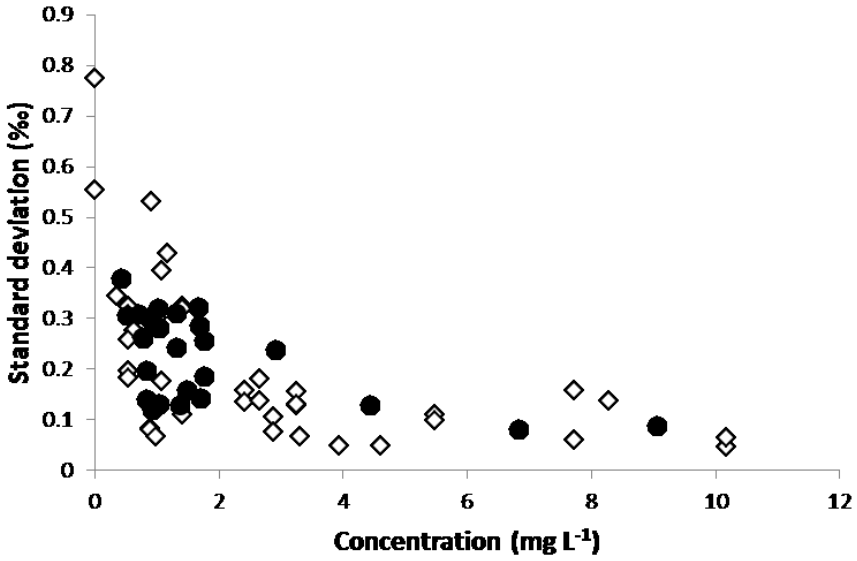

Figure 4-5: Increase in reproducibility (‰) of calibration standards (white diamonds) and natural samples (black circles) with increased C concentration of samples. Standard deviations are reported for samples having between 3 and 5 replicates, run consecutively. These measurements were performed over 8 months of analysis on three DOC analyzer combustion columns.

Sample carry-over

Cross-contamination between samples can influence δ^{13}C-DOC signature and DOC concentration especially for vastly different samples run in series (Panetta et al., 2008; Qian and Mopper, 1996). Sample carry-over or memory effects originate from the "sticking" of CO_2 or DOC molecules to the sample loops, the combustion column and various other DOC analyzer mechanical components.

We analyzed a sequence of DOC solutions bracketed by blank injections (acidified TOC grade water) that flush out residual carbon from the previously injected sample. Carry-over into the blanks was determined by comparison to the normalized true blank height (average height of the last 3 injections out of a series of 5 blanks). The solution concentrations were prepared to cover a range of concentrations between 2 and 8 mg C L^{-1} but the injection volume was adjusted from 200 to 1500 µL to keep the mass of carbon from each injection nearly constant (1.52 ± 0.15

µg). Because increased carry-over from higher concentration solutions was observed (Figure 4-6) even when the same quantity of carbon was injected into the combustion column, cross-contamination from non-combusted/adsorbed species on column packing materials, or from mechanical components downstream from the combustion column can be discounted. Carry-over therefore likely originates from organic molecules that adhere to the sample loops and sparging chamber located between the sample vial and the combustion column. Solutions containing natural DOC (algae-extracted DOC) cross-contaminate more than β-alanine solutions; this is likely because natural DOC contains more "sticky", hydrophobic molecules, that adhere to PTFE tubing.

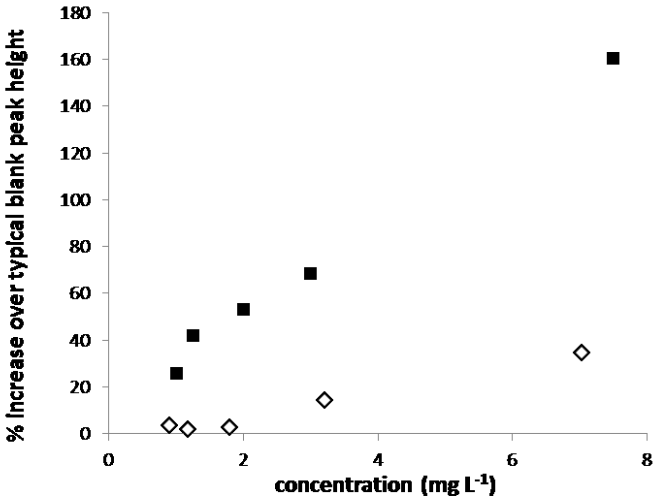

Figure 4-6: Carry-over into blank water following the analysis of algal DOC (black squares) and β-alanine (white diamonds) solutions at varying concentrations (mg L^{-1}). The total mass of carbon injected was kept constant for each DOC solution by adjusting the injection volume. The magnitude of carry-over was normalized to the true blank intensity (average intensity of 3 blank injections).

When analyzing samples in sequence, we recommend the use of at least one blank injection between each sample to minimize carry-over. Alternatively, it may be advantageous to program the DOC analyzer to rinse the sample loop and sparging chamber with blank water more than

once between each sample. Many blank injections are required when analyzing $\delta^{13}C$ at enriched levels. After the injection of a highly enriched ($\delta^{13}C$ >100‰) sample, the system needed at least two successive injections to recover accurate $\delta^{13}C$ values for natural abundance samples or standards (data not shown).

Sample matrix effects

Combined to low DOC concentrations, salts have historically been at the root of most problems associated with DOC-IRMS analysis of seawater samples. Salts from natural seawater, have been reported to cause a decrease in combustion efficiency due to the fouling of catalytic sites (Benner and Strom, 1993; Skoog et al., 1997), trigger the production of random ghost peaks due to the flaking of salt deposits into the column hot zone (Qian and Mopper, 1996), and most importantly, cause unavoidable system maintenance issues (Bouillon et al., 2006; Lang et al., 2007; Panetta et al., 2008). As salts are inherently associated with samples from both aquatic and terrestrial ecosystems, their influence on DOC combustion as well as on $\delta^{13}C$ measurements must be assessed. Using a standard addition method, we tested the response factor of the DOC combustion by adding sucrose to a deep Pacific seawater sample (collected in 2006). The response factors for sucrose dissolved in freshwater and saltwater were identical, indicating that there is no difference in combustion, trapping or detection efficiency.

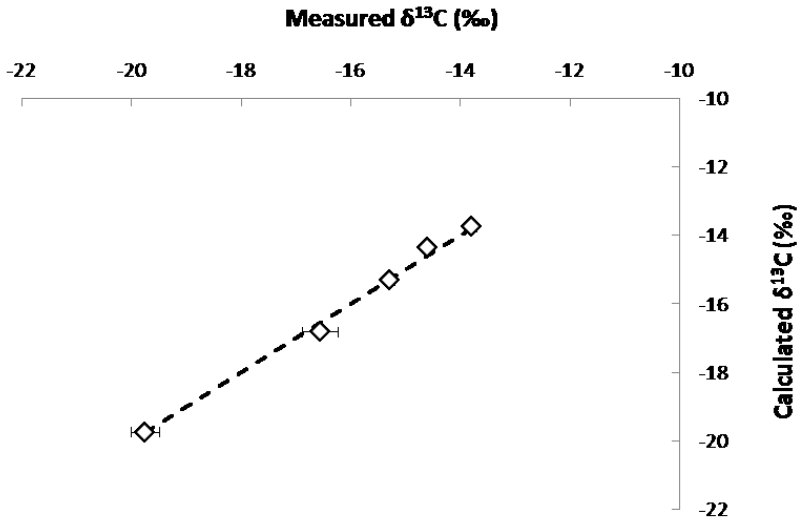

Figure 4-7: Predicted versus calculated $\delta^{13}C$ value for the standard addition of IAEA sucrose ($\delta^{13}C$ = -10.47‰) to deep pacific water ($\delta^{13}C$ =-19.75‰, 1.09 mg L^{-1}). With an intercept of 0, the slope of the line is 1.005 (R^2 = 0.985).

Though salts do not seem to affect DOC combustion efficiency, accounting for salt build-up in the combustion column is crucial. Salts are deposited within the upper centimeter of the quartz pellet bedding and are not displaced by repeated injections of freshwater. The thickness and density of the salt build-up depends on the size of the quartz chips, with a more tightly packed and flow-restricting salt layer accumulating on smaller chips. After about 100 mL of seawater are injected on the column (the equivalent of 3.5g of salt), carrier gas flow starts to be impinged by the accumulating salt, retarding and broadening peaks on the DOC analyzer. Further injection of salty water can completely clog the DOC column; at this point, the explosive vaporization of water upon injection can cause the column to shatter. In order to minimize column breakage, it is therefore crucial to clean and repack the combustion column regularly when analyzing high volumes of salty samples.

At high temperatures, salts precipitated on the combustion column also generate volatile species that could partake in ion-molecule reactions if allowed to enter the mass spectrometer

source. Though not systematically studied, ion source chemistry has been suspected to cause most nonlinearity effects as well as instrument drifts in IRMS (http://isogeochem.wikispaces.com/). Most contaminating species were cleaned from sample CO_2 in the GD-100 trap by rinsing the peak with ultrapure He gas (45 seconds) prior to being sent to the IRMS. Residual contaminants may however linger if they have a strong affinity for the molecular sieve. We therefore installed a Cu reduction/scrubbing furnace containing Cu pellets and cobaltous/ic oxide (silvered) between the molecular sieve and the IRMS to remove sulfur/halide and nitrogen oxide (NO_x) gases (similarly to Lang et al., 2007 and Panetta et al., 2008). We obtained much better precision and accuracy on isotopic signatures after the installation of the scrubbing furnace, especially for salty samples. Prior to the installation of the Cu furnace, raw isotopic signatures for standard compounds were more depleted than their true values and not as reproducible (3 to 3.5x higher standard deviation). Residual volatiles from the DOC analyzer are not only major contributors to the reduction system precision but may also corrode IRMS components and reduce the source filament life.

Contribution of the blank

HTC-DOC analyzers generate notoriously high blank values, contributing up to 40% of the DOC in a 100 µL injection of a typical deep seawater sample (Peterson et al., 2003). Unstable and/or elevated blanks that are not weighted or overlooked have historically generated erroneously high DOC values (Sharp et al., 1993; Sugimura and Suzuki, 1988). The major part of the DOC blank comes from the column packing (Benner and Strom, 1993; Cauwet, 1994; Sharp et al., 1993) that needs to be “conditioned” before use through a series of pure water injections. The injection of water on the column packing prompts the release of adsorbed CO_2 and produces the reactive oxygen species that are required for the oxidation of carbonaceous species embedded in the catalyst and other column packing materials (Chen et al., 2002). During conditioning, the

quantity of CO_2 released from the column packing follows a hyperbolic decrease to a low and stable value (Peterson et al., 2003). Reagent blanks (from blank water and acid) are also important to consider. A cleaning procedure for water was outlined by Benner and Strom in 1993, reducing DOC contamination to less than 24 μg L^{-1} (Benner and Strom, 1993). Since then, research laboratories have produced certified low carbon water (http://yyy.rsmas.miami.edu/groups/biogeochem/CRM.html, < 12 μg L^{-1}); TOC-grade water (Sigma, < 1.2 μg L^{-1}) is now also commercially available.

CO_2 released from the injection of blank TOC-grade water is called the "water blank". We calculate the water blank from the DOC analyzer response factor to be between 60 and 110 μg L^{-1} of carbon for a 1500-μL injection. Our results are similar to those of Cauwet (1994) (48 – 96 μg L^{-1}), Qian and Mopper (1996) (84 μg L^{-1}), Sharp et al. (2002) (48 – 96 μg L^{-1}) and Peterson et al. (2003) (36 – 108 μg L^{-1}). The water blank contributes about 10% of the DOC peak intensity of a deep seawater DOC sample (Florida Straight water provided by Hansell CRM program Batch 13 Lot # 05-13, 490 – 530 μg L^{-1}), which contains the lowest concentration of DOC measured in this study. Assuming that TOC-grade water (Sigma < 1.2 μg L^{-1}) contains an insignificant concentration of DOC, the water blank corresponds almost entirely to CO_2 ejected from the catalyst bed. The purity of the water from ultra-purification systems (Milli-Q water, Millipore Simplicity 185 equipped with a Simpak1 cartridge) should be verified when it is used to prepare calibration standards and blanks, especially when analyzing low DOC samples as 18.2 MΩ·cm water was found to contain 0.5 to 63 μg L^{-1} of adventitious DOC.

Blank water injections generate CO_2 peaks that are measurably large throughout the service life of the combustion column. Nevertheless, the formation of blank peaks does not discount the possibility that CO_2 is continuously released from the combustion column packing without the

help of injected water; or that atmospheric CO_2 leaks are carried into the system along the carrier gas flow path (Peterson et al., 2003). This CO_2 bleed is not separable from the analytical baseline and is called the “system blank”. The system blank is known to be an even more significant source of background CO_2 than the water blank (Lang et al., 2007). Omitting major CO_2 contamination resulting in low signal to noise ratios, this increased baseline does not affect routine DOC analyses. Nevertheless problems arise during the subsequent characterization of CO_2 using stable carbon isotope analysis since sample CO_2 is combined to contaminating/blank CO_2 in the trap upstream from the IRMS.

Two components therefore make up the IRMS blank: the system blank and the water blank. The system blank depends on the amount of time that the GD-100 Graden trap collects CO_2 (about 5 minutes per injection) and can be directly measured by passing the DOC analyzer carrier gas without injecting water on the DOC column. The IRMS response factor is then used to deduce the carbon content of the system blank from the height of the IRMS peak. Although the system blank is highly stable during one series of analysis, it can vary from one combustion column to another, likely due to usage and mass differences in column packing materials. As the column ages and accumulates salts, the surface characteristics of column packing material may change (e.g., devitrification of the quartz beads and column walls, as well as loss of the platinum coating from catalyst beads; Peterson et al. 2003). The lowest system blank measured in this study, approximately 0.176 µg, was generated from a column containing new, conditioned catalyst and gradually increased to > 1.0 µg over one year of catalyst use (≈ 3000 injections). Regular evaluation of the system blank is important since high system blanks are not compatible with isotopic analysis of low-carbon samples (sample blank corrections are discussed in the following section). As the system blank does not vary with injected volume, the relative contribution of carbon from the sample can be increased relative to the blank carbon by injecting higher sample

volumes. For example, the total blank contribution for a 500-µL injection of Deep Florida Straight water (CRM Batch 13 Lot # 05-13, D. Hansell, U. Miami) is about 50% of the total IRMS peak area, compared to about 33% for an injection of 1500 µL.

Unlike the system blank, the water blank is proportional to the volume of water injected (Figure 4-8; Benner and Strom, 1993; Cauwet, 1994; Lang et al., 2007). The water blank was generally less significant than the system blank, accounting for between 14 and 55% of a 1500-µL blank injection (consistent with Lang et al. 2007). Like the system blank, the water blank varies during the life of one DOC column, however more significant water blanks are observed on new (but conditioned) columns (Figure 4-8).

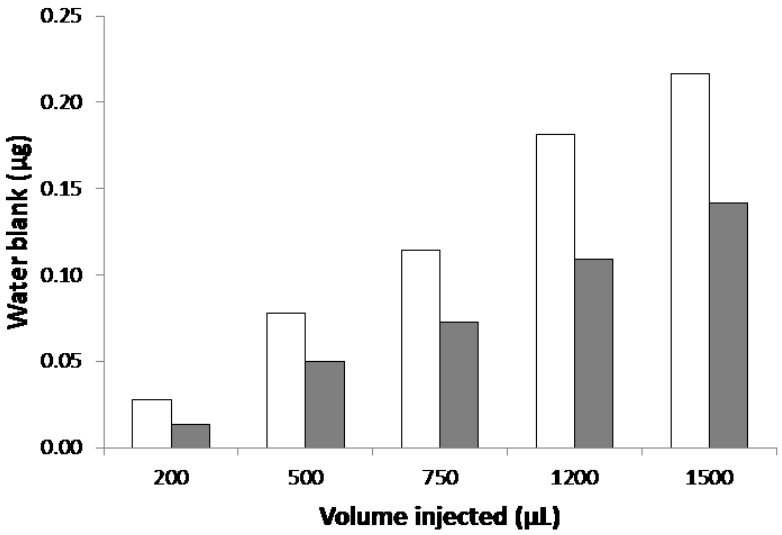

Figure 4-8: Water blank (µg C) for new column packing (white) and old column packing (grey) as a function of the DOC injection volume (µL). The system blank is not included (subtracted from total blank signal).

Concentrations can be calculated from either the DOC area or the IRMS peak height (or area), however the proper statistical treatment of the blank is especially important when dealing with the IRMS peak height, which is affected by both the water blank and the system blank. When

comparing low DOC water concentration measurements, such as those for the CRM Deep Florida Straight water, comparable concentrations are calculated from either the DOC calibration (0.494 ± 0.014 mg L^{-1}) or the IRMS calibration (0.486 ± 0.028 mg L^{-1}) when the intercepts from the DOC area or IRMS height *vs.* concentration standard curves are subtracted. Obtained values are within the community accepted concentration range (0.49 – 0.53 mg L^{-1}, http://yyy.rsmas.miami.edu/groups/biogeochem/CRM.html). The necessity of blank subtraction shows that the combination of the water blank and the system blank is equally present in both the samples and standards implying that blanks likely arise mainly from the catalyst and column packing and, corroborating the very low/insignificant reagent blank estimated in this work.

Background $\delta^{13}C$ and sample correction

Like for DOC quantitation, background determination largely controls the feasibility of isotopic analysis by DOC-IRMS. Indeed, most problems of accuracy and reproducibility of low-carbon $\delta^{13}C$ measurements are rooted in the intrinsic variability of the fractional contribution of the blank and its $^{13}C/^{12}C$ ratio. The contribution of blank CO_2 to total signal intensity increases exponentially with decreasing sample DOC concentration, as does the statistical error associated to blank $\delta^{13}C$. For instance, if the blank $\delta^{13}C$ precision is ± 2‰, the standard deviation that results from blank $\delta^{13}C$ variability becomes less than 0.02‰ for high concentration samples such as sewage water or DOC concentrates (50 mg L^{-1}, ≈1% blank contribution), about 0.14‰ standard deviation for a typical lacustrine samples (3 mg L^{-1}, ≈7% blank contribution) and 0.66‰ standard deviation for low-concentration marine samples such as Deep Florida Straight water (≈0.5 mg L^{-1}, ≈33% blank contribution). Measured standard deviations of sample and standard $\delta^{13}C$-DOC are shown in Figure 4-5 and follow the expected exponential decrease with sample concentration. Analytical precision is comparable for samples and standards of similar concentration and thus does not seem to depend on sample complexity (Figure 4-5).

Instrumental IRMS performance is not expected to be problematic, even for the lowest concentration samples since all samples generated peaks above 1 nA, above which IRMS precision is adequate (<0.1‰).

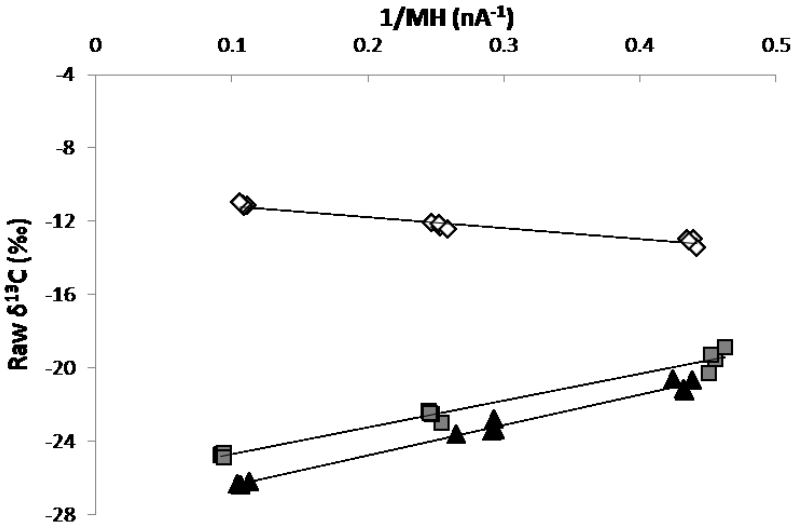

Figure 4-9: Measured $\delta^{13}C$ versus the inverse of the IRMS signal intensity for standard solutions of β-alanine (grey squares), potassium hydrogen phthalate (KHP) (black triangles) and IAEA-sucrose (white diamonds). Three solutions of each compound were prepared with concentrations of approximately 0.7, 1.7 and 5 mg L^{-1}. Linear functions were used to determine the blank-corrected $\delta^{13}C$ of the standards as well as the isotopic composition of the blank.

Though ideally less variable, the blank contribution and its $\delta^{13}C$ signature are stable enough to be measured. The most convenient and most accurate way of determining the blank $\delta^{13}C$ is through plotting the measured isotopic signature (δ_m) of 3 or 4 standard solutions at different concentrations versus the inverse of peak intensity ($1/\eta_m$, nA^{-1}) (Fry et al., 1992; Panetta et al., 2008). If the blank and standard compounds are the only contributors of CO_2 in the IRMS peak, a straight line should be generated, such as shown in Figure 4-9. On this graph, the blank-corrected $\delta^{13}C$ (δ_{bc}) is the *y*-intercept; blank $\delta^{13}C$ (δ_b) can be calculated from the slope using the intensity of the blank (η_b):

$$\delta_b = (\text{Slope} / \eta_b) + \delta_{bc}$$

To verify the reproducibility of the obtained values, determination of the isotopic signature of the blank was performed using three standard compounds dissolved in TOC-grade water (Figure 4-9). At the time of these analyses, δ_b was -14.71 ± 1.15‰.

Although not as accurate owing to the lower precision of the IRMS at low amplitudes (≈0.5 nA), the isotopic signature of the blank can also be monitored directly from IRMS peaks generated from the injection of TOC-grade water. During the course of one day of analysis, δ_b can vary considerably even when the magnitude of the blank appears to be stable. For example, when the O_2 carrier gas flow is interrupted, the isotopic signature of the blank typically becomes 5-10‰ more depleted than δ_b from a properly conditioned column. About 100 injections of TOC-grade water are required to stabilize a new combustion column for isotopic analysis (containing new catalyst beads) after exposure to air; fewer injections (about 30) are required when old catalyst is cleaned and reused. Once stabilized, the blank still fluctuates from one sample to another (over sequences lasting 24 to 48 hours), but does not seem to follow any observable isotopic drifts or patterns. Nevertheless, throughout the service life of the column, the CO_2 evolving from the blank typically starts from fairly depleted values (-18 to -20‰) and drifts towards more enriched values (-15 to -12‰) after extensive use (3-4 months, >1000 injections). These blank isotopic signatures are in the ballpark of previously reported values; δ_b was −19.2‰ to −24.3‰ for Lang et al. (2007) and -15.51 to -17.78‰ for Panetta et al. (2008). Changes in the isotopic signature of the blank during the life of the column likely arise from changes in the column packing; e.g. devitrification of the quartz chips/column as well as loss of platinum coating from catalyst beads (Peterson et al. 2003).

After determination of the blank isotopic ratio and signal intensity, the following isotope mass balance equation is applied to a measured sample (Panetta et al. 2008):

$$\delta_s = \frac{\partial_m \eta_m + \partial_b \eta_b}{\eta_m - \eta_b}$$

where δ_s is the stable isotope ratio of the analyte and η_m and η_b are the measured and blank intensities, respectively. Other parameters are defined above.

It should be noted that the more the signature of the sample deviates from that of the blank, the larger the discrepancy between the measured and the actual $\delta^{13}C$. For example, a marine seawater sample containing 1 mg C L^{-1} DOC at $\delta^{13}C$ = -20‰ generates a peak having a 16.5 to 83.5 blank CO_2 to sample CO_2 intensity ratio, and a measured signature of -19.1‰ ($\delta^{13}C$ difference of 0.9‰). In contrast, a sample enriched in ^{13}C ($\delta^{13}C$ = +100‰) having the same concentration (and therefore the same blank contribution) is measured at +81.1‰ ($\delta^{13}C$ difference of 18.9‰). For an enriched sample ($\delta^{13}C$ = +100‰), a small error in blank contribution therefore translates into a relatively large error on isotopic measurements: 1% blank contribution error equates to a 1.2‰ error on the isotopic measurement.

Discussion

When the first inter-comparison studies were launched in the 1990s, DOC measurements were still of uncertain quality (Sharp et al., 1993). Over the past decades, superior precision/accuracy and increased spatial coverage have not only led to better estimations of the overall size of the oceanic DOC pool but have also led to the detailed documentation of DOC transport, sources and sinks in freshwater and marine systems (Hedges, 2002b). DOC concentration gradients from ocean surfaces to bottom-waters suggest production in the surface waters and consumption at depth (Bauer, 2002; Druffel et al., 1992). Lateral gradients along the path of bottom-water

ocean circulation are more subtle and the DOC influxes and effluxes responsible for these gradients are more difficult to identify, but may include inputs from marginal seas and continental shelves (Bauer and Druffel, 1998), inputs due to the dissolution of sinking biogenic particles, and consumption by microbes (Hansell, 2002). There may also be other unidentified DOC production and removal processes.

Unlike DOC concentrations, δ^{13}C-DOC measurements have limited spatial and temporal coverage in saltwater systems, likely due to the difficulty of the analyses. Thus far, δ^{13}C-DOC data point to the nearly purely marine origin for dissolved organic matter in the open ocean (Bauer, 2002; Bauer et al., 1992) but increased resolution and precision may better constrain DOC sources and help identify DOC fractionation processes. δ^{13}C-DOC measurements have also been used to track carbon in the mixing water bodies of estuaries and river plumes (Osburn and Stedmon, 2011; Raymond and Bauer, 2001a). Renewed interest in freshwater systems, especially riverine systems that discharge in the ocean, recently initiated an IAEA funded project aiming to expand the knowledge base on riverine systems through the application of a wide range of isotopic hydrology methods, including δ^{13}C-DOC (http://isogeochem.wikispaces.com).

Using our optimized system, we analyzed natural water samples from a broad range of environmental settings including rivers and lakes, a freshwater to seawater estuarine transect as well as bottom water from the Florida Strait (CRM material). δ^{13}C reproducibility was similar to that of standards (Figure 4-5). Out of all natural waters, seawater samples generally have the lowest DOC concentrations (0.40 to >1mg L^{-1}, Hansell 2002 and references therein), and are therefore typically the most difficult to analyze. The consensus reference material (CRM Batch 13 Lot # 05-13, Hansell lab 2013) was the lowest concentration sample analyzed in this study (0.49-0.53 mg L^{-1}). After thorough calibration of the instrument and careful blank

determination/correction, values obtained for this sample were –19.9 ± 0.4‰ (n = 4) and -20.6 ± 0.3‰ on separate DOC-IRMS systems, corroborating Bouillon (2006), Lang et al. 2007 and Panetta et al. (2008) for a similar sample provided by the same laboratory.

Figure 4-10 shows $\delta^{13}C$ values for samples collected in the St. Lawrence Estuary. Going seaward from the mouth of the river comprising mainly continentally-derived material ($\delta^{13}C$-DOC = -26.1 ± 0.2‰), isotopic signatures become progressively more enriched, reaching a value of -19.9 ± 0.3‰ in the Gulf as a result of degradation and dilution of terrestrially-derived material and addition of marine-derived DOC through primary productivity. These $\delta^{13}C$-DOC measurements are precise and comparable to previously reported values (Hélie and Hillaire-Marcel, 2006; Panetta et al., 2008). It is of note that all these samples - as well as calibration standards - were run within a single sequence lasting less than 24 hours. Increased throughput, simplicity and reliability of $\delta^{13}C$-DOC measurements may bring about the more thorough examination of carbon sources and cycling in aquatic systems, especially marine, coastal and estuarine waters. To the authors' knowledge, this $\delta^{13}C$-DOC method has the highest reported throughput and the highest tolerance for salts. More importantly, it is also the only automated method for determination of $\delta^{13}C$-DOC in saltwater samples. Another noteworthy advantage of this method is its amenability to both freshwater and saltwater samples with no special considerations needed to measure both types of samples within the same sequence of analyses. Low concentration freshwater samples (<1.5 mg L^{-1}) are more reproducible using wet oxidation due to lower blanks and to the higher volume tolerances (Bouillon et al., 2006; Osburn and St-Jean, 2007; St-Jean, 2003). However, since naturally-occurring freshwater samples are typically rich in DOC (1.5 mg L^{-1}), HTC-DOC is almost always as reliable as wet oxidation.

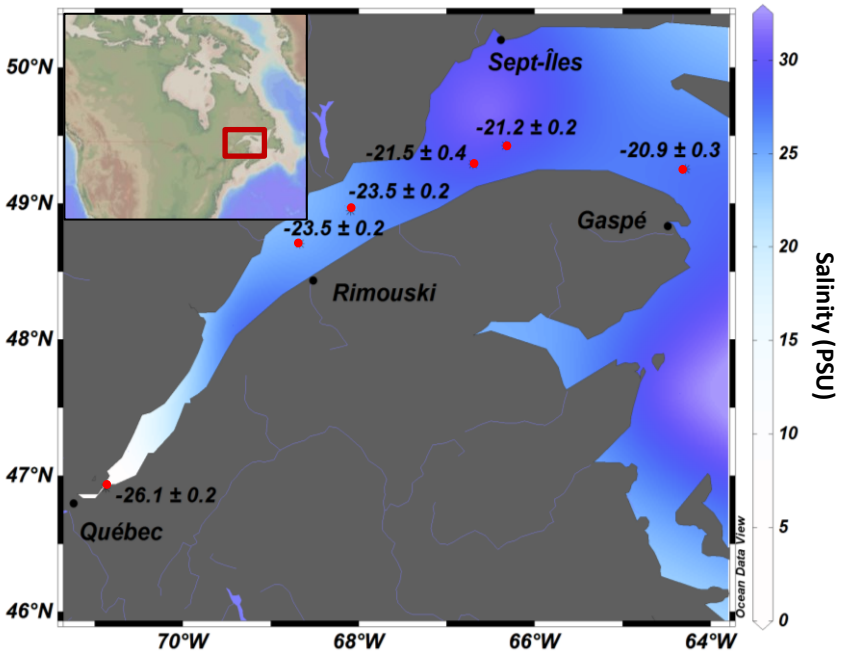

Figure 4-10: δ^{13}C-DOC isotopic signatures (‰) of surface water samples collected from the St. Lawrence Estuary transect with increasing salinity. (Ocean Data View: Schlitzer, R., Ocean Data View 4, http://odv.awi.de, 2013.)

Comments and recommendations:

The hyphenation of an Aurora 1030C DOC analyzer, a GD-100 CO_2 trap and a continuous flow IRMS has made possible the high-throughput, automated measurements of δ^{13}C-DOC in freshwater and seawater samples. The analysis time is ≈20 min per sample and series can be run overnight. In our experience, fairly rugged δ^{13}C-DOC are easily measured for samples containing >1.5 mgC L^{-1}, but, with blank contributions as high as 40% of the total sample intensity, analysis of lower concentration solutions (<1.5 mg C L^{-1}) must be met with caution: proper conditioning of the combustion column, precise determination of blank contribution and δ^{13}C signature, as well as appropriate blank corrections are essential for accurate measurements. δ^{13}C blank fluctuations are however innate to high temperature combustion as blanks originate mainly from the continuous desorption/ejection of CO_2 from the catalyst/column packing. Throughout

the service life of the combustion column, random blank variations limit the maximum precision of low-concentration isotopic measurements (approximately ± 0.3-0.5‰ for typical deep seawater samples, Figure 4-5). Higher reproducibility has not yet been achieved at these low concentrations, but might be possible if the catalyst and column packing materials were swapped with cleaner materials generating lower and/or more stable blanks (possible materials include copper oxide (Panetta et al., 2008; Qian and Mopper, 1996) or platinum-coated quartz wool (Cauwet, 1994)). Unlike WO, HTC combustion is not affected by the sample matrix even at low DOC concentrations, though the instrument can only tolerate approximately 3.5 g of salt accumulation before flow restrictions arise.

Future avenues of applications for the DOC analyzer and CO_2 trap include same sample $\delta^{13}C$ determination of dissolved inorganic and organic carbon (total dissolved inorganic carbon is typically much more concentrated than DOC in seawater samples, therefore a large linear dynamic range or a He dilutor would be necessary for these samples). Other possible future applications may include CO_2 generation and trapping for accelerator mass spectrometry ^{14}C dating, since $\Delta^{14}C$ and $\delta^{13}C$ used in conjunction serve as unique source and age tracers that are especially useful in studies of marine carbon cycling through the DOC pool (Bauer, 2002; Raymond and Bauer, 2001a). Provided enough starting material and a suitable trap for the nitrogen oxides produced upon dissolved organic matter combustion in the HTC analyzer, e.g.(Wang et al., 2009), dual isotopic analysis may also extend to $\delta^{15}N$ measurements (Huygens et al., 2007).

Chapter 5: Revisiting the disappearance of terrestrial dissolved organic matter in the ocean: A $\delta^{13}C$ study

Abstract

Organic carbon (OC) depleted in ^{13}C is a widely used tracer for terrestrial OM in aquatic systems. Photochemical reactions can however change $\delta^{13}C$ of dissolved organic carbon (DOC) when chromophoric, aromatic-rich terrestrial OC is selectively mineralized. We assessed the robustness of the $\delta^{13}C$ signature of DOC ($\delta^{13}C_{DOC}$) as a tracer for terrestrial OM by estimating its change during the photobleaching of chromophoric DOM (CDOM) from ten large rivers. These rivers cumulatively account for approximately 1/3 of the world's freshwater discharge to the global ocean. Photobleaching of CDOM by simulated solar radiation was associated with the photochemical mineralization of 16 to 43% of the DOC and, by preferentially removing compounds depleted in ^{13}C, caused a 1 to 2.9‰ enrichment in $\delta^{13}C$ in the residual DOC. Such solar radiation-induced photochemical isotopic shift biases the calculations of terrestrial OM discharge in coastal oceans towards the marine end-member. Shifts in terrestrial $\delta^{13}C_{DOC}$ should be taken into account when constraining the terrestrial end-member in global calculation of terrestrially derived DOM in the world ocean.

Introduction

The oceanic dissolved organic carbon (DOC) pool is large (662 x 10^{15} g OC;(Hansell et al., 2009)), representing a quantity of carbon that is approximately equal to that of carbon dioxide in the atmosphere and terrestrial plant biomass (Hedges, 2002a). The turnover of OC within the oceanic reservoir is supported by marine and continental photosynthesis, with vascular plant detritus and soil organic matter mainly transported to the ocean by continental erosion and riverine discharge. Apportioning these sources is challenging since oceanic DOM has a complex, highly altered structure, consisting mainly of relatively small molecules in fairly uniform and very dilute concentrations (Benner et al., 1997). Most evidence points to a nearly purely marine origin for oceanic DOM, as indicated by 1) its marine-like $\delta^{13}C$ signature (Bauer, 2002; Druffel et al., 1992); 2) the low abundance or absence of terrestrially-derived molecular biomarkers within the DOM pool (Ogawa and Tanoue, 2003; Opsahl and Benner, 1997) and 3) the compositional and optical dissimilarities between riverine and seawater DOM (Blough and Del Vecchio, 2002).

Though oceanic DOM is predominantly marine-like, there is evidence that a small yet non-negligible component of DOM has a terrestrial origin. Studies using resin and ultrafiltration-isolated lignin molecules have shown that the terrestrial component varies between 4 and 10% of the isolated fractions of DOM (Meyers-Schulte and Hedges, 1986; Opsahl and Benner, 1997). These are likely underestimations since solar radiation-induced photochemical reactions break apart large aromatic-rich molecules like lignin, tannin and cutin (Dittmar et al., 2007; Hernes and Benner, 2003; Vähätalo et al., 1999) into molecular fragments that can be difficult to isolate from seawater's salty matrix (too hydrophilic for hydrophobic resins or too small for ultrafiltration) and identify as terrestrial compounds using current analytical methods (Rossel et al., 2013).

Optical parameters (absorbance and fluorescence) that are specific to riverine DOM are also particularly susceptible to photochemical transformation since the light-absorbing, chromophoric riverine DOM components are selectively removed upon exposure to UV radiation in a process called photobleaching (Blough and Del Vecchio, 2002; Helms et al., 2008). Photobleaching of terrestrial DOM is associated with the photochemical mineralization of DOC, acting as a partial sink for terrestrial DOC (Moran et al., 2000). The residual non-mineralized fraction of photobleached terrestrial DOM has optical properties that are similar to marine DOM; its terrestrial origin cannot be fully recognized using the currently available optical methods (Helms et al., 2008; Spencer et al., 2009; Vähätalo and Wetzel, 2008). Fichot and Benner (2012) recently proposed a spectral tracer for terrestrial DOM in river-influenced ocean margins based on the spectrophotometric measurement of the spectral slope coefficient of chromophoric DOM (CDOM) between 275 and 295 nm ($S_{275\text{-}295}$). This method, however, is based on the assumption that the kinetics of the two main processes driving the degradation of terrestrial DOM, namely photodegradation of CDOM and microbial degradation of the non-chromophoric components, are similar on the timescales of ocean margin dynamics (Fichot and Benner, 2012). Although not mentioned in their report, it also assumes that the extent of degradation of the chromophoric and non-chromophoric components is similar, therefore the complete removal of chromophoric DOM would also suggests the complete removal of photochemically and microbially recalcitrant DOC in riverine DOM. These assumptions have not been systematically verified.

Stable isotopes of carbon are typically used to trace terrestrial DOM in coastal, estuarine and marine systems since they are thought to incur little to no change in their isotopic signature upon partial OC degradation (Druffel et al., 1992; Maher and Eyre, 2011; Raymond and Bauer, 2001a; Raymond and Bauer, 2001b). Photochemical transformations have however been shown

to shift the stable isotope signature of DOC derived from a plant leachate or collected from a humic lake and three rivers of different size (Opsahl and Zepp, 2001; Osburn et al., 2001; Spencer et al., 2009; Vähätalo and Wetzel, 2008).

Direct (complete mineralization to CO_2) or indirect (increase in the bioavailability of DOC followed by rapid biological mineralization to CO_2) photochemical transformations are important pathways in the mineralization of terrestrial DOM (Miller and Zepp, 1995; Mopper et al., 1991; Spencer et al., 2009). Together, these processes can possibly explain the removal of up to 80% of riverine DOC (Obernosterer and Benner, 2004). However the remaining, non-photoreactive and biologically recalcitrant DOC, representing >20% of the global riverine input, is still large enough to support more than half the steady-state turnover of oceanic DOC (0.1 x 10^{15} g C yr^{-1}) (Williams and Druffel, 1987). Thus it remains puzzling that terrestrial DOM accounts for such a small percentage of oceanic DOM. It is possible that riverine DOM remains in oceanic waters but is altered beyond recognition through photodegradation and bacterial relabeling during passage in the microbial loop, allowing it to escape from the analytical windows of traditional measurement methods.

In the present work, we study the effect of photochemical and microbial transformations on isotopic signatures of riverine DOC. We measured the potential isotopic shifts of DOC $\delta^{13}C$ during 1) abiotic photochemical mineralization of a portion of the DOC pool to CO_2 and other purgeable organics and inorganics associated with a nearly complete photochemical decomposition of riverine chromophoric DOM (CDOM) and 2) the bacterial mineralization of biologically labile DOC produced during the photochemical transformation of DOC. The riverine DOC was collected from ten major rivers, cumulatively representing 1/3rd of the world's freshwater discharge and 28% of the marine input of continental DOC (Cauwet, 2002) allowing

us to appropriately constrain the continental end-member. We calculate the percentage of DOC that resists photochemical and microbial degradation and measure the $\delta^{13}C_{DOC}$ signature of DOC before and after the photochemical treatment and microbial degradation. We show how a photochemical shift in $\delta^{13}C_{DOC}$ signatures influences the use of ^{13}C isotopes for quantifying terrigenous DOC in the oceans.

Materials and methods

Riverine samples

The rivers selected in this study are responsible for nearly one third of both freshwater discharge and DOC flux to the ocean, respectively (Table 1). They drain 25% of the continental land area in a wide range of ecosystems and climates on five continents (Milliman and Farnsworth, 2011). The selected rivers provide a representative end-member of riverine DOC, which can be used as a predictive sample set for the behavior of riverine DOC in oceanic waters.

A water sample was collected from each river during the season of high discharge in 10-L polyethylene containers (cleaned with detergent, rinsed with acid and Milli-Q water). All samples were collected in one location upstream from the fresh-water – salt-water transition zone. The samples were thus representative of the DOC discharged to the coastal ocean at the time of sampling. The Amazon River is the only exception: owing to sampling constraints, it was collected at two locations upstream of the confluence point of Rio Negro and Rio Solimoes. Samples from the two locations were mixed in an appropriate ratio (1:3 Rio Negro to Rio Solimoes) to represent the bulk Amazon River discharge.

Table 5-1: Concentration and $\delta^{13}C$ of total and NL-DOC reactivity classes for each riverine sample. Standard deviations are given in parentheses. $\delta^{13}C$ values are not given when NL-DOC concentrations were below 1 mg/L, due to the poor reproducibility of these measurements. The percentage of photodegraded and microbially degraded NL-DOC represents the losses of NL-DOC occurring each of these processes and average values are normalized to discharge rates (Cauwet, 2002) and NL-DOC concentrations.

River name	Latitude	Longitude	Discharge rate ($km^3\ yr^{-1}$ or $10^{12} L\ yr^{-1}$)	NL-DOC ($mg\ L^{-1}$)	NL-DOC $\delta^{13}C$ (‰)	Photooxidation (% loss)	Photooxidation $\delta^{13}C$ of residual (‰)	Microbial degradation (% loss)	Microbial degradation $\delta^{13}C$ of residual (‰)
Amazon	03°08'00''S	59°54'10''W	5780	4.0 *(0.1)*	-29.0 *(0.2)*	37.4 *(0.7)*	-27.4 *(0.0)*	33.0 *(3.0)*	-27.4 *(0.3)*
Danube	45°13'38''N	28°44'05''E	198	2.3 *(0.0)*	-28.4 *(0.2)*	33.5 *(4.2)*	-27.0 *($0._2$)*	33.1 *(0.3)*	*n.a.*
Yangtze	31°45'49"N	121°2'22"E	925	1.7 *(0.0)*	-27.6 *(0.4)*	34.5 *n.a.*	-27.1 *n.a.*	28.7 *(0.6)*	*n.a.*
Congo	04°18'18''S	15°28'32''E	1300	5.9 *(0.1)*	-27.1 *(0.2)*	43.4 *(0.1)*	-25.4 *(0.5)*	37.7 *n.a.*	-26.2 *n.a.*
Parana	34°18'07''S	58°32'47''W	470	2.9 *(0.0)*	-27.0 *(0.0)*	30.9 *(2.1)*	-24.0 *(0.0)*	28.7 *n.a.*	-26.5 *n.a.*
Lena	71°54'14''N	127°15'16''E	505	5.4 *(0.2)*	-26.9 *(0.1)*	29.6 *(1.8)*	-25.4 *(0.1)*	25.0 *(0.0)*	-25.5 *(0.0)*
Mississippi	29°02'20''N	89°19'20''W	410	3.4 *(0.1)*	-26.6 *(0.1)*	25.1 *(2.1)*	-25.7 *(0.4)*	31.7 *(1.6)*	*n.a.*
Ganges-Brahmaputra	23°34'12"N	90°10'54"E	971	0.8 *(0.0)*	-26.5 *(0.9)*	34.0 *(4.4)*	-25.8 *(0.4)*	21.9 *(2.07)*	*n.a.*
St. Lawrence	46°54'45''N	70°52'32''W	413	3.6 *(0.1)*	-26.1 *(0.2)*	16.0 *n.a.*	-25.5 *n.a.*	31.9 *(0.8)*	-25.2 *(0.0)*
Mekong	11°33'28''N	104°56'53''E	666	1.4 *(0.1)*	-26.0 *(0.2)*	16.6 *n.a.*	-24.5 *n.a.*	25.1 *n.a.*	*n.a.*
Weighted average				**3.6** ***(0.1)***	**-28.1** ***(0.2)***	**35.9** ***(1.8)***	**-26.6** ***(0.2)***	**32.6** ***(2.4)***	**-26.2** ***(0.9)***

The polyethylene containers were cleaned at the University of Helsinki and shipped to the local operators at each river. The containers were filled in the center of the stream by direct immersion below the surface from a boat, except for the Mississippi and St. Lawrence Rivers where near surface water (about 3 m below the surface) was collected with Niskin bottles and directly transferred to the polyethylene containers. All samples were immediately placed in a box to shield the water from sun and artificial light. They were left unfiltered/unkilled upon shipment and storage at the University of Helsinki (the time lag between sampling and measurement was between 80-390 days) so that the most labile fraction of the DOC (L-DOC) in all samples was decomposed prior to the measurement reported in this study (see below). The samples were not refrigerated during transportation (about one week in most cases) but they were stored at 4°C in the dark upon arrival in Helsinki. The same water samples used here have been also examined for the concentration of dissolved black carbon and the contribution of iron to CDOM (Jaffé et al., 2013; Xiao et al., 2013). Additional samples from the St. Lawrence River were collected at the same time as the polyethylene container, filtered on-board (pre-combusted GF/F filters, 0.7 µm nominal pore size), acidified with ultrapure HCl to a pH <2, and stored in pre-combusted glass vials.

Irradiation experiment followed by a bioassay

All samples were sterile filtered (0.2 µm, Sartobran 300, Sartorius) and separated into two batches of duplicates: one duplicate set of irradiated samples for each river, to be compared to a corresponding duplicate set of dark control samples. Irradiated samples were placed in clean and combusted (> 2 h, 450°C) UV-transparent 750-mL quartz vials fitted with ground glass stoppers. A headspace corresponding to 10% of the vial internal volume was filled with O_2 gas, and replenished after 4 days of irradiation to support complete oxidation of the UV-sensitive

DOM fraction (Vähätalo and Wetzel, 2008). The samples were placed horizontally 1 cm below the surface of water on a stainless steel grid in a flow-through pool of tap water regulated to 24.5 ± 1.0°C. They were exposed for 10 days to simulated solar radiation adjusted to a power that mimics the global mean of a half-year UV dose of solar radiation. The simulated solar radiation was generated using a metal halide lamp (Thorn OQ 1000, UK) and fluorescent tubes (UVA-340, Q-Lab Corp., Canada), and measured with a Macam SR 991 spectroradiometer in air 2-cm above the quartz flasks. The spectral irradiance of the artificial light source comprised the photochemically active part of UV radiation present in natural sunlight but excluded any environmentally non-relevant short-wavelength UV radiation absent from solar radiation incident to the ocean (Figure 5-1B) (Chu and Liu, 2009). Dark controls were treated in the same way (sterile filtered, but kept at 21.6 ± 2.1°C in the dark). We preserved samples with ultrapure HCl (pH < 2) for DOC concentration and $\delta^{13}C$ measurements at the beginning and end of the irradiation.

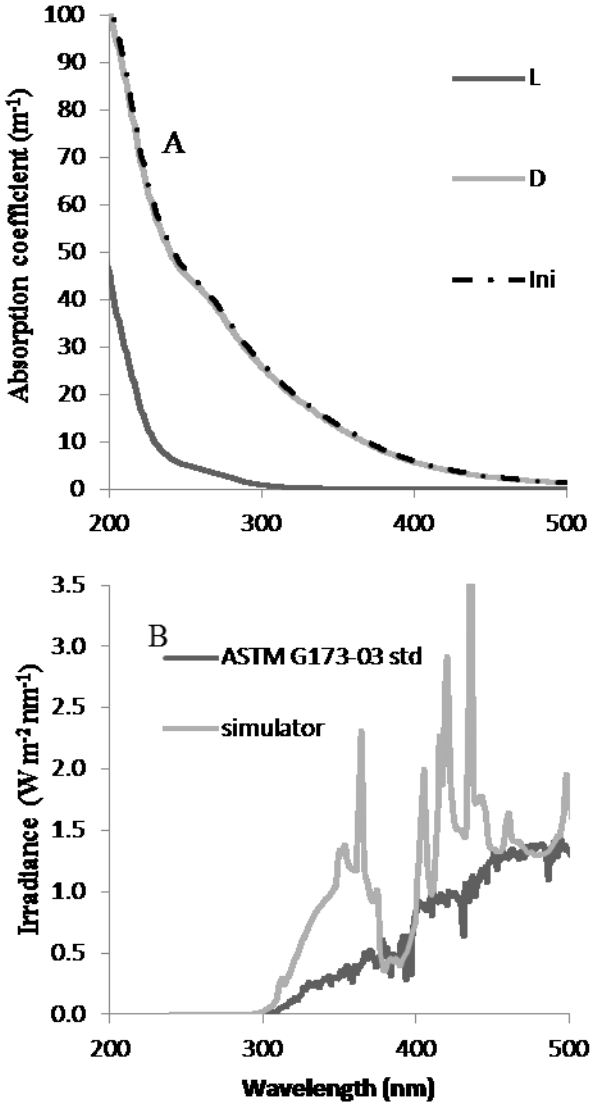

Figure 5-1: (A) Absorption coefficients of chromophoric dissolved organic matter in the initial (Ini), the irradiated (L) and the dark control (D) of Amazon River, and (B) the spectral irradiance of solar simulator (simulator) and natural solar radiation (ASTM G173-03 std; Lu et al., 2013). Note that the absorption spectra for Ini and D are almost perfectly superimposed in (A).

In order to quantify the microbial mineralization of labile DOC produced during the abiotic photochemical transformation of riverine DOM, we introduced a microbial inoculum into the irradiated and the dark control samples. Each sample received KH_2PO_4 to the final concentration of 133 P μg L^{-1} and unfiltered water from its corresponding river (1% vol/vol) as a source of phosphorus nutrient and microbial inoculum, respectively. These bioassay flasks contained an

air headspace and were incubated in the dark at 22.0 ± 0.5 °C. After 28 days of incubation, the samples were filtered and preserved with HCl for the measurement of DOC concentration and its $\delta^{13}C$ signature as explained above.

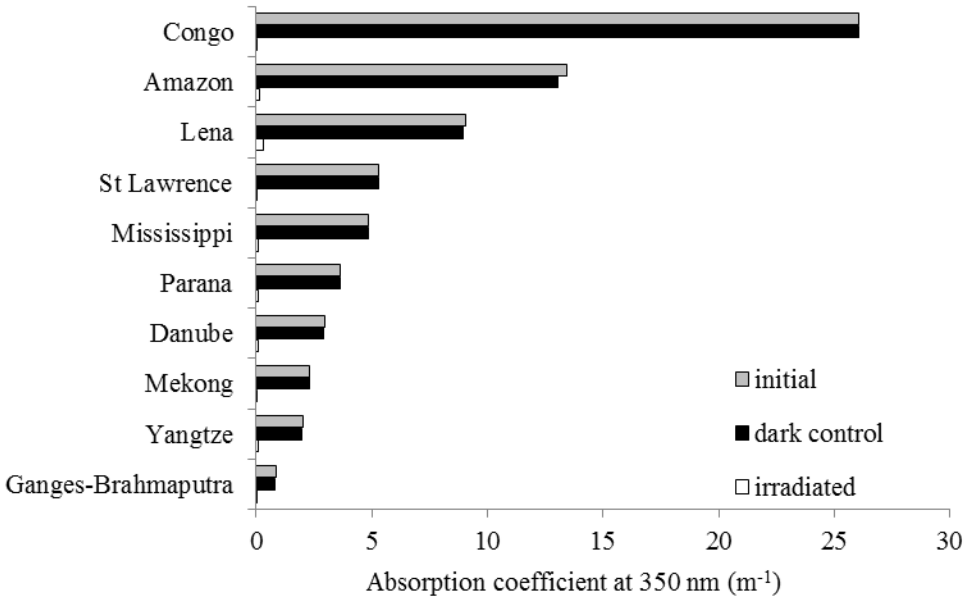

Figure 5-2: Absorption coefficient of chromophoric DOM at 350nm in the samples before (initial, grey) and after irradiation experiment in the irradiated (white) and the dark controls (black)

Note that the biologically labile organic compounds (L-DOC) present in the original water samples were degraded during sample shipment and storage through microbial processes that do not affect $\delta^{13}C$ signature of DOM to a significant extent (Lu et al., 2013; Obernosterer and Benner, 2004; Stutter et al., 2013). The DOC sample that was used at the start of the irradiation experiment therefore corresponds almost entirely to non-biologically labile DOC (NL-DOC). NL-DOC comprises semi-labile and refractory DOC, which have degradation rates on the order of years to centuries (Obernosterer and Benner, 2004). Note also that we report changes in the concentration and the $\delta^{13}C$ signature of NL-DOC ($\delta^{13}C_{NL\text{-}DOC}$) during a two-stage process: 1) the

photobleaching of NL-DOC under sterile conditions, followed by 2) the biodegradation of the residual non-photosensitive organic compounds. Complete photobleaching causes the mineralization of the chromophoric DOC pool and/or its transformation to non-chromophoric DOC molecules. The DOC that is impervious to photooxidation is measured in the irradiated DOC sample (irr-DOC). The DOC that resists both the photobleaching and microbial degradation treatments because it is both transparent to UV-radiation and biologically recalcitrant is defined as the recalcitrant DOC fraction (R-DOC). R-DOC is therefore the residual DOC, measured directly after sequential treatments.

In natural systems, the degradation of NL-DOC by photooxidative and microbial pathways take place simultaneously rather than consecutively. Our experimental design thus probably overestimates the relative importance of photochemical degradation since in natural environments, there is competition for DOC substrates that are both bioavailable and photodegradable during daily light/dark cycles. However, as photobleaching leads to significant changes in $\delta^{13}C$ signatures while the effect of biodegradation is much smaller and inconsistent (Table 1), we focused mostly on $\delta^{13}C$-DOC shifts occurring during photobleaching when interpreting the fate NL-DOC in the ocean.

High- temperature catalytic oxidation DOC-IRMS measurements

A combustion total organic carbon (TOC) analyzer (OI Analytical Model 1010, College Station, TX) was modified to reduce background contamination from atmospheric CO_2 by replacing all gas-permeable polytetrafluoroethylene (PTFE) tubing with polyether ether ketone (PEEK) tubing. Ultra-high purity oxygen carrier gas and platinum-coated silica particles (5% Pt (w/w)) were used for combustion of samples. Prior to analysis, the instrument furnace was kept at temperature of 680^{o}C, under clean O_2 for several hours, followed by the injection of a total of about 100 blanks,

ensuring low background CO_2 levels. Trapping the background CO_2 without injecting a liquid sample on the combustion column produced a peak corresponding to 0.18 µgC. The results obtained for the samples were corrected for this low background contribution.

The TOC analyzer was interfaced to an Isoprime isotope ratio mass spectrometer (IRMS) through a Graden instrument chemical CO_2 trap (GD-100), which allows quantitative recovery of CO_2 while switching the carrier gas from ultra-high purity oxygen to ultra-high purity helium. Each sample injection therefore provided both the DOC concentration (by NDIR on the TOC analyzer and by the measured current on the IRMS) and $\delta^{13}C$ isotopic composition. The correlation coefficient between the NDIR and voltage-derived concentrations was > 0.98. Dry certified sucrose standard ($\delta^{13}C$ = -10.45 ± 0.03‰) from the International Atomic Energy Agency (IAEA-CH-6) and β-alanine (Sigma-Aldrich, -26.18 ± 0.33‰ standardized in-house against several certified materials by elemental analysis-IRMS) were dissolved in ultrapure water and used as calibration and reference compounds.

The injection volume was adjusted to 750 µL, generating enough CO_2 for high precision concentration and isotopic measurements without compromising combustion efficiency. Twin vials of each sample were run in either duplicate or triplicate, yielding standard deviations of ≤ 0.15 mg/L and ≤ 0.3 ‰ for concentration and isotopic measurements, respectively. Isotope data is reported with standard notation ($\delta^{13}C$) in parts per thousand (‰) relative to the Pee Dee Belemnite standard.

Results

Riverine NL-DOC concentrations and $\delta^{13}C_{NL\text{-}DOC}$ signatures

The measured NL-DOC concentrations in the rivers examined ranged from $0.8 \pm 0.0_3$ mg L^{-1} (Ganges-Brahmaputra) to 5.9 ± 0.1 mg L^{-1} (Congo) with a yearly discharge-weighted average of 3.6 ± 0.1 mg L^{-1} (Table 5-1) for all rivers. The $\delta^{13}C_{NL\text{-}DOC}$ signatures ranged from -29.0 ± 0.2 ‰ (Amazon) to -26.0 ± 0.2 ‰ (Mekong) with a yearly discharge-weighted average of -28.1 ± 0.2 ‰ (Table 5-1). These weighted average NL-DOC concentrations and $\delta^{13}C_{NL\text{-}DOC}$ values could be used as a first-order estimate for terrestrial riverine DOC discharged in the ocean. Additional studies are however needed to improve the accuracy of this estimate by taking into account the quantitatively important rivers not sampled in this project, as well as potential seasonal and inter-annual variability in NL-DOC concentrations and $\delta^{13}C_{NL\text{-}DOC}$ signatures.

The concentrations of NL-DOC and $\delta^{13}C_{NL\text{-}DOC}$ signatures reported in Table 5-1 do not include the biologically labile fraction of DOC (L-DOC). L-DOC is rapidly consumed by microbes (hourly to daily time scales; in this study, L-DOC was biodegraded during the shipping and storage of unkilled samples), therefore it is too reactive to contribute to the oceanic reservoir of DOC. L-DOC was not measured directly in samples other than the St. Lawrence River where the L-DOC fraction accounted for 19 ± 1% (n=3) of total DOC (measured on separate aliquots collected on the sampling day), consistent with previously reported estimates of 13 and 28% in lacustrine and swamp settings (Obernosterer and Benner, 2004) or 22 ± 12% of total DOC in the coastal ocean (Lønborg and Álvarez-Salgado, 2012).

The $\delta^{13}C_{DOC}$ signatures measured for St. Lawrence River total DOC (including L-DOC, -26.4 ± 0.4‰) and NL-DOC (-26.1 ± 0.2‰) suggest that the removal of L-DOC by biodegradation does

not alter $\delta^{13}C_{DOC}$ signatures, in agreement with several earlier studies (Lu et al., 2013; Obernosterer and Benner, 2004; Stutter et al., 2013).

Effect of irradiation and microbial incubation on NL-DOC concentration and $\delta^{13}C$ signature

Irradiation with artificial sunlight destroyed photochemically the chromophores that absorbed in the UV and blue regions of the spectrum, nearly completely extinguishing the DOC absorption at > 350nm for all samples (Figures 5-1 and 5-2). A fraction of the DOC in samples was converted to CO_2 (or other small purgeable organic molecules) during the irradiation, as indicated by the lower irr-DOC concentration compared to NL-DOC. The loss of NL-DOC by photomineralization ranged from 16% (St. Lawrence) to 43% (Congo), with an average of 36% for the all rivers examined (Table 5-1), corroborating previously reported literature values (Obernosterer and Benner, 2004). No well-stained bacteria were found in the irradiated samples by epifluorescence microscopy, indicating that the partial mineralization of NL-DOC (to DIC), as well as any structural, spectral and isotopic modifications of the NL-DOC pool were incurred due to a purely abiotic photochemical process. In contrast to the irradiated samples, the light absorption by CDOM or the concentration of NL-DOC did not change significantly in the dark control samples during the ten-day irradiations (Figures 5-2 and 5-3B).

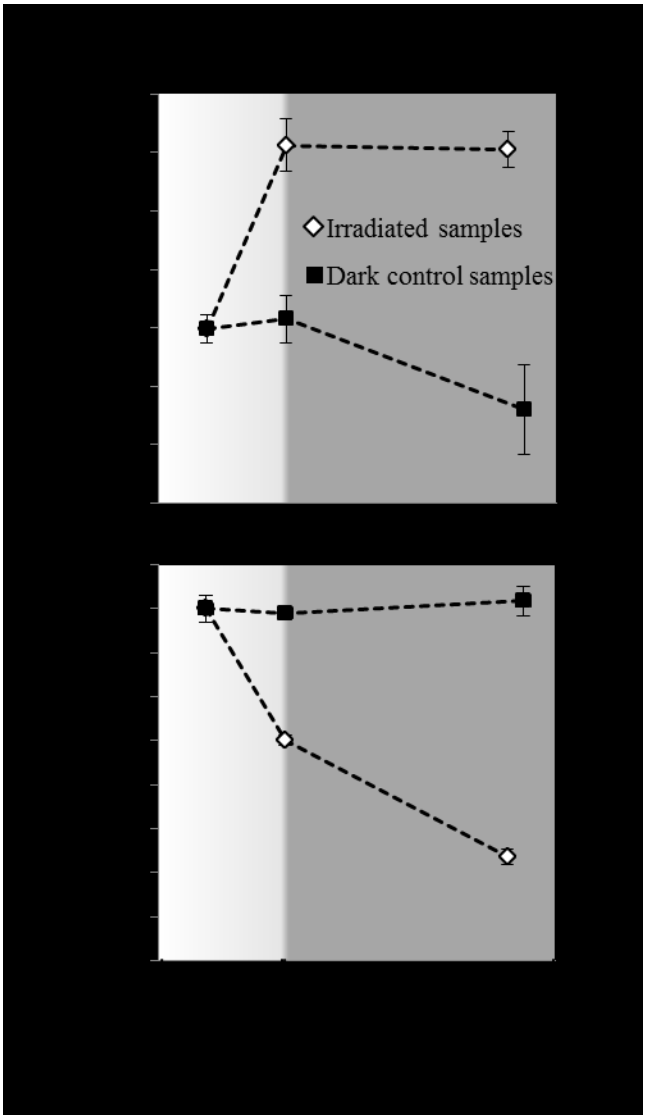

Figure 5-3: Concentration of NL-DOC and its $\delta^{13}C$ value in a representative riverine sample (the Amazon River) during the 10 day abiotic photooxidation and the following 28-day microbial degradation initiated by inoculation with unfiltered riverine water containing indigenous bacteria. Irradiated samples are shown in white, while the dark controls are shown in black)

In our study, $\delta^{13}C_{irr\text{-}DOC}$ was consistently enriched relative to NL-DOC in every irradiated riverine samples by 0.5 ‰ (Yangtze) to 2.3 ‰ (Parana) indicating the mineralization of a pool of DOC that was depleted relative to NL-DOC. The complete mineralization of photo-sensitive DOC therefore shifted the signature of the average riverine DOC by 1.5 ‰ (from -28.1 ‰ to -26.6 ‰, Table 5-1 and Figure 5-4). Dark control samples did not change during the course of the

irradiation step as they were protected from the radiation and sterile filtered. Consequently, no changes in the light absorption by CDOM or the concentration of DOC incurred in the dark control samples during the ten day irradiation (Figures 5-2 and 5-3B).

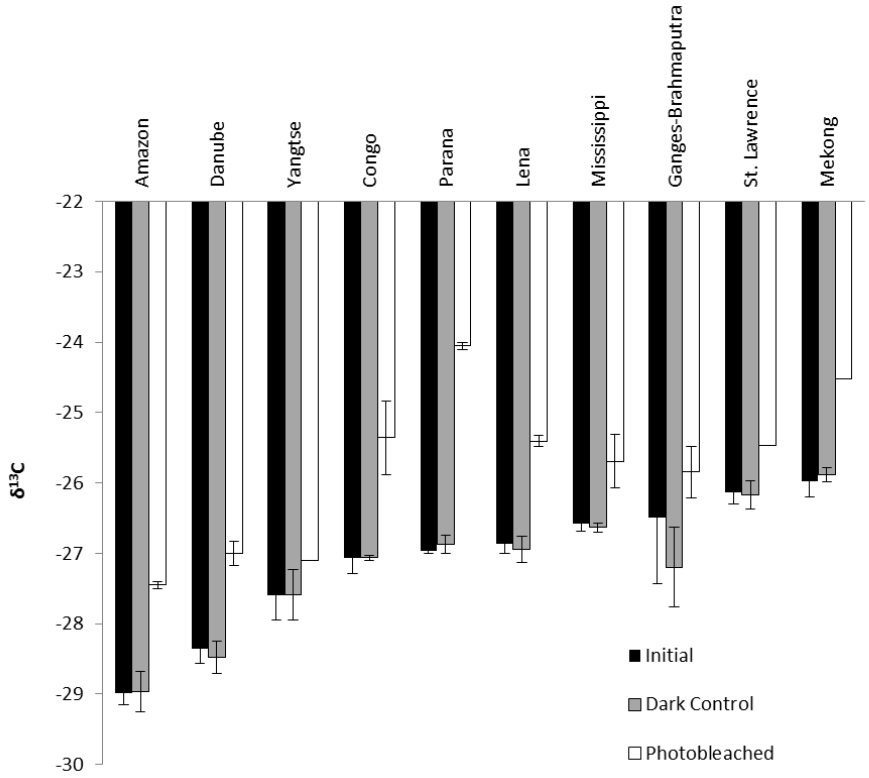

Figure 5-4: Change in NL-DOC isotopic signature ($\delta^{13}C$) as a result of photodegradation. Error bars represent standard deviation

UV radiation produced bioavailable, labile DOC that was consumed during the course of theincubation. This DOC pool represented between 21.9 % (Ganges-Brahmaputra) and 37.7 % (Congo) (average of 32.6 ± 2.4%) of the NL-DOC pool (Figure 5-3B and Table 5-1). The corresponding microbial consumption in the dark control samples was negligible (5 ± 7% of NL-DOC in all ten rivers) as exemplified for the Amazon River in Figure 5-3B, indicating the absence of biologically labile compounds within non-irradiated samples. After the completion of the irradiation/inoculation experiment, a residual, recalcitrant DOC fraction (R-DOC) remained. The

R-DOC fraction ranged between 18.9% (Congo) and 58.3% (Mekong) with a weighted average of 31.5 ± 1.5% (Figure 5-5, Table 5-1).

The NL-DOC pool is therefore separable into 3 fractions, each comprising roughly one third of the DOC: 1) a fraction that is directly mineralized to DIC (or degraded into small purgeable organics) during photobleaching, 2) a fraction of DOC that becomes labile as a result of UV-induced molecular transformations and 3) a residual, recalcitrant fraction (R-DOC).

Riverine NL-DOC samples that were most depleted in ^{13}C contained the smallest R-DOC fraction (Figure 5-5 A). The Congo River was an exception to the $\delta^{13}C$ trend (Figure 5-5 A), experiencing the highest NL-DOC losses of all rivers but displaying relatively enriched values. The fraction of R-DOC was also related to the amount of CDOM indicated by an absorption coefficient at 350 nm ($aCDOM_{350}$) of NL-DOC (Figure 5-5 B).

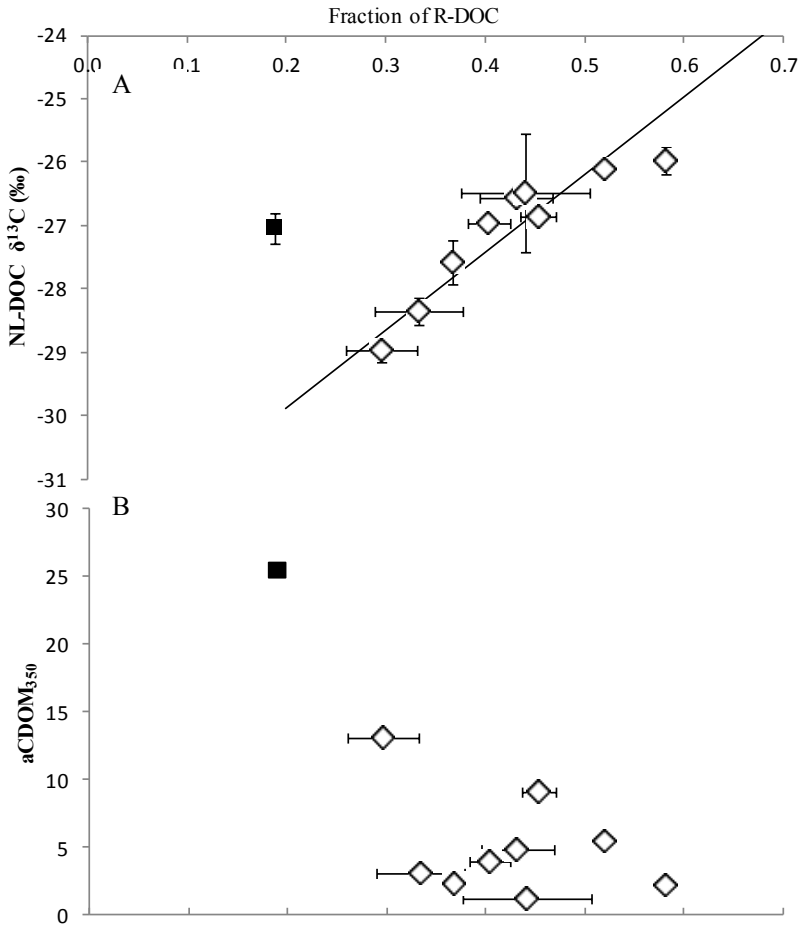

Figure 5-5: (A) Fraction of NL-DOC resistant to photooxidation followed by bacterial incubation (R-DOC) as a function of the $\delta^{13}C$ signature of NL-DOC, and (B) the absorption coefficient at 350 nm for all riverine samples. The error bars in (A) represent the propagated uncertainty for the fraction of NL-DOC remaining following the two treatments. The R-DOC fraction was calculated using the percentages of NL-DOC degraded during photobleaching and microbial degradation in Table 5-1 (100% - %photobleached - %microbially degraded, divided by 100). The trendline describes a Model II linear regression model including all data except the Congo River.

Discussion

Photochemically induced shift in $\delta^{13}C_{NL\text{-}DOC}$ signatures and optical parameters

Our irradiation experiment was designed to simulate the photochemical transformations of riverine DOC upon photobleaching of CDOC in the mixed layer of the coastal ocean (Figures 5-1 and 5-2). Photochemical destruction by simulated solar radiation most effectively targets chromophores that absorb in the regions of the spectrum that overlap with the most intense

irradiance bands (Figure 5-1A) and results in the virtually complete loss of DOC absorption at these wavelengths. We observed the nearly complete disappearance of the terrestrial optical signal (loss of DOM absorption at 350 nm ($aCDOM_{350}$)) for all riverine samples (Figure 5-2), which has previously been demonstrated by other irradiation experiments and field studies measuring CDOM *in-situ* or by remote sensing (Fichot and Benner, 2012; Nelson et al., 2010; Vähätalo and Wetzel, 2008; Vodacek et al., 1995). It is known that photochemical reactions specifically target certain molecular moieties/types, absorbing light in the blue and UV region of the spectrum (high $a_{\lambda<350\ nm}$) (Mopper and Kieber, 2002). The chromophoric DOC component constitutes the major portion of the organic carbon in many lakes, rivers, and even some coastal waters, and is structurally similar to soil humics, with a characteristic brown color (Blough and Del Vecchio, 2002; Hedges and Oades, 1997). It is composed of a mixture of lignocellulose-derived polyelectrolytes that result mainly from the decay of terrestrial vegetation and aquatic detritus (Dittmar et al., 2007; Gonsior et al., 2008). The photobleaching of CDOM was concomitant to the photochemical mineralization of a portion of NL-DOC, as illustrated by a loss of DOC in the irradiated samples (irr-DOC) (Figure 5-3B and Table 5-1). The photomineralization of the NL-DOC pool ranged from 16% (St. Lawrence) to 43% (Congo), with an average of 36% for the all rivers examined (Table 5-1).

A removal process, such as photooxidation, that targets specific types of molecules, ultimately causes a change in the chemical composition of DOC in the irradiated samples. This change in the molecular makeup of DOC was reflected by an isotopic enrichment from $\delta^{13}C_{NL\text{-}DOC}$ to $\delta^{13}C_{irr\text{-}DOC}$ following photodegradation (0.5 ‰ (Yangtze) to 2.3 ‰ (Parana); Table 5-1 and Figure 5-4). The average riverine $\delta^{13}C_{NL\text{-}DOC}$ shifted by 1.5 ‰ (from -28.1 ‰ to -26.6 ‰; $\delta^{13}C_{NL\text{-}DOC}$ and $\delta^{13}C_{irr\text{-}DOC}$ are statistically different at a 99% confidence interval, Table 5-1 and Figure 5-4). Other studies have also highlighted similar shifts towards heavier δ^{13}C-DOC values upon

photochemical mineralization of DOC. These shifts have averaged 6 ‰ for a plant leachate, 1.2 ‰ for a humic lake, 0.7 ‰ for the Altamaha River, 1.6 ‰ for the Satilla River, and 3.1 ‰ for the Congo River (Lu et al., 2013; Opsahl and Zepp, 2001; Osburn et al., 2001; Spencer et al., 2009; Vähätalo and Wetzel, 2008). The photochemical isotopic shift measured in this study for the Congo River was not as pronounced as reported by Spencer et al. (2009) for the same river (1.7 ‰ *vs.* 3.1 ‰, respectively). This apparent disagreement may be related to differences in the temperature and the source of irradiation, but more likely to different initial δ^{13}C-DOC signatures in the two studies (-29.2 ‰ in this study *vs.* -27.1 ‰ for Spencer et al., 2009); the δ^{13}C signature of irr-DOC was similar in both studies (-26.2 ‰ *vs.* -26.3 ‰). The δ^{13}C signature of total DOC can vary by few ‰ at least in headwaters catchments during storm events (Lambert et al., 2013) and at the mouth of Arctic rivers between rivers and/or seasons (Neff et al., 2006; Raymond et al., 2007), with more depleted signatures corresponding to recently synthesized fresh plant materials.

In our study, $\delta^{13}C_{irr\text{-}DOC}$ of irradiated riverine samples was consistently enriched relative to $\delta^{13}C_{NL\text{-}DOC}$ (Table 5-1, Figure 5-4). The enriched δ^{13}C of UV-resistant irr-DOC relative to NL-DOC occurs due to the mineralization of ^{13}C-depleted NL-DOC components, varying between -25.8‰ and -33.9‰ and averaging -30.8‰ (calculated by isotopic and mass balances of NL-DOC and irr-DOC from the 10 studied rivers). Naturally photosynthesized ^{13}C-depleted components of terrestrial plants include, amongst others, macromolecular aromatic compounds such as lignin, tannins and cutins, which are depleted by 4-7‰ relative to the bulk plant material (Goñi et al., 2005; Hayes, 2001). It is possible that partial photooxidative breakdown can damage these compounds sufficiently to produce low molecular weight, oxygenated compounds that bear little or no resemblance to their parent molecules, but that match closely the small, molecularly uncharacterized molecules that make up the bulk of deep-ocean DOC (Benner et al., 1997).

Photobleaching can therefore simultaneously explains the three main changes in DOC that make riverine DOC appear deceivingly more marine in nature: 1) the decrease in average molecular size (Dittmar et al., 2007; Hernes and Benner, 2003; Opsahl and Benner, 1998); 2) the reduction in the abundance of aromatic/unsaturated functionalities that absorb UV light (such as lignin (Vähätalo et al., 1999); and 3) the overall enrichment in $\delta^{13}C$.

Does biodegradation shift the $\delta^{13}C$ signature of terrestrial NL-DOC?

Photochemical enhancement of DOM bioavailability has previously been shown to be an important factor in the alteration of estuarine and coastal heterotrophy (Chin-Leo and Benner, 1992; Vähätalo et al., 2011; Zepp, 2005). We therefore extended the irradiation experiment with a bioassay to assess microbial decomposition of irradiated DOC samples (irr-DOC). Microbes consumed photo-produced, labile DOC, comprising between 21.9 % (Ganges-Brahmaputra) and 37.7 % (Congo) (average of 32.6 ± 2.4%) of the initial NL-DOC sample (Figure 5-3B and Table 5-1), a DOC fraction that was similar in size to the directly photo-mineralized DOC (Table 5-1). Microbial consumption in the corresponding dark control samples was negligible (5 ± 7% of NL-DOC in all ten rivers, data not shown) as exemplified for Amazon in Figure 5-3B. Our results are in agreement with earlier studies, which have found labile photoproducts to be quantitatively important components of DOC photooxidation (Aarnos et al., 2012; Obernosterer and Benner, 2004; Pullin et al., 2004; Vähätalo et al., 2003).

In the samples from Amazon, Lena and St. Lawrence rivers, the isotopic shifts associated to the mineralization of labile photoproducts were smaller than the average standard deviation of $\delta^{13}C_{DOC}$ measurements (≈ 0.3‰) (Table 5-1). These negligible isotopic shifts are in agreement with the lack of shifts in the biodegradation L-DOC fraction of the St. Lawrence River sample and with data reported in earlier studies (Lu et al., 2013; Obernosterer and Benner, 2004; Stutter et

al., 2013). The $\delta^{13}C$ signature of other two samples, the Congo and the Parana rivers, decreased by 1.2 and 2.5‰, respectively (Table 5-1). Though more work is needed to better understand the reason for this ^{13}C depletion, it could be explained by the consumption of microbially labile photoproducts that are more enriched in ^{13}C, possibly produced by the C4 carbon fixation pathway. Note however that this shift does not affect the main conclusions of this work as the $\delta^{13}C$ signatures of the R-DOC fraction were still less depleted than the initial NL-DOC signatures.

Relationship between NL-DOC photochemical susceptibility and $\delta^{13}C_{NL\text{-}DOC}$

The extent of photodegradation of riverine samples was evaluated by the concentration of the residual UV and microbially-resistant component (R-DOC). R-DOC was inversely correlated to absorption of NL-DOC at 350 nm ($aCDOM_{350}$) (Figure 5-5B). As aromatic compounds such as lignin are the primary components of DOC that absorb light (Hernes and Benner, 2003), it is likely that samples with the lowest relative R-DOC contribution contain the freshest terrestrial NL-DOC (less photobleached) collected in rivers with low residence time and/or efficient shielding from light (DOM self-shielding, high particulate loads and/or forested banks).

Riverine NL-DOC samples that were most depleted in ^{13}C had increased susceptibility towards direct abiotic photodegradation and photo-production/biodegradation of labile DOC compounds (Figure 5-5 A). The initial $\delta^{13}C_{NL\text{-}DOC}$ was most depleted (-29.0‰; Table 5-1, Figure 5-5 A) in the Amazon River sample, where the fraction of residual DOC (R-DOC) resisting photodegradation was low (0.296, Figure 5-5A); abiotic photooxidation and the following microbial decomposition accounted for fractions of 0.374 and 0.330, respectively (Table 5-1). The fraction of R-DOC was highest (0.583) in the river sample with the highest initial $\delta^{13}C_{NL\text{-}DOC}$ (-26.0‰; Mekong, Table 5-1, Figure 5-5 A). Plots of the fraction of R-DOC versus $\delta^{13}C_{NL\text{-}DOC}$ for all rivers (the Congo River was treated as an outlier, see below) yielded a linear plot with a high

correlation coefficient (0.925) and a relatively low standard error on the slope (±1.69 ‰) and y-intercept (±0.73 ‰). The model II linear regression shown in Figure 5-5A (fraction R-DOC = $\delta^{13}C_{NL\text{-}DOC}$ + 32.35)/12.31) could therefore potentially be used as predictive tool for estimating the maximum photochemical and bacterial removal of riverine NL-DOC in the ocean using the $\delta^{13}C_{NL\text{-}DOC}$ of riverine samples.

We draw more information from the Figure 5-5A correlation by operationally separating NL-DOC into two distinct DOC pools: mineralizable DOC (either through abiotic photooxidation or bacterial decomposition) and recalcitrant DOC (R-DOC). Each riverine sample has a different fractional contribution of these 2 DOC pools, depending on light exposure history, residence time and organic carbon source. With no contribution from R-DOC, NL-DOC is the most ^{13}C-depleted ($\delta^{13}C_{NL\text{-}DOC}$ = -32.35 ± 0.73‰). This signature corresponds to purely photodegradable/biodegradable compounds, which explains its closeness to the calculated $\delta^{13}C$ signature of the DIC lost during abiotic mineralization (average $\delta^{13}C_{DIC}$ =-30.8‰). The higher limit of $\delta^{13}C_{NL\text{-}DOC}$ refers to the theoretical signature of purely recalcitrant DOC (-20.04 ± 0.42‰), which is interestingly similar to the signature of purely marine DOC (≈ -20‰, see below; (Bauer, 2002)).

The Congo River was an outlier to the $\delta^{13}C$ trend (dark square in Figure 5-5 A), experiencing the highest NL-DOC losses of all rivers but displaying relatively enriched values. This outlier could result from a relatively high discharge of C4 vascular plant material compared to the other rivers (these plant materials have more enriched $\delta^{13}C$ values but have similar, optical properties and molecular characteristics to those of C3 vascular plants, imparting them with similar propensities toward photodegradation). In one of the main tributaries of the Congo River, the $\delta^{13}C$ signature of total DOC varies greatly between seasons (-30.6 to -25.8‰) depending on

hydrological cycle and multiple sources of DOC with contrasting $\delta^{13}C$ signatures, including C4 plants (Bouillon et al., 2012). The relationship of Figure 5-5A might not apply to rivers carrying a high load of C4 plant-derived materials.

The effect of photochemical $\delta^{13}C$-shift when calculating the contribution of terrestrial NL-DOC to the oceanic DOC reservoir

The results of the present study show that the R-DOC pool is variable, always large and in some cases the dominant pool of riverine DOC. There was a 3-fold difference in the contribution of R-DOC amongst rivers, ranging from 18.9% (Congo) to 58.3% (Mekong) of the NL-DOC pool, with a weighted average of 31.5 ± 1.5% (Table 5-1, Figure 5-5). Though terrestrial in nature, R-DOC is nearly transparent to UV radiation (Figure 5-2) owing to the removal of chromophoric DOC. Our irradiation and incubation experiment therefore predicts that nearly 1/3 of the global riverine export of terrestrial DOC is undistinguishable from the genuine marine DOC pool using the currently used optical and molecular-level methods, which both target the same aromatic, light absorbing moieties derived from lignin-like compounds. As R-DOC is the fraction that is most likely to resist degradation in oceanic waters (slower turnover than the total riverine DOC pool), relying on these tracers to track terrestrial DOC within coastal systems and in the ocean likely greatly underestimated the terrestrial component, especially for waters having an extensive exposure to sunlight.

The highest exposure of DOM to sunlight occurs at the mouth of estuaries and river plumes, where fresh riverine waters are spread into a thin surface layer or are mixed into denser, more translucent saline waters. The exact half-life of riverine CDOM however depends on the depth of the photolytic zone (transparency related to particulate load and DOM shielding), as well as the time of exposure and the intensity of sunlight. Previous studies report CDOM half-lives at

approximately 1.5 yr in irradiated seawater (Miller and Zepp, 1995) or 1000 to 4200 yrs in the mixed world ocean (Mopper et al., 1991). Based on these values, the non-refractory component of terrestrial DOC is not expected to be immediately photodegraded after its discharge into coastal/estuarine waters, but likely succumbs to UV-light or microbial decay during the course of the turnover of the oceanic DOC pool; this is consistent with the nearly complete absence of terrestrial chromophoric/lignin-containing molecules in the mid-ocean and deep bottom waters (Benner et al., 1997; Blough and Del Vecchio, 2002).

We extrapolate the mass of the recalcitrant R-DOC discharged into the global ocean using the size of R-DOC (as a fraction of NL-DOC) measured in our ten large rivers. Firstly, the global riverine NL-DOC export ranges from 0.18 to 0.22 x 10^{15} gC yr^{-1}, assuming that NL-DOC is 72% to 87% (Obernosterer and Benner, 2004) of the total global riverine DOC export of 0.25 x 10^{15} gC yr^{-1} (Cauwet, 2002). The theoretical maximal degradation of NL-DOC resulting from the combination of photobleaching and microbial degradation leaves behind the residual R-DOC fraction of 19 to 58% of NL-DOC, therefore we predict that the riverine R-DOC export ranges between 0.034 and 0.128 x 10^{15} gC yr^{-1}. Though it represents only a fraction of the total riverine DOC export, this yearly contribution of UV-resistant material equates to more than half the estimated turnover of DOC in the ocean (0.1 x 10^{15} gC yr^{-1}) (Williams and Druffel, 1987).

Photochemical degradation shifts $\delta^{13}C_{DOC}$ signatures toward marine values, thus leading to underestimations of the terrestrial component and complicating the use of δ^{13}C-DOC for tracking terrigenous DOC in the ocean. The problem is exacerbated by the fact that the δ^{13}C signatures of both the marine and terrestrial DOC components of oceanic waters are not well constrained (Bauer, 2002). These factors combined preclude the use of a two end-member

isotopic mixing model, as shown in Eq. 1, to directly calculate the fraction (f) of terrestrial DOC in mid-ocean and deep ocean water samples.

$$\partial^{13}C_{measured} = f_{marine}\partial^{13}C_{marine} + f_{riverine}\partial^{13}C_{riverine} \quad \text{Eq.1}$$

The marine DOC end-member is difficult to measure directly, but can be inferred from the predominant C3 fixation pathway in phytoplankton having a theoretical 19‰ fractionation from dissolved DIC in the ocean at temperatures of about 20°C (Bauer, 2002; Yu et al., 2008). A representative signature of -20‰ has been used to track organic matter sources in coastal systems (Bauer, 2002), however the application of a $\delta^{13}C$ signature that is representative of the global marine DOC pool is confounded by factors such as local ocean temperatures and phytoplankton species that influence this value ($\delta^{13}C_{marine}$ ranges from -17.5 to 25‰; most values are between -18 and -22‰) (Fontugne and Duplessy, 1981). Constraining the stable isotopic signature of the riverine end-member is also difficult and requires that natural variability (Bouillon et al., 2012; Neff et al., 2006; Raymond et al., 2007) and processes that potentially shift the $\delta^{13}C$ values be adequately considered.

The importance of photobleaching (both direct photobleaching and bacterial mineralization caused by a photochemically induced increase in bioavailability) as a sink for terrestrial DOC in the ocean is being increasingly recognized. Appropriately constraining the $\delta^{13}C$ signature of the terrestrial DOC component that mixes with oceanic DOC is therefore requires us to account for the isotopic shifts occurring during the photochemical/microbial removal of a large fraction of the riverine DOC pool. Instead of using well-constrained $\delta^{13}C$ values for the marine and terrestrial end-members ($\delta^{13}C_{marine}$ and $\delta^{13}C_{riverine}$, respectively), we used a range of realistic $\delta^{13}C_{marine}$ values to assess the effect of photobleaching of riverine DOC on the calculated proportion of terrigenous DOC on a range of measured $\delta^{13}C$ ($\delta^{13}C_{measured}$) values. Figure 5-6

shows the percent difference in the proportion of terrestrial DOC in the a measured DOC sample calculated using the $\delta^{13}C$ of two possible riverine end-members: 1) the average unaltered riverine water (weighted using NL-DOC concentrations and riverine discharge rates, $\delta^{13}C_{NL\text{-}DOC}$ = -28.1‰), and 2) the average photobleached riverine DOC (irr-DOC), on average 1.5‰ more enriched than the unaltered riverine NL-DOM ($\delta^{13}C_{irr\text{-}DOC}$ = -26.6‰). We plot the percent difference in the calculated proportion of the terrestrial component using our two possible riverine end-members. With theoretical $\delta^{13}C_{measured}$ values that vary between -20 and -26‰ and three possible $\delta^{13}C_{marine}$ values (-18, -20 and -22‰), we obtain relative increases in contributions ranging between 0 and 22% using the new, photobleached riverine $\delta^{13}C_{irr\text{-}DOC}$ value compared to the $\delta^{13}C$ signature of unaltered riverine water ($\delta^{13}C_{NL\text{-}DOC}$). Increases in the % terrigenous contribution were most significant when the signatures of the marine and terrestrial end-members were most alike. It is of note however that these calculations represent maximum values as they are based on the complete photobleaching of the CDOM fraction.

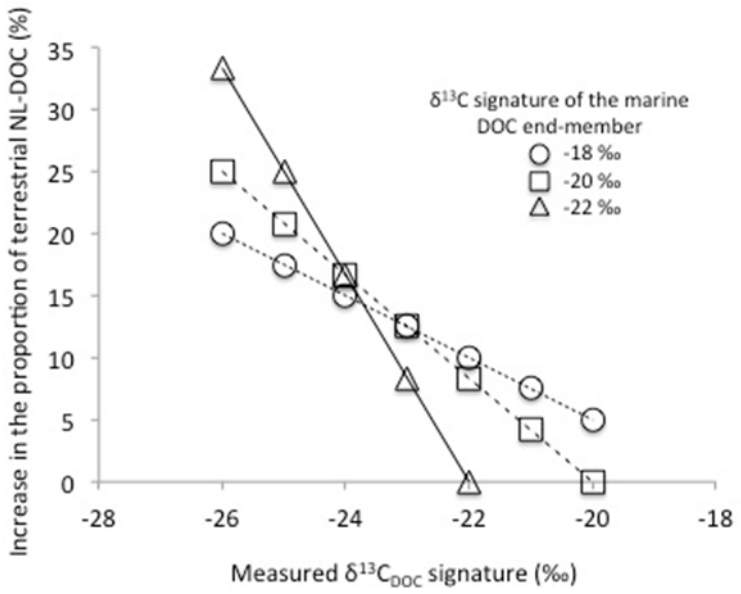

Figure 5-6: Change in the contribution of terrestrial DOC to total (measured) NL-DOC using a simple two end-member mixing model over a range of measured $\delta^{13}C$ signatures for total NL-DOC and three theoretical $\delta^{13}C$ values for the marine DOC end-member. The percentages represent the difference in the calculation of the terrestrial contribution (100 x fraction terrestrial from Eq. 1) when using the weighted average riverine end-member $\delta^{13}C$ signature for unaltered riverine water (-28.1 ‰) or photooxidized and microbially degraded riverine water (-26.2 ‰). The range of $\delta^{13}C_{marine}$ end-member values (-18, -20 and -22 ‰) cover the vast majority of possible signatures for phytoplankton-derived DOC in the world ocean (Bauer, 2002; Yu et al., 2008)

Conclusion

Only about 15% of each river's NL-DOC discharge would have to be incorporated into the oceanic DOC pool to account for a 30% terrestrial contribution (assuming that the turnover time of the terrestrial oceanic component of oceanic DOC is similar to that of total oceanic DOC). This riverine DOC would most likely be composed of the residual, most recalcitrant fraction of the global riverine DOC. This low value is consistent with the exhaustiveness of the photobleaching and other removal processes for terrestrial DOM, such as microbial degradation and salt-induced coagulation/precipitation.

The scarceness of lignin and the $\delta^{13}C$ range measured for marine DOM have however previously precluded a terrestrial DOC component of any significance in the open-ocean (Williams and Druffel, 1987) though it is possible that the breadth and extent of chemical reactions that alter riverine DOC also affect our ability to molecularly and optically characterize the overall composition of DOM and to identify specific terrestrial proxies in photobleached DOM. We predict the ultimate removal of approximately 2/3 of the original NL-DOC pool in the sunlit waters of ocean margins and mid-ocean regions, which suggests that 1/3 of the riverine pool is either undetected in oceanic waters or is in some other way degraded during its travel in oceanic waters. This work is instrumental in constraining photochemically-induced shifts in $\delta^{13}C_{NL\text{-}DOC}$ signatures, providing geochemists with critical information for determining the source and reactivity of different components of oceanic DOM. Accounting for $\delta^{13}C$ shifts also allows tracking more efficiently the transfer of organic matter from land to sea, which is a key link in the global carbon cycle, providing the most important pathway for ultimate preservation of terrigenous production (Hedges, 1992).

The natural variability in the $\delta^{13}C$ signatures of the terrestrial and marine end-members precludes the application of simple two end-members isotopic mixing model to calculate the proportion of terrestrial DOC in the world ocean. However, such model could be exploited on regional scales, in areas where the $\delta^{13}C$ signatures of the end-members are well constrained in time and space. Along with new proxies (Hopmans et al., 2004), methods (Minor et al., 2012) and computer simulations (Belicka and Harvey, 2009) designed to track terrestrial DOM in the oceans, our results contribute to the on-going effort to further elucidate the addition and removal processes of DOM during the turnover of oceanic waters. More specifically, new approaches are needed to detect and quantify the photobleached terrestrial compounds that fall outside of the analytical window of optical and molecular-level methods, which account for

a large and variable proportion of terrestrial DOC (18 to 58% of the NL-DOC fraction for the 10 major rivers studied in this work).

Chapter 6: General conclusions

The objective of this project was to demonstrate that strong interactions exist between OM and iron in sediments which “refractorizes” a large portion of sedimentary OM and allows its preservation. The main focus of our research was to understand the interactions between iron and OM, not only in terms of the mechanism of formations (through adsorption of OM onto iron oxides or through co-precipitation or coagulation of OM and iron(III) at redox interfaces) but also in terms of the nature of the bonds (whether inner-sphere, outer-sphere or electrostatic) and the chemical conditions that favor their formation.

Using a well-established iron reduction method that we have modified to measure concomitant losses of iron (ICP-MS) and OM (Elemental Analysis (EA)) from a series of stabilized sediment samples from a variety of depositional settings, we established that the association of OM with iron was universal and sequesters a quantitatively significant portion of the OM in sediments. The operationally-defined iron-associated OM in extracted sediments was ^{13}C-rich and exhibited a low atomic C to N ratio, possibly indicating the preferential association of carbohydrate and protein-like biomolecules to iron. The large quantity of OC co-extracted with iron, suggests that these interactions form through the coagulation or co-precipitation of both elements rather than through the simple adsorption of OM onto iron oxides.

The main criticism from reviewers of this first paper was that, though we could demonstrate a quantitatively significant association between OM and iron oxides, we could not ascertain the sheltering and preservative effect of these associations for OC, nor could we unambiguously prove inner-sphere complexation. In answer to this critique, we designed an incubation experiment demonstrating that, over a 250 day period, iron-OM interactions increased the longevity and preservation potential of OM in sediment slurries. Like many scientific experiments however, this incubation was more successful at demonstrating a number of

phenomenon that are peripheral to iron's preservative effect. For instance, we showed that an enrichment in reactive iron oxides enhances the solid-solution partitioning of DOM, causing DOM to become immobilized to particle surfaces. Increased DOM retention decreases its mobility and consequently DOM becomes less bioavailable, which possibly enhances carbon sequestration in iron-rich sediments. An additional unexpected effect of iron enrichment in our sediment slurries was the increase in the mineralization rate of organic nitrogen. This effect was contrary to the expected increase in organic nitrogen stability, experienced by organic carbon in the same sediments. Accelerated nitrogen losses were explained by Feammox, an alternative pathway of nitrogen mineralization in sediments that catalyzes the oxidation of ammonium to either nitrate, nitrite or dinitrogen. This process has not yet been demonstrated in unaltered marine sediments.

δ^{13}C-DOC measurements also allowed us to demonstrate an exchange between mineral-bound OM and DOM in sediment porewaters. The direct relationship between porewater DOM and mineral-bound OM, was postulated almost two decades ago by Hedges and Keil (1995), who hypothesized that the large pool of mineral-bound OC exerts a strong control over the concentration and composition of the much smaller pool of porewater DOC. The relationship between these two pools is however often obscured by complex overriding transport processes that lead to the addition or removal of DOC (diffusion, bioirrigation, remineralization) and particulate OC (sedimentation, burial, bioturbation, anabolic uptake). In using an algal tracer having a depleted carbon isotopic signature relative to the native, mineral-bound OM, we could monitor the isotopic composition of DOC in solution. The signature changed from the depleted signature of the tracer to a more enriched signature, as a result of the desorption of native DOM from the sediment. We were also able to show the preferential immobilization of ^{13}C-enriched

DOM through coagulation with iron oxides, corroborating the enriched $\delta^{13}C$ of iron-bound OC shown in Chapter 2.

The need for the $\delta^{13}C$-DOC measurements described in our incubation experiment pushed us to develop a method of analyzing simply and routinely $\delta^{13}C$-DOC in salty solutions. We hyphenated a DOC analyzer to an open-split IRMS using a chemical trap. Using this system, we measured $\delta^{13}C$ in a wide-range of freshwater and saltwater samples. The use of a chemical trap, rather than a cryogenic trap, enabled the facile automation of the DOC-IRMS system, increasing sample throughput, reducing user error and improving reproducibility. Higher sample throughput also allowed for more thorough calibration of the instrument as well as a better understanding of system capabilities.

In contrast to previously described DOC-IRMS methods, which aimed predominantly at proving the feasibility of these measurements, our system is capable of sustaining a large number of sample determinations (weekly, about 150 injections of low concentration salty samples, or > 300 freshwater samples). Until now however, due to the difficulty of $\delta^{13}C$-DOC measurements, there have been only limited measurements of $\delta^{13}C$-DOC in saltwater systems. The small number of $\delta^{13}C$-DOC measurements done since the 1970s, along with lignin biomarker work, point to a nearly purely marine origin for DOM in the open ocean (Bauer, 2002; Druffel et al., 1992) but increased resolution and precision may better constrain the signature of DOC sources and help identify DOC fractionation processes. $\delta^{13}C$-DOC measurements is also a useful technique to track carbon in the mixing water bodies of estuaries and river plumes.

After developing and optimizing the DOC-IRMS system, we were presented with a unique opportunity to participate in an international sampling effort (The Big River Project, launched by Anssi Vähätalo) to study river systems around the world. We used the DOC-IRMS technique to

monitor the isotopic composition of riverine waters during photooxidation with simulated UV light. With our system, we were able to show the ^{13}C-enrichment of DOC of continentally-derived DOC upon photooxidation, which affects the estimation of continentally-derived DOC in the ocean using ^{13}C as a tracer.

Future directions

Offshoots of the main axis of the project have started to take shape in response to a number of unanswered questions. These pertain mainly to the mechanism, formation conditions and persistence of iron-OM interactions as well as their influence on carbon cycling in the environment. Some areas of interest are highlighted here:

1. Redox conditions in various depositional environments alter the chemistry of redox-sensitive elements such as iron, and their possible associations to OM and other elements. "Extreme" depositional settings such as the fluidized mud belts of river deltas as well as sediments underlying anoxic bottom waters contain unusually low and unusually high OM contents respectively. Deltaic muds can quickly alternate between oxic and anoxic conditions, creating an ideal environment for the use of iron oxides as an important electron acceptor. The accelerated breakdown of iron-associated OM in these muds may be a by-product of the utilization of iron oxides as an OM oxidant, which might in part explain the lower OM content of these sediments.

In contrast, in oxygen minimum zones, where anoxic bottom waters begin to impinge on the sediment bed (such as off the western coast of Mexico), we expect iron to play a more limited role in the burial and sequestration of OM. The diagenetic recycling of iron may no longer take place in these sediments but in the overlying water column where iron(II) can diffuse to meet higher oxygen concentrations. We are interested in the effect that these differences may have on the structure of iron(III)-OM complexes.

In chapter 2, we also noted that a significant fraction of the OC of a lake sediment was attached to iron phases, perhaps demonstrating a difference in the mechanism of interaction between iron and OM in lacustrine settings which possibly also reverberates to the greater carbon cycle within these systems.

2. We are also interested in determining the effect of the iron oxide-rich surficial layer of the sediment on fluxes of DOC to oceanic bottom waters. Iron and manganese phases display distinctly higher affinities for DOC than the phyllosilicate minerals that make up the bulk of the mineral matrix of typical sediments. As explained previously, reactive iron and manganese oxides are dissolved reductively in anoxic environments and, upon the diffusion of Fe(II) and Mn(II) to the oxic layer, are re-precipitated as authigenic phases. The redox cycles of iron and manganese have long been recognized to regulate the geochemical behaviour and fluxes of phosphate and various trace metals in sediments. We postulate that the oxide-rich surface sediment layer plays a similarly important role in buffering the fluxes of DOC from sediments to the water column. DOC comprises a complex mixture of fresh and aged/altered organic compounds that exhibit a wide diversity in chemical composition and structure, likely reflected by an equally wide range of adsorption affinities. The preferential binding of specific DOC compound classes to particle surfaces likely leads to molecular and isotopic fractionation of DOC. We hope to design a laboratory experiment to demonstrate the fractionation of the porewater DOC pool passing through iron and manganese-rich sediments (or co-precipitating with iron and manganese oxides) by monitoring the solution composition using a wide-range of methods such as high-resolution mass spectrometry, NMR and δ^{13}C-DOC measurements. As global estimates of sedimentary DOC fluxes are on the same scale as the total oceanic input of riverine DOC, the current paradigm recognizes sediments as an important source of aged, re-worked and recalcitrant DOC for marine waters. Iron and manganese oxide-rich sediments may

modulate sedimentary DOC fluxes, therefore altering a source of DOC that possibly supports a large fraction of the oceanic DOC turnover. Similar work conducted by Riedel (2013) demonstrated the specific binding of aromatic and pyrogenic DOC compounds at redox interfaces of peats and fens. Riedel et al. (2013) explain that a similar effect in surficial sediments, would indeed render the oxic-anoxic interface of marine sediment into "a selective yet intermediate barriers that limit the flux of DOM to oceanic waters."

3. We also hope to probe the macrostructure of OM in a wide range of depositional environments using microscopic methods, such as TEM and X-Ray absorption spectroscopic techniques. As explained, we expect that the changing redox chemistry of different depositional settings like river deltas and sediment underlying high productivity and/or anoxic waters will also impart differences in the role that iron plays in the preservation of OM. These differences may be reflected by either a change in the quantity of OM that binds to iron phases, or even a change in the macrostructure of the Fe-OM phases which may be visible using TEM microscopy using the same method described by Ransom et al. (1997). Through X-ray absorption spectroscopy (Fe-EXAFS, Fe-XANES), it would be interesting to determine the chemical environment of iron atoms (its valence number, type of its neighbours and inter-atomic distances) interacting with OM in different environments. This technique may allow us to confirm that inner-sphere complexation occurs between iron and OM. Alternatively, a multi-element approach using soft X-ray techniques (NEXAFS spectra/scanning transmission x-ray microscopy) would allow us to determine the speciation of carbon and nitrogen (transitions between the molecular orbitals that correspond to different functional groups) co-localized to iron at a nanometer resolution.

References

Aarnos, H., Ylöstalo, P. and Vähätalo, A.V., 2012. Seasonal phototransformation of dissolved organic matter to ammonium, dissolved inorganic carbon, and labile substrates supporting biomass across the Baltic Sea. Journal of Geophysical Reseach, 117.

Aller, R.C. and Aller, J.Y., 1998. The effect of biogenic irrigation intensity and solute exchange on diagenetic reaction rates in marine sediments. Journal of Marine Research, 56(4): 905-936.

Aller, R.C., Blair, N.E., Xia, Q. and Rude, P.D., 1996. Remineralization rates, recycling, and storage of carbon in Amazon shelf sediments. Continental Shelf Research, 15(5/6): 753-786.

Anschutz, P., Sundby, B., Lefrançois, L., Luther Iii, G.W. and Mucci, A., 2000. Interactions between metal oxides and species of nitrogen and iodine in bioturbated marine sediments. Geochimica et Cosmochimica Acta, 64(16): 2751-2763.

Arnarson, T.S. and Keil, R.G., 2000. Mechanism of pore water organic matter adsorption to montmorillonite. Marine Chemistry, 71: 309-320.

Arnarson, T.S. and Keil, R.G., 2007. Changes in organic matter-mineral interactions for marine sediments with varying oxygen exposure time. Geochimica et Cosmochimica Acta, 71: 3545-3556.

Arneel, J.J., Axler, R.P. and Owen, C.J., 1993. Persulfate digestion for determination of total nitrogen and total phosphorous in low-nutrient waters. American Environmental Laboratory, 10: 1-11.

Arnosti, C., 2011. Microbial extracellular enzymes and the marine carbon cycle. Annual Review of Marine Science, 3: 401-425.

Baas Becking, L.G.M. and Moore, D., 1959. The relation between iron and organic matter in sediments. Journal of sedimentary petrology, 29(3): 454-458.

Bastviken, D., Persson, L., Odham, G. and Tranvik, L., 2004. Degradation of dissolved organic matter in oxic and anoxic lake water. Limnology and Oceanography, 49(1): 109-116.

Bauer, J.E. (Editor), 2002. Carbon isotopic composition of DOM. Biogeochemistry of Marine Dissolved Organic Matter. Academic Press, San Diego, 405-453 pp.

Bauer, J.E. and Druffel, E.R.M., 1998. Ocean margins as a significant source of organic matter to the deep ocean. Nature, 392: 482-485.

Bauer, J.E., Williams, P.M. and Druffel, E.R.M., 1992. Recovery of submilligram quantities of carbon dioxide from gas streams by molecular sieve for subsequent determination of isotopic (13C and 14C) natural abundances. Analytical Chemistry, 64: 824-827.

Baxby, M., Patience, R.L. and Bartle, K.D., 1994. The origin and diagenesis of sedimentary orgnaic nitrogen. Journal of Petroleum Geology, 17(2): 211-230.

Beaupré, S.R., Druffel, E.R.M. and Griffin, S., 2007. A low-blank photochemical extraction system for concentration and isotopic analyses of marine dissolved organic carbon. Limnology and Oceanography: Methods, 5: 174-184.

Belicka, L.L. and Harvey, H.R., 2009. The sequestration of terrestrial organic carbon in Artic Ocean sediments: A comparison of methods and implications for regional carbon budgets. Geochimica et Cosmochimica Acta, 73(20): 6231-6248.

Benner, R., 2002. Chemical Composition and Reactivity. In: D.A. Hansell and C.A. Carlson (Editors), Biogeochemistry of marine dissolved organic matter. Academic Press, pp. 59-85.

Benner, R., Biddanda, B., Black, B. and McCarthy, M., 1997. Abundance, size distribution, and stable carbon and nitrogen isotopic compositions of marine organic matter isolated by tangential-flow ultrafiltration. Marine Chemistry, 57: 243-264.

Benner, R. and Strom, M., 1993. A critical evaluation of the analytical blank associated with DOC measurements by high-temperature catalytic oxidation. Marine Chemistry, 41: 153-160.

Berner, R.A., 1970. Sedimentary pyrite formation. American Journal of Science, 268: 1-23.

Berner, R.A., 1976. Inclusion of adsorption in the modelling of early diagenesis. Earth and Planetary Science Letters, 29(2): 333-340.

Berner, R.A., 1980. Early diagenesis: A theoretical approach, Princeton, NJ, 241 pp.

Berner, R.A., 1989. Biogeochemical cycles of carbon and sulfur and their effect on atmospheric oxygen over phenerozoic time. Palaeogeography, Palaeoclimatology, Palaeoecology, 75(1-2): 97-122.

Berner, R.A., 2003. The long-term carbon cycle, fossil fuels and atmospheric composition. Nature, 426: 323-326.

Berner, R.A. and Canfield, D.E., 1989. A new model for atmospheric oxygen over Phanerozoic time. American Journal of Science, 289: 333-361.

Blough, N.V. and Del Vecchio, R., 2002. Chromophoric DOM in the coastal environment. In: D.A. Hansell and D.E. Canfield (Editors), Biogeochemistry of Marine Dissolved Organic Matter. Elsevier, San Diego, pp. 509-540.

Boudot, J.-P., Bel Hadj, B.A., Steiman, R. and Seigle-Murandi, F., 1989. Biodegradation of synthetic organo-metallic complexes of iron and aluminum with selected metal to carbon ratios. Soil Biology and Biochemistry, 21: 961-966.

Boudreau, B.P., 1986. Mathematics of tracer mixing in sediments; II, Nonlocal mixing and biological conveyor-belt phenomena. American Journal of Science, 286(3): 199-238.

Bouillon, S., Kornheuer, M., Baeyens, W. and Dehairs, F., 2006. A new automated setup for stable isotope analysis of dissolved organic carbon. Limnology and Oceanography: Methods, 4: 216-226.

Bouillon, S. et al., 2012. Organic matter sources, fluxes amd greenhouse gas exchange in the Oubangui River (Congo River basin). Biogeosciences, 9: 2045-2062.

Buckley, D.E. and Cranston, R.E., 1988. Early diagenesis in deep sea turbidites: The imprint of paleo-oxidation zones. Geochimica et Cosmochimica Acta, 52: 2925-2939.

Burdige, D.J., 1993. The biochemistry of manganese and iron reduction in marine sediments. Earth-Science Reviews, 35: 249-283.

Burdige, D.J., 2002. Chapter 13 - Sediment Pore Waters. In: A.H. Dennis and A.C. Craig (Editors), Biogeochemistry of Marine Dissolved Organic Matter. Academic Press, San Diego, pp. 611-663.

Burdige, D.J., 2006. Geochemistry of marine sediments. Princeton University Press, Woodstock, 609 pp.

Burdige, D.J. and Gardner, K.G., 1998. Molecular weight distribution of dissolved organic carbon in marine sediment pore waters. Marine Chemistry, 62: 45-64.

Canfield, D.E., 1997. The geochemistry of river particulates from the continental USA: Major elements. Geochimica et Cosmochimica Acta, 61: 3349-3365.

Canfield, D.E., Habicht, K.S. and Thamdrup, B., 2000. The Achean sulfur cycle and the early history of atmospheric oxygen. Science, 288: 658-661.

Cattaneo, A. and Prairie, Y.T., 1995. Temperal variability in the chemical characteristics along the Rivière de l'Achigan: How many samples are necessary to describe stream chemistry? Canadia Journal of Fisheries and Aquatic Sciences, 52: 828-835.

Cauwet, G., 1994. HTCO method for dissolved organic carbon analysis in seawater: influence of catalyst on blank estimation. Marine Chemistry, 47(55-64).

Cauwet, G., 2002. DOM in the coastal zone. In: D.A. Hansell and C.A. Carlson (Editors), Biogeochemistry of Marine Dossolved Organic Matter. Elsevier, San Diego, pp. 579-602.

Chen, W., Zhao, Z., Koprivnjak, J.-F. and Perdue, E.M., 2002. A mechanistic study of the high-temperature oxidation of organic matter in a carbon analyzer. Marine Chemistry, 78: 185-196.

Chin-Leo, G. and Benner, R., 1992. Enhanced bacterioplacton production and respiration at intermediate salinities in the Mississippi River plume. Marine Ecology Progress Series, 87: 87-103.

Christensen, J.P., 1994. Carbon export from continental shelves, denitrification and atmospheric carbon dioxide. Continental Shelf Research, 14: 547-576.

Chu, S.X. and Liu, L.H., 2009. Analysis of terrestrial solar radiation energy. Solar Energy, 83(3): 1390-1404.

Clément, J.-C., Shresthat, J., Ehrenfeld, J.G. and Jaffé, P.R., 2005. Ammonium oxidation coupled to dissimilatory reduction of iron under anaerobic conditions in wetland soils. Soil Biology and Biochemistry, 17: 2323-2328.

Colley, S., Thomson, J., Wilson, T.R.S. and Higgs, N.C., 1984. Post-depositional migration of elements during diagenesis in brown clay and turbidite sequences in the North East Atlantic. Geochimica et Cosmochimica Acta, 48(6): 1223-1235.

Couture, R.-M., Gobeil, C. and Tessier, A., 2008. Chronology of atmospheric deposition of arsenic inferred from reconstruction sedimentary records. Environmental Science and Technology, 42(17): 6508-6513.

Cowie, G.L., Hedges, J.I., Prahl, F.G. and de Lance, G.J., 1995. Elemental and major biochemical changes across an oxidation front in a relict turbidite: An oxygen effect. Geochimica et Cosmochimica Acta, 59(1): 33-46.

Crowe, S.A., Canfield, D.E., Mucci, A., Sundby, B. and Maranger, R., 2012. Anammox, denitrification and fixed-nitrogen removal in sediments from the Lower St. Lawrence Estuary. Biogeosciences, 9: 4309-4321.

Deflandre, B., Mucci, A., Gagné, J.-P., Guignard, C. and Sundby, B., 2002. Early diagenetic processes in coastal marine sediments disturbed by a catastrophic sedimentation event. Geochimica et Cosmochimica Acta, 66: 2547-2558.

Devol, A.H. (Editor), 2008. Denitrification including Anammox. Nitrogen in the Marine Environment. Elsevier, 263-289 pp.

Dittmar, T., Whitehead, K., Minor, E.C. and Koch, B.P., 2007. Tracing terrigenous dissolved organic matter and its photochemical decay in the ocean by using liquid chromatography/mass spectrometry. Marine Chemistry, 107: 378-387.

Druffel, E.R.M., Williams, P.M., Bauer, J.E. and Ertel, J.R., 1992. Cycling of dissolved and particulate organic matter in the open ocean. Journal of Geophysical Research, 97(C10): 15639-15659.

Eglinton, T.I., 2012. A rusty carbon sink. Nature, 483: 165-166.

Emerson, S. and Hedges, J.I., 1988. Processes controlling the organic carbon content of open ocean sediments. Paleoceanography, 3: 621-634.

Farquar, G.D., Ehleringer, J.R. and Hubick, K.T., 1989. Carbon isotope discrimination and photosynthesis. Annual Review of Plant Physiology and Plant Molecular Biology, 40: 503-537.

Fichot, C.G. and Benner, R., 2012. The spectral slope coefficient of chromophoric dissolved organic matter ($S_{275-295}$) as a tracer of terrestrial dissolved organic carbon in river-influenced ocean margins. Limnology and Oceanography, 57(5): 1453-1466.

Fontugne, M.R. and Duplessy, J.C., 1981. Organic carbon isotopic fractionation be marine plankton in the temperature range -1 to 30^{o}C. Oceanological Acta, 4: 85-90.

Fowler, S.W. and Knauer, G.A., 1986. Role of large particles in the transport of elements and organic compounds through the ocean water column. Progress in Oceanogrpahy, 16: 147-194.

Froelich, P.N. et al., 1979. Early oxidation of organic matter in pelagic sediments of the eastern equatorial Atlantic: suboxic diagenesis. Geochimica et Cosmochimica Acta, 43(7): 1075-1090.

Fry, B., Brand, W., Mersch, F.J., Tholke, K. and Garritt, R., 1992. Automated analysis system for coupled δ15N measurements. Analytical Chemistry, 64: 288-291.

Fry, B., Hullar, S.S. and Peterson, B.J., 1993. Platinum-catalyzed combustion of DOC in sealed tubed for stable isotopic analysis. Marine Chemistry, 41: 187-193.

Gélinas, Y., Baldock, J.A. and Hedges, J.I., 2001. Organic carbon composition of marine sediments: effect of oxygen exposure on oil generation potential. Science, 294: 145-148.

Goñi, M.A., Yunker, M.B., Macdonald, R.W. and Eglinton, T.I., 2005. The supply and preservation of ancient and modern components of organic carbon in the Canadian Beaufort Shelf of the Arctic Ocean. Marine Chemistry, 93(1): 53-73.

Gonsior, M., Peake, B.M., Cooper, W.T., D'Andrilli, J. and Cooper, W.J., 2008. Photochemically induced changed in dissolved organic matter identified by ultrahigh resolution fourier transform iron cyclontron resonance mass spectrometry. Environmental Science and Technology, 43(698-703): 698.

Gu, B., Schmitt, J., Chen, Z., Liang, L. and McCarthy, J.F., 1995. Adsorption and desorption of different organic matter fractions on iron oxides. Geochimica et Cosmochimica Acta, 59(2): 219-229.

Guggenberger, G. and Kaiser, K., 2003. Dissolved organic matter in soil: challenging the paradigm of sorptive preservation. Geoderma, 113: 293-310.

Hansell, D.A., 2002. DOC in the global ocean carbon cycle. In: D.A. Hansell and C.A. Carlson (Editors), Biogeochemistry of marine dissolved organic matter. Academic press, pp. 685-711.

Hansell, D.A., Carlson, C.A., Repeta, D.J. and Schlitzer, R., 2009. Dissolved organic matter in the ocean: New insights stimulated by a controversy. Oceanography, 22: 52-61.

Hart, P.J., 1969. The Earth's crust nd upper mantle: Structure, Dynamic processes, and their relation to deep-seated geological phenomena. American Geophysical Union.

Hayes, J.M., 2001. Fractionation of carbon and hydrogen isotopes in biosynthetis processes. Reviews in Mineralogy and Geochemistry, 43(1): 225-277.

Hease, R.R. et al., 1997. Iron species determination to investigate early diagenetic reactivity in marine sediments. Geochimica et Cosmochimica Acta, 61: 63-72.

Hedges, J.I., 1992. Global biogeochemical cycles: progress and problems. Marine Chemistry, 39: 67-93.

Hedges, J.I. (Editor), 2002a. Why dissolved organic matter? Biogeochemistry of Marine Dissolved Organic Matter. Elsevier, New York, 774 pp.

Hedges, J.I., 2002b. Why dissolved organic matter? In: D.A. Hansell and A.C. Craig (Editors), Biogeochemistry of marine dissolved organic matter. Academic Press, pp. 1-27.

Hedges, J.I. et al., 2000. The molecularly-uncharacterized component of nonliving organic matter in natural environments. Organic Geochemistry, 31: 945-958.

Hedges, J.I. and Keil, R.G., 1995. Sedimentary organic matter preservation: an assessment and speculative synthesis. Marine Chemistry, 49: 81-115.

Hedges, J.I., Keil, R.G. and Benner, R., 1997. What happens to terrestrial organic matter in the ocean? Organic Geochemistry, 27: 195-212.

Hedges, J.I. and Oades, J.M., 1997. Comparative organic geochemistries of soils and marine sediments. Organic Geochemistry, 27(7/8): 319-361.

Hedges John, I., Hu, F.S., Devol, A.H., Hartnett, H.E. and Keil, R.G., 1999. Sedimentary organic matter preservation: a test for selective degradation under oxic consitions. American Journal of Science, 229: 529-555.

Hélie, J.-F. and Hillaire-Marcel, C., 2006. Sources of particulate and dissolved organic carbon in the St Lawrence River: isotopic approach. Hydrological Processes, 20: 1945-1959.

Helms, J.R. et al., 2008. Absorption spectral slopes ratios as indicators of molecular weight, source and photobleaching of chromophoric dissolved organic matter. Limnology and Oceanography, 53(3): 955-969.

Henrichs, S.M., 1992. Early diagenesis of organic matter in marine sediments: progress and perplexity. Marine Chemistry, 39: 119-149.

Henrichs, S.M., 1995. Sedimentary organic matter preservation: an assessment and speculative synthesis - a comment. Marine Chemistry, 49: 127-136.

Hernes, P.J. and Benner, R., 2003. Photochemical and microbial degradation of dissolved lignin phenols: Implications for the fate of terrigenous dissolved organic matter in marine environments. Journal of Geophysical Research, 108(C9): 3291-3299.

Hollister, C.D., Silva, A.J. and Driscoll, A., 1973. A giant piston-corer. Ocean Engineering, 2: 159-168.

Hopmans, E.C. et al., 2004. A novel proxy for terrestrial organic matter in sediments based on branched and isoprenoid tetraether lipids. Earth and Planetary Science Letters, 224(1-2): 107-116.

Hulth, S. et al., 2005. Nitrogen removal in marine environments: recent findings and future research challenges. Marine Chemistry, 94(1–4): 125-145.

Huygens, D. et al., 2007. On-line technique to determine the isotopic composition of total dissolved nitrogen. Analytical Chemistry, 79: 8644-8649.

Ingalls, A.E., Lee, C., Wakeham, S.G. and Hedges, J.I., 2003. The role of biominerals in the sinking flux and preservation of amino acids in the Southern Ocean along 170^{o}W. Deep-Sea Research Part II: Topical Studies in Oceanography, 50: 713-738.

Jaffé, P.R. et al., 2013. Global charcoal mobilization from soils via dissolution and rivering transport to the oceans. Science, 340: 345-347.

Johnson, K.S., Gordon, R.M. and Coale, K.H., 1997. What controls dissolved iron in the world ocean? Marine Chemistry, 57: 137-161.

Jones, D.L. and Edwards, A.C., 1998. Influence of sorption on the biological utilization of two simple carbon substrates. Soil Biology and Biochemistry, 30: 1895-1902.

Kaiser, K. and Guggenberger, G., 2000. The role of DOM sorption to mineral surfaces in the preservation of organic matter in soils. Organic Geochemistry, 31: 711-725.

Katsev, S., Chaillou, G., Sundby, B. and Mucci, A., 2007. Effect of progressive oxygen depletion on sediment diagenesis and fluxes: A model for the Lower St. Lawrence River Estuary. Limnology and Oceanography, 52(2555-2568): 2555.

Keil, R.G., Montluçon, D.B., Prahl, F.G. and I., H.J., 1994. Sorptive preservation of labile organic matter in marine sediments. Nature, 370: 549-552.

Kennedy, M.J. and Wagner, T., 2011. Clay mineral continental amplifier for marine carbon sequestration in a greenhouse ocean. Proceedings of the National Academy of Science, 108(24): 9776-9781.

Komada, T. et al., 2013. Dissolved organic carbon dynamics in anaerobic sediments of the Santa Monica Basin. Geochimica et Cosmochimica Acta, 110: 253-273.

Kraemer, S.M., 2004. Iron oxide dissolution and solubility in the presence of siderophores. Aquatic Sciences, 66: 3-18.

Laidler, K.J. and Meiser, J.H., 1999. Physical Chemistry. Houghton Mifflin, Boston.

Lalonde, K., Mucci, A., Ouellet, A. and Gélinas, Y., 2012. Preservation of organic matter in sediments promoted by iron. Nature, 483(7388): 198-200.

Lambert, T. et al., 2013. New insights from the use of carbon isotopes as tracer of DOC sources and DOC transport processes in headwater catchments. Biogeosciences, 10: 17965-18007.

Lang, S., Lilley, M.D. and Hedges, J.I., 2007. A method to measure the isotopic composition of dissolved organic carbon using a high temperature combustion instrument. Marine Chemistry, 103: 318-326.

LaRowe, D.E. and Van Cappellen, P., 2011. Degradation of natural organic matter: A thermodynamic analysis. Geochimica et Cosmochimica Acta, 75(8): 2030-2042.

Liu, G.-R., Ye, C.-S., He, J.H. and Jiang, H., 2009. Lake sediment treatment with aluminum, iron, calcium and nitrate additives to reduce phosphorus release. Journal of Zhejiang University Science A, 10(9): 1367-1373.

Lønborg, C. and Álvarez-Salgado, X.A., 2012. Recycling versus export of bioavailable dissolved organic matter in the coastal ocean and efficiency of the continental shelf pump. Global Biogeochemical Cycles, 26.

Lu, Y. et al., 2013. Photochemical and microbial alteration of dissolved organic matter in temperate headwater streams associated with different land use. Journal of Geophysical Reseach, 188(2): 566-580.

Luther III, G.W., Sundby, B., Lewis, B.L., Brendel, P.J. and Silverberg, N., 1997. Interactions of manganese with the nitrogen cycle: Alternative pathway to dinitrogen. Geochimica et Cosmochimica Acta, 61(19): 4043-4052.

Mackay, D.J. and Zirino, A., 1994. Comments on trace metal speciation in seawater or do “onions” grow in the sea? Analytica Chimica Acta, 284: 635-647.

Magen, C., Mucci, A. and Sundby, B., 2011. Reduction Rates of Sedimentary Mn and Fe Oxides: An Incubation Experiment with Arctic Ocean Sediments. Aquatic Geochemistry, 17(4-5): 629-643.

Maher, D. and Eyre, B.D., 2011. Insights into estuarine benthic dissolved organic carbon (DOC) dynamics using δ^{13}C-DOC values, phospholipid fatty acids and dissolved organic nutrient fluxes. Geochimica et Cosmochimica Acta, 75: 1889-1902.

Mariotti, A. et al., 1981. Experimental determination of nitrogen kinetic isotope fractionation: Some principles; illustration for the denitrification and nitrification processes. Plant and Soil, 62(3): 413-430.

Mason, B.H., 1966. Principles of geochemistry. Wiley.

Mayer, L.M., 1994. Surface area control on organic carbon accumulation in continental margin sediments. Geochimica et Cosmochimica Acta, 58: 1271-1284.

Mayer, L.M., 1995. Speculative organic matter preservation: an assessment and speculative synthesis – a comment. Marine Chemistry, 49: 123-126.

Mayer, L.M., 1999. Extent of coverage of mineral surfaces by organic matter in marine sediments. Geochimica et Cosmochimica Acta, 63: 207-215.

Mehra, O.P. and Jackson, M.L., 1960. Iron oxide removal from soils and clays by a dithionite-citrate system buffered with sodium bicarbonate. Clays and Clay Minerals, 7: 317-327.

Meyers-Schulte, K.J. and Hedges, J.I., 1986. Molecular evidence for a terrestrial component of organic matter dissolved in ocean water. Nature, 321: 61-63.

Michaud, E., Desrosiers, G., Mermillod-Blondin, F., Sundby, B. and Stora, G., 2005. The functional group approach to bioturbation: The effects of biodiffusers and gallery-diffusers of the Macoma balthica community on sediment oxygen uptake. Journal of Experimental Marine Biology and Ecology, 326(1): 77-88.

Middelburg, J.J. et al., 2000. The fate of intertidal microphytobenthos carbon: An in situ ^{13}C-labeling study. Limnology and Oceanography, 45(6): 1224-1234.

Miller, W.L. and Zepp, R.G., 1995. Photochemical production of dissolved inorganic carbon from terrestrial organic matter: Significance to the oceanic organic carbon cycle. Geophysical Research Letters, 22(4): 417-420.

Milliman, J.D. and Farnsworth, K.L., 2011. River discharge to the coastal ocean - a global synthesis. Cambridge University Press.

Minor, E.C., Steinbring, C.J., Longnecker, K. and Kujawinski, E.B., 2012. Characterization of dissolved organic matter in Lake Superior and its watershed using ultrahigh resolution mass spectrometry. Organic Geochemistry, 43: 1-11.

Mopper, K. and Kieber, D.J. (Editors), 2002. Photochemistry and the cycling of carbon, sulfur, nitrogen and phosphorous. Biogeochemistry of Marine Dissolved Organic Matter. Elsevier, San Diego, 456-503 pp.

Mopper, K., Zhou, X., Kieber, D.J., Sikorski, R.J. and Jones, R.N., 1991. Photochemical degradation of dissolved organic carbon and its impact on oceanic carbon cycle. Nature, 353: 60-62.

Moran, M.A., Sheldon Jr., W.M. and Zepp, R.G., 2000. Carbon loss and optical property changes during long-term photochemical and biological degradation of estuarine dissolved organic matter. Limnology and Oceanography, 45(6): 1254-1264.

Morgan, J.W. and Anders, E., 1980. Chemical compostion of Earth, Venus and Mercury. Proceedings of the National Academy of Science, 71(12): 6973-6977.

Mucci, A. et al., 2000. The fate of carbon in continental shelf sediments of eastern Canada: a case study. Deep Sea Research Part II: Topical Studies in Oceanography, 47(3–4): 733-760.

Navrotsky, A., Mazeina, L. and Majzlan, J., 2008. Size-driven structural and thermodynamic complexity in iron oxides. Science, 319: 1635-1638.

Neff, J.C. et al., 2006. Seasonal changes in the age and structure of dissolved organic carbon in Siberian rivers and streams. Geophysical Research Letters, 33: L23401-C7616.

Nelson, N.B., Siegel, D.A., Carlson, C.A. and Swan, S.M., 2010. Tracing global biogeochemical cycles and merional overturning circulation using chromophoric dissolved organic matter. Geophysical Research Letters, 37(3).

O'Sullivan, D.W., Hanson Jr, A.K. and Kester, D.R., 1995. Stopped flow luminol chemiluminescence determination of Fe(II) and reducible iron in seawater at subnanomolar levels. Marine Chemistry, 49(1): 65-77.

Obernosterer, I. and Benner, R., 2004. Competition between biological and photochemical processes in the mineralization of dissolved organic carbon. Limnology and Oceanography, 49(1): 117-124.

Ogawa, H. and Tanoue, E., 2003. Dissolved organic matter in oceanic waters. Journal of Oceanography, 59: 129-147.

Opsahl, S. and Benner, R., 1997. Distribution and cycling of terrigenous dissolved organic matter in the ocean. Nature, 386: 480-482.

Opsahl, S. and Benner, R., 1998. Photochemical reactivity of dissolved lignin in river and ocean waters. Limnology and Oceanography, 43: 1297-1304.

Opsahl, S. and Zepp, R.G., 2001. Photochemically-induced alteration of stable carbon isotope ratios in terrigenous dissolved organic carbon. Geophysical Research Letters, 28(12): 2417-2420.

Osburn, C.L., Morris, D.P., Thorn, K.A. and Moeller, R.E., 2001. Chemical and optical changes in freshwater dissolved organic matter exposed to solar radiation. Biogeochemistry, 54: 251-278.

Osburn, C.L. and St-Jean, G., 2007. The use of wet chemical oxidation with high-amplification isotope ratio mass spectrometry (WCO-IRMS) to measure stable isotope values of dissolved organic carbon in seawater. Limnology and Oceanography: Methods, 5: 296-308.

Osburn, C.L. and Stedmon, C.A., 2011. Linking the chemical and optical properties of dissolved organic matter in the Baltic–North Sea transition zone to differentiate three allochthonous inputs. Marine Chemistry, 126: 281-294.

Ouellet, A. et al., 2012. Assessing carbon dynamics in natural and perturbed boreal aquatic systems. Journal of Geophysical Reseach: Biogeosciences, 117: G001943-G001956.

Panetta, R.J., Ibrahim, M. and Gélinas, Y., 2008. Coupling a high-temperature catalytic oxidation total organic carbon analyzer to an isotope ratio mass spectrometer to measure natural-

abundance δ^{13}C-dissolved organic carbon in marine and freshwater samples. Analytical Chemistry, 80: 5232-5239.

Peterson, B.J., Lang, S., Aufdenkampe, A.K. and I., H.J., 2003. Dissolved organic carbon measurement using a modified high-temperature combustion analyzer. Marine Chemistry, 81: 89-104.

Poulton, S.W. and Raiswell, R., 2005. Chemical and physical characteristics of iron oxides in riverine and glacial meltwater sediments. Chemical Geology, 218: 203-221.

Prahl, F.G., De Lange, G.J., Scholten, S. and Cowie, G.L., 1997. A case of post-depositional aerobic degradation of terrestrial organic matter in turbidite deposits from the Madeira Abyssal Plain. Organic Geochemistry, 27(3–4): 141-152.

Pullin, M.J., Bertilsson, S., Goldstone, J.V. and Voelker, B.M., 2004. Effects of sunlight and hydroxyl radical on dissolved organic matter: Bacterial growth efficiency and production of carboxylic and other substrates. Limnology and Oceanography, 49(6): 2011-2022.

Qian, J. and Mopper, K., 1996. Automated high-performance, high-temperature combustion total organic carbon analyzer. Analytical Chemistry, 68: 3090-3097.

Raiswell, R. and Canfield, D.E., 2012a. The iron biogeochemical cycle past and present. Geochemical Perspectives, 1(1): 1-215.

Raiswell, R. and Canfield, D.E., 2012b. Supplementary Information. Geochemical Perspectives, 1(1): 187-210.

Ransom, B., Bennet, R.H., Baerwald, R. and Shea, K., 1997. TEM study of in situ organic matter on continental margins: occurrence and the “monolayer” hypothesis. Marine Geology, 138: 1-9.

Ransom, B., Kim, D., Kastner, M. and Wainwright, S., 1998a. Organic matter preservation on continental slopes: importance of mineralogy and surface area. Geochimica et Cosmochimica Acta, 62(8): 1329-1345.

Ransom, B., Shea, K.F., Burkett, P.J., Bennet, R.H. and Baerwald, R., 1998b. Comparison of pelagic and nepheloid layer marine snow: implications for carbon cycling. Marine Geology, 150: 39-50.

Raymond, P.A. and Bauer, J.E., 2001a. DOC cycling in a temperate estuary: A mass balance approach using natural ^{14}C and ^{13}C isotopes. Limnology and Oceanography, 46(3): 655-667.

Raymond, P.A. and Bauer, J.E., 2001b. Riverine export of aged organic matter to the North Atlantic Ocean. Nature, 409: 497-499.

Raymond, P.A. et al., 2007. Flux and age of DOC exported to the Artic Ocean: A carbon isotopic study of the five largest artic rivers. Global Biogeochemical Cycles, 21: GB4011.

Rickels, W. et al., 2011. Large-Scale intentional interventions into the climate system? Assessing the climate engineering debate. . Kiel Earth Institute, Kiel.

Riedel, T., Zak, D., Biester, H. and Dittmar, T., 2012. Iron traps terrestrially derived dissolved organic matter at redox interfaces. Proceedings of the National Academy of Science, 110(25): 10101-10105.

Rossel, P.E., Vähätalo, A.V., Witt, M. and Dittmar, T., 2013. Molecular composition of dissolved organic matter from a wetland plant (Juncus effusus) after photochemical and microbial decomposition (1.25 yr): Common features with deep sea dissolved organic matter. Organic Geochemistry, 60: 62-71.

Rue, E.L. and Bruland, K.W., 1995. Complexation of iron(III) by natural organic ligands in the Central North Pacific as determined by a new competitive ligand equilibration/adsorptive cathodic stripping voltammetric method. Marine Chemistry, 50: 117-138.

Sawayama, S., 2006. Possibility of anoxic ferric ammonium oxidation. Journal of Bioscience and Bioengineering, 101(1): 70-72.

Schindler, D.W., 1974. Eutrophication and and recovery in experimental lakes: Implications for lake management. Science, 184(4139): 897-899.

Schwertmann, U., 1966. Inhibitory effect of soil organic matter on the crystallization of amorphous iron hydroxide. Nature, 212: 645-646.

Sharp, J.H. et al., 1993. Re-evaluation of high temperature combusition and chemical oxidation measurements of dissolved organic carbon in seawater. Limnology and Oceanography, 38: 1774-1782.

Sharp, J.H. et al., 2002. Final dissolved organic carbonbroad community intercalibration and preliminary use of DOC reference materials. Marine Chemistry, 77: 239-253.

Silva, A.J., Hollister, C.D., Laine, E.P. and Beverly, B.E., 1976. Geotechnical properties of deep sea sediments: Bermuda rise. Marine Geotechnology, 1(3): 195-232.

Skoog, A., Thomas, D., R., L. and Ritchter, K.-U., 1997. Methodological investigations on DOC determinations by the HTCO method. Marine Chemistry, 56: 39-44.

Skoog, D.A., Holler, F.J. and Nieman, T.A., 1998. Principles of instrumental analysis. Brooks/Cole.

Smith, J.N. and Schafer, C.T., 1999. Sedimentation, bioturbation, and Hg uptake in the sediments of the estuary and Gulf of St. Lawrence. Limnology and Oceanography, 44(1): 207-219.

Solomon, D. et al., 2012. Micro- and nano-environments of carbon sequestration: Multi-element STXM-NEXAFS spectromicroscopy assessment of microbial carbon and mineral associations. Chemical Geology, 329: 53-73.

Spencer, R.G.M. et al., 2009. Photochemical degradation of dissolved organic matter and dissolved lignin phenols from the Congo River. Journal of Geophysical Research, 114: 1-12.

St-Jean, G., 2003. Automated quantitative and isotopic (13C analysis of dissolved inorganic carbon and dissolved organic carbon in continuous-flow using a total organic carbon analyzer. Rapid Communications in Mass Spectrometry, 17: 419-428.

Stookey, L.L., 1970. Ferrozine - A new spectroscopy reagent for iron. Analytical Chemistry, 42(7): 779-781.

Stumm, W. and Morgan, J.J., 1970. Aquatic Chemistry: An introduction emphasizing chemical equilibria in natural waters, Volume 1. Wiley-Interscience, 583 pages pp.

Stutter, M.I., Richards, S. and Dawson, J.C.C., 2013. Biodegradability of natural dissolved organic matter collected from a UK moorland stream. Water Research, 47: 1169-1180.

Sugimura, Y. and Suzuki, Y., 1988. A high-temperature catalytic oxidation method for the determination of non-volatile dissolved organic carbon in seawater by direct injection of a liquid sample. Marine Chemistry, 24: 105-131.

Sundby, B., Gobeil, C., Silverberg, N. and Mucci, A., 1992. The phosphorus cycle in coastal marine sediments. Limnology and Oceanography, 37(6): 1129-1145.

Suzuki, Y., 1993. On the measurement of DOC and DON in seawater. Marine Chemistry, 41: 287-288.

Thomson, J., Jarvis, I., Green, D.R. and Green, D., 1998. 32. Oxidation fronts in Madeira Abyssal Plain turbidites: persistence of early diagenetic trace-element enrichments during burial, site 950, Proc. ODP, Sci. Res, pp. 559-571.

Tipping, E., Woof, C. and Cooke, D., 1981. Iron oxide from seasonally anoxic lake. Geochimica et Cosmochimica Acta, 45(9): 1411-1419.

Trovo, A.G., Santos Melo, S.A. and Fernandes Pupo Nogueira, R., 2008. Photodegradation of the pharmaceuticals amoxicillin, bezafibrate and paracetamol by the photo-Fenton process - Application to sewage treatment plant effluent. Journal of Photochemistry and Photobiology A: Chemistry, 198(2-3): 215-220.

Vähätalo, A.V., Aarnos, H., Hoikkala, L. and Lignell, R., 2011. Photochemical transformation of terrestrial dissolved organic matter supports hetero-and autotrophic production in coastal water. Marine Ecology Progress Series, 423: 1-14.

Vähätalo, A.V., Salonen, K., Münster, U., Järvinen, M. and Wetzel, R.G., 2003. Photochemical transformation of allochtonous organic matter provides bioavailable nutrients in a humic lake. Archiv für Hydrobiologie, 156: 287-314.

Vähätalo, A.V., Salonen, K., Salkinoja-Salonen, M. and Hatakka, A., 1999. Photochemical mineralization of synthetic lignin in lake water indicates enhanced turnover of aromatic organic matter under solar radiation. Biodegradation, 10: 415-420.

Vähätalo, A.V. and Wetzel, R.G., 2008. Long-term photochemical and microbial decomposition of wetland-derived dissolved organic matter with alteration of ^{13}C:^{12}C mass ratio. Limnology and Oceanography, 53(4): 1387-1392.

Van der Zee, C., Roberts, D.R., Rancourt, D.G. and Slomp, C.P., 2003. Nano-goethite is the dominant reactive oxyhydroxide phase in lake and marine sediments. Geology, 31: 993-996.

Van Geldern, R. et al., 2013. Stable carbon isotope analysis of dissolved inorganic carbon (DIC) and dissolved organic carbon (DOC) in natural waters – Results from a worldwide proficiency test. . Rapid Communications in Mass Spectrometry, 27: 2099-2107.

Viollier, E., Inglett, P.W., Hunter, K., Roychoudhury, A.N. and Van Cappellen, P., 2000. The ferrozine method revisited: Fe(II)/Fe(III) determination in natural waters. Applied Geochemistry, 15(6): 785-790.

Vodacek, A. et al., 1995. The use of in situ and airborne fluorescence measurements to determine UV absorption coefficients and DOC concentrations in surface waters. Limnology and Oceanography, 40(2): 411-415.

Wagai, R. and Mayer, L.M., 2006. Sorptive stabilization of organic matter in soils by hydrous iron oxides. Geochimica et Cosmochimica Acta, 71: 25-35.

Wang, X., Ma, X., Zhao, S., Wang, B. and Song, C., 2009. Nanoporous molecular basket sorbent for NO2 and SO2 capture based on a polyethylene glycol-loaded mesoporous molecular sieve. Energy and Environmental Science, 2: 878-882.

Wang, X.C. and Druffel, E.R.M., 2001. Radiocarbon and stable carbon isotope compositions of organic compound classes in sediments from the NE Pacific and Southern Oceans. Marine Chemistry, 73: 65-82.

Wang, Z.-C., Druffel, E.R.M., Griffin, S., Lee, C. and Kashgarian, M., 1998. Radiocarbon studies of organic compound classes in plankton and sediment of the Northeastern Pacific Ocean. Geochimica et Cosmochimica Acta, 62: 1365-1378.

Weiss, M.S. et al., 1991. Molecular architecture and electrostatic properties of a bacterial porin. Science, 254: 1627-1630.

White, H.K., Reddy, C.M. and Eglinton, T.I., 2005. Isotopic constraints on the fate of petroleum residues sequestered in salt march sediments. Environmental Science and Technology, 39: 2545-2551.

Williams, P.M., 1968. Stable carbon isotopes in the dissolved organic matter in the sea. Nature, 219: 152-153.

Williams, P.M. and Druffel, E.R.M., 1987. Radiocarbon in dissolved organic matter in the central North Pacific Ocean. Nature, 330(6145): 246-248.

Williams, P.M. and Gordon, L.I., 1970. Carbon-13:carbon-12 ratios in dissolved and particulate organic matter in the sea. Deep-Sea Research, 17: 17-27.

Xiao, Y.-H., Sara-Aho, T., Hartikainen, H. and Vähätalo, A.V., 2013. Contribution of ferric iron to light absorption by chromophoric dissolved organic matter. Limnology and Oceanography, 58(2): 653-662.

Yang, W.H., Weber, K.A. and Silver, W.L., 2012. Nitrogen loss from soil through anaerobic ammonium oxidation coupled to iron reduction. Nature Geoscience, 5: 538-541.

Yu, J., Elderfield, H. and Piotrowski, A.M., 2008. Seawater carbonate ion-$\delta^{13}C$ systematics and applications to glacial-interglacial North Atlantic ocean circulation. Earth and Planetary Science Letters, 271: 209-220.

Zepp, R.G., 2003. Solar UVR and aquatic carbon, nitrogen , sulfur and metals cycles. In: W. Helbling and H. Zagarese (Editors), UV effects in aquatic organisms and ecosystems. The Royal Society of Chemistry, pp. 139-171.

Zepp, R.G., 2005. Light and environmental chemistry: Influence of changing solar radiation on aquatic photoreactions. IUVA News, 7(1): 9-14.

Zonneveld, K.A.F. et al., 2010. Selective preservation of organic matter in marine environments; processes and impact on the sedimentary record. Biogeosciences, 7: 483-511.

Appendix A2

This Appendix presents the details of the method used to measure organic carbon (OC) associated with iron (Fe), and the control experiments. Results from this extraction method are shown in Chapter 2 of this thesis. Also listed in two tables are the results for the control experiments and the extractions, the detailed calculations used to obtain our estimate of 21.5 ± 8.6% of global sedimentary OC associated with Fe and finally two graphs showing the relationships between $\delta^{13}C$ and $\delta^{15}N$, as well as between $\delta^{13}C$ and the C/N molar ratio for the Fe-OM and the non-Fe-OM fractions.

Extraction method and control experiment

The method used in this work was adapted from the work of Mehra and Jackson (1960). This method, hereafter called the CBD method, has been shown to extract all reactive iron oxides while being gentle on clay minerals (Poulton and Raiswell, 2005). Briefly, freeze-dried sediment samples were added to a solution containing a buffer (sodium bicarbonate, pH 7.3) and a metal ion complexing agent (trisodium citrate) in capped 40-mL Teflon tubes and heated to 80 ºC in a water bath. A reducing agent (sodium dithionite) was added to the mixture and maintained at 80 ºC for 15 min. To determine how much organic carbon (OC) is readily desorbed from the sediment, control experiments were carried out in which the samples were extracted under the same conditions (solid:solution ratio, temperature, time) as the reduction treatment, but replacing trisodium citrate and sodium dithionite by sodium chloride at an equivalent ionic strength. The reduction treatment and control experiment were carried out on all samples. Following both treatments, the supernatant was separated from the solid fraction by centrifugation at 3000 g for 10 minutes. The solid fraction was then rinsed three times with artificial seawater, and the rinse water and supernatant were combined. The supernatant and

rinse water were then acidified and filtered on pre-combusted and acid-rinsed GFF filters (nominal pore size of 0.7 µm). Dissolved iron in the supernatant/rinse water solution was analyzed by ICP-MS (Agilent), whereas OC and TN losses (plus changes in stable $\delta^{13}C$ and $\delta^{15}N$) upon treatment were evaluated by elemental analysis (Eurovector) coupled to a GV Instrument Isoprime isotope ratio mass spectrometer by analyzing the freeze-dried solid sample before and after treatment while accounting for mass losses during treatment. The following table presents the different steps for the reduction method and control experiment used in this work.

Table 8-1: Conditions used in the reduction method and control experiment

Reduction method	***Control experiment***
0.25 g of dry sediment	0.25 g of dry sediment
+ 15 mL of a 0.27 M trisodium citrate ($Na_3C_6H_5O_7 \cdot 2H_2O$; ionic strength = 1.6 M) and 0.11 M sodium bicarbonate ($NaHCO_3$)	+ 15 mL of a 1.6 M sodium chloride (NaCl; ionic strength = 1.6 M) and 0.11 M sodium bicarbonate ($NaHCO_3$)
Heat to 80ºC in a water bath	Heat to 80ºC in a water bath
+ 0.25 g sodium dithionite (0.1 M solution of $Na_2S_2O_4$; ionic strength increases by 0.25 M)	+ 0.22 g of sodium chloride (0.25 M solution of NaCl; ionic strength increases by 0.25 M)
Keep at 80ºC for 15 min	Keep at 80ºC for 15 min
Centrifuge (3000 g, 10 min) and remove supernatant	Centrifuge (3000 g, 10 min) and remove supernatant
Rinse 3 times with artificial seawater and remove supernatant by centrifugation	Rinse 3 times with artificial seawater and remove supernatant by centrifugation
Combine rinse water and supernatant, acidify to pH<2 with HCl, and filter on pre-combusted and acid-rinsed GFF filter	Combine rinse water and supernatant, acidify to pH<2 with HCl, and filter on pre-combusted and acid-rinsed GFF filter

On average, 7.2 ± 5.4% of the total OC was released from the samples in the control experiment (compared to <3% of total OC when extracting the samples with OC-free seawater at room temperature). The amount of OC released in the control experiment is significant with respect to our estimates of the OC that is intimately associated with Fe (buffered dithionite extraction). Consequently, results of the individual control experiments were subtracted from the amount of OC released from the dithionite extraction to obtain our Fe-associated OC estimate for each sample. In other words, all the results presented and discussed in the paper are control-corrected values. The entire data set is now presented below, in Tables 2 (control experiment) and 3 (reduction treatment).

To ensure that trisodium citrate and sodium bicarbonate do not contaminate our samples with adventitious OC, which would lead to underestimations of the pool of Fe-associated OC, the reacted solid phase was rinsed three times with artificial seawater following the dithionite extraction. Bicarbonate contamination is unlikely since all our samples were decarbonated with HCl (vapour phase) prior to elemental analysis. We estimated the contamination from citrate using two natural low OC samples (oxidized Madeira turbidite sample containing 0.11%OC [with about 50% biogenic calcite and lesser amounts of quartz and clay], and deep-core sediment from the St-Lawrence Estuary (Stn 16) containing 0.14%OC [glacial marine clays]), as well as five sediments pretreated with hydrogen peroxide (5 successive 24-hour treatments with 30% H_2O_2 at 50^{o}C, which typically remove >95% of native OC) and covering a broad range of mineralogies and native OC concentrations (Equatorial Pacific 9^{o}N [OC-poor red ooze enriched in clays and iron oxides]; Mexican Margin 303 and 306 [clayey sample enriched in marine OM]; St. Lawrence Estuary 23 [iron oxide-rich sample overlain by hypoxic bottom waters and containing a mix of terrestrial and marine OC]; Mackenzie River Delta [silt and clay-size marine mud]). Based on the measured %OC gains and an assumed 25% loss of native iron-associated OC (removed during

the dithionite extraction) for the first two samples, we expect that contamination does not exceed more than 0.05-0.08% of the dry sediment weight, which is insignificant for the samples in our data set. Furthermore, the isotopic signature of citrate used in this work is -22.0‰. Since most of our bulk samples' OC $\delta^{13}C$ compositions are more negative than citrate and become more negative after the iron extraction, it is not likely that citrate contributes significantly to the post-extraction samples.

We also assessed the specificity of our method for the fraction of total OC associated with iron by running the following experiment. We used a planktonic biomass sample (cultured *Nannochloropsis* cells (44 wt% OC), purchased from Reed Mariculture, CA, USA), and soil litter from the boreal forest (42 wt% OC, sampled in the summer of 2008 in the Abitibi area, QC, Canada), as representative samples from marine and terrestrial environments, respectively. The plankton sample was quickly frozen in liquid nitrogen and thawed three times to break the cells open. An aliquot of the sample was filtered through a 0.45-µm GF/F filter to separate the soluble material from the solid organic mass which accumulated on the filter. The dry litter sample was ground to <1 mm in a mortar, suspended in Milli-Q water, and filtered as above. Both solid samples were then extracted with salty and warm water buffered with bicarbonate, under the same conditions as in the control experiment (Table 8-1), and then extracted with the CBD solution, under the same conditions as the sediment samples. Losses of OC were negligible in both cases, accounting for <2% of the initial OC mass. To further address the issue of method specificity, we repeated a second time the CDB extraction on three St. Lawrence Estuary samples (Stations 25 [more terrestrial], 23 [intermediate] and 20 [more marine]) that had already been treated for iron oxide removal. A very minute fraction of additional OC (approximately 2% of the sedimentary OC) was lost when extracting iron oxides a second time, confirming that the CBD extraction only removes iron-associated OC.

Caption for Tables 2 and 3: Tables 2 and 3 (on following pages) show all measured parameters for the studied set of sediments. These parameters are meant to highlight isotopic and chemical differences between the original sediment samples and the same samples after the control experiment (Table 2), and between the original sediment samples and the same samples after the iron extraction (Table 3). The initial and final organic carbon (%OC initial, %OC after ext.) and total nitrogen contents (%TN initial, %TN after ext.) as well as the carbon (δ^{13}C initial, δ^{13}C after ext.) and nitrogen (δ^{15}N initial, δ^{15}N after ext.) isotopic compositions of the sediments were measured using an elemental analyzer coupled to an isotope ratio mass spectrometer. The %OC and %TN associated with extractable iron (OC-Fe and TN-Fe) was calculated from the loss of OC and TN following the extraction. The iron removed during the extraction was measured using inductively-coupled plasma mass spectrometry and is expressed in µg of iron per gram of dry sediment. Surface area measurements were performed on sediments from which organic matter was removed using concentrated hydrogen peroxide as described above. Sulfidic sediments are highlighted in red, anoxic and seasonally anoxic in orange, typical continental margin sediments bathed by oxic waters in yellow, deltaic and estuarine samples in green and deep-sea sediments in blue.

Table 8-2

Sample	depth	% OC	% OC-H_20	$\delta^{13}C$	$\delta^{13}C$	$\delta^{13}C$	% TN	% TN-Fe	$\delta^{15}N$	$\delta^{15}N$	$\delta^{15}N$	C/N	C/N	C/N
	(cm)	*before*		*initial*	*after ext.*	$OC-H_20$	*initial*		*initial*	*after ext.*	$TN-H_20$	*initial*	*after ext.*	$OC-H_20$
Black Sea	0 to 0.5	4.61	2.91	-26.60	-26.18	-40.63	0.34	0.00	1.73	2.53		15.69	15.24	
	9 to 11	4.21	12.12	-25.58	-25.59	-25.51	0.30	0.00	0.91	1.16		16.16	14.20	
Mexican margin 306	0 to 0.5	6.66	1.83	-22.06	-22.12	-18.84	0.84	0.00	9.77	10.41		9.27	9.10	
	3 to 4	6.98	7.05	-22.03	-22.04	-21.90	0.96	3.33	10.29	10.53	9.01	8.49	8.17	17.97
	16 to 19	6.65	9.23	-21.17	-21.25	-20.38	0.91	0.00	10.62	10.37		8.51	7.73	
Indian Margin	0 to 3	5.18	4.64	-23.09	-23.11	-22.67	0.76	5.82	8.29	7.16	26.55	7.99	8.08	6.38
Lake Brock	0 to 1	1.18	27.53	-27.96	-27.92	-28.06	0.12	33.62	4.96	4.94	4.99	11.14	12.17	9.13
	9 to 11	2.00	19.22	-27.24	-27.32	-26.90	0.22	20.84	5.46	5.78	4.25	10.41	10.62	9.60
Saanish intlet	0 to 20	2.21	7.87	-22.45	-22.52	-20.51	0.34	7.39	9.31	9.24	10.22	7.51	7.47	8.00
Madeira turbidite 7-8-9		0.95	4.45	-21.93	-22.11	-18.07	0.07	0.00	6.25	6.50		15.04	14.38	
Mexican margin 305	0 to 0.5	2.82	10.34	-21.50	-21.55	-21.06	0.37	10.21	9.94	11.06	0.10	9.00	8.99	9.11
	4 to 5	2.75	10.40	-21.40	-21.60	-19.68	0.41	9.30	10.76	10.90	9.43	7.78	7.69	8.71
	22 to 27	2.66	4.24	-21.34	-21.51	-17.51	0.33	0.00	10.17	10.32		9.46	9.06	
Mexican margin 304	0 to 0.5	2.36	10.30	-22.27	-22.29	-22.09	0.27	15.28	12.28	12.80	9.42	10.32	10.92	6.95
	5 to 6	2.25	8.45	-22.21	-22.41	-20.04	0.30	7.85	12.30	12.55	9.42	8.64	8.59	9.30
	19 to 22	2.27	4.09	-22.66	-22.92	-16.57	0.27	0.00	12.26	12.31		9.89	9.49	
Arabian Sea	0 to 0.5	1.11	7.39	-21.65	-22.00	-17.26	0.16	0.00	11.40	11.06		8.04	7.44	
	10 to 12	1.03	1.06	-22.35	-22.41	-16.75	0.13	0.00	9.85	11.28		9.37	9.27	
Mexican margin 303	0 to 0.5	1.42	12.47	-21.66	-21.81	-20.61	0.19	12.20	11.53	11.86	9.15	8.84	8.81	9.04
	14 to 16	1.44	14.15	-22.16	-22.18	-22.04	0.17	13.07	12.19	12.29	11.52	9.69	9.57	10.50
	22 to 27	1.51	8.35	-22.30	-22.77	-17.14	0.17	12.18	11.91	12.19	9.89	10.46	10.92	7.17
Wash Coast 205	11 to 12	2.24	7.14	-22.32	-22.55	-19.44	0.21	10.60	8.61	8.20	12.12	12.20	12.67	8.22
Wash. Coast 215	11 to 12	3.00	0.00	-22.91	-22.68		0.27	0.00	10.12	9.83		12.75	12.75	
Wash. Coast 213	11 to 12	2.10	0.00	-23.69	-23.52		0.28	0.00	9.32	9.17		8.72	8.72	
St-Lawrence 20	0 to 35	1.36	9.10	-22.55	-22.75	-20.55	0.14	9.05	6.27	6.62	2.75	11.24	11.24	11.30
St-Lawrence Gulf	1.5 to 5	2.13	4.50	-22.40	-22.56	-19.00	0.36	1.12	9.81	9.80	9.98	6.86	6.63	27.66
	470 to 500	0.91	8.97	-23.11	-23.05	-23.71	0.11	12.36	9.89	10.14	8.07	9.91	10.30	7.19
Wash. Coast 202	11 to 12	1.33	5.08	-22.02	-21.97	-23.07	0.11	8.12	11.26	11.54	8.01	13.65	14.10	8.54
Wash Coast 204	11 to 12	1.40	0.00	-24.00	-24.13		0.10	3.28	8.29	7.88	20.49	15.76	16.30	0.00
St-Lawrence 23	0 to 35	1.43	6.96	-24.34	-24.60	-20.87	0.13	13.02	4.84	5.34	1.50	12.83	13.72	6.86
Wash Coast 206	11 to 12	1.67	10.29	-21.85	-22.63	-15.04	0.16	8.89	9.49	9.49	9.51	11.99	11.80	13.88
Wash. Coast 203	11 to 12	2.15	9.10	-23.46	-23.62	-21.86	0.28	5.98	8.19	8.75	-0.61	8.96	8.66	13.61
St-Lawrence 25	0 to 35	1.12	7.92	-24.57	-24.62	-23.99	0.09	11.09	4.98	5.48	0.97	13.80	14.29	9.86
Wash. Coast 201	11 to 12	1.14	9.31	-22.87	-22.90	-22.58	0.15	9.47	10.04	11.62	-5.06	8.70	8.71	8.55
Eel iver basin	0 to 1	1.11	8.24	-25.25	-25.42	-23.36	0.10	13.80	6.00	5.12	11.52	12.49	13.30	7.46
	15 to 20	0.99	1.42	-25.51	-25.45	-29.68	0.09	1.31	5.75	5.48	26.13	12.92	12.90	14.04
MaKenzie river delta	0 to 1	1.18	5.64	-26.17	-26.70	-17.31	0.19	5.89	2.22	2.92	-8.96	7.35	7.37	7.04
Southern Ocean	8 to 12	0.45	0.00	-23.59	-23.84									
Station M	0 to 1	1.39	4.60	-23.50	-23.70	-19.36	0.23	1.68	10.23	10.36	2.94	7.19	6.98	19.64
	15 to 20	1.21	7.65	-23.62	-23.92	-20.00	0.18	11.37	10.64	10.94	8.31	7.88	8.21	5.30
Equatorial Pacific 0^oN	0 to 0.5	0.27	0.00	-21.56	-22.60									
Equatorial Pacific 9^oN	10 to 12	0.30	0.00	-22.45	-22.80									

Table 8-3

Sample	depth	% OC	%OC-Fe	$\delta^{13}C$	$\delta^{13}C$	$\delta^{13}C$	% TN	% TN-Fe	$\delta^{15}N$	$\delta^{15}N$	$\delta^{15}N$	C/N	C/N	C/N	Fe	SA		OC:Fe
	(cm)	*before*		*initial*	*after ext.*	*Fe-OC*	*initial*		*initial*	*after ext.*	*Fe-TN*	*initial*	*after ext.*	Fe-OC		*initial*	*after ext.*	
															µg/g	m2/g		
Black Sea	0 to 0.5	4.48	24.98	-26.18	-26.48	-25.28	0.34	29.55	2.53	2.77	1.95	15.24	16.23	12.89	1695			30.79
	9 to 11	3.70	6.84	-25.59	-26.02	-19.76	0.30	22.04	1.16	1.22	0.95	14.20	16.97	4.40	1000	20.21	36.20	11.80
Mexican margin 306	0 to 0.5	6.54	22.31	-22.12	-22.24	-21.68	0.84	24.84	10.41	10.19	11.09	9.10	9.40	8.17	4018			16.95
	3 to 4	6.49	22.83	-22.04	-22.58	-20.20	0.93	31.53	10.53	10.69	10.19	8.17	9.20	5.91	2603	43.17	50.78	26.56
	16 to 19	6.04	18.41	-21.25	-21.62	-19.61	0.91	27.43	10.37	10.63	9.66	7.73	8.69	5.19	1642			31.59
Indian Margin	0 to 3	4.94	26.59	-23.11	-23.01	-23.93	0.71	18.52	7.16	8.05	3.26	8.08	8.85	4.72	3519	25.52	32.78	7.08
Lake Brock	0 to 1	0.85	26.41	-27.92	-27.73	-28.45	0.08	18.99	4.94	4.94	4.94	12.17	11.03	17.03	1963	4.23	2.71	5.39
	9 to 11	1.61	10.81	-27.32	-26.73	-28.97	0.18	32.53	5.78	5.77	5.80	10.62	11.58	8.62	2500			7.96
Saanish intlet	0 to 20	2.03	28.09	-22.52	-22.72	-22.00	0.32	30.78	9.24	8.75	10.34	7.47	7.76	6.82	5610			4.75
Madeira turbidite 7-8-9		0.90	29.76	-22.11	-22.62	-20.92	0.07	15.81	6.50	6.90	4.39	14.38	11.99	27.06	1314			9.56
Mexican margin 305	0 to 0.5	2.53	12.70	-21.55	-21.81	-19.74	0.33	10.71	11.06	10.46	16.00	8.99	8.79	10.66	4679			3.20
	4 to 5	2.46	9.10	-21.60	-22.00	-17.65	0.37	20.82	10.90	10.76	11.43	7.69	8.82	3.36	3781			2.76
	22 to 27	2.55	13.00	-21.51	-21.75	-19.91	0.33	27.07	10.32	10.64	9.44	9.06	10.80	4.35	1069			14.48
Mexican margin 304	0 to 0.5	2.12	30.03	-22.29	-22.35	-22.15	0.23	11.25	12.80	12.35	16.37	10.92	8.61	29.17	5800			5.12
	5 to 6	2.06	22.31	-22.41	-23.02	-20.29	0.28	34.42	12.55	11.88	13.81	8.59	10.17	5.57	6021	54.44	61.14	3.55
	19 to 22	2.18	19.65	-22.92	-23.19	-21.85	0.27	30.89	12.31	12.12	12.75	9.49	11.03	6.03	2513			7.94
Arabian Sea	0 to 0.5	1.02	26.89	-22.00	-22.36	-21.01	0.16	47.78	11.06	10.29	11.90	7.44	10.42	4.19	2799	35.00	33.87	4.59
	10 to 12	1.02	18.78	-22.41	-22.89	-20.32	0.13	26.81	11.28	10.40	13.70	9.27	10.29	6.49	1574	28.02	42.82	5.69
Mexican margin 303	0 to 0.5	1.24	18.71	-21.81	-22.89	-17.15	0.16	27.40	11.86	11.63	12.45	8.81	9.87	6.02	9215			1.18
	14 to 16	1.23	7.79	-22.18	-22.86	-14.18	0.15	18.18	12.29	11.55	15.58	9.57	10.78	4.10	5229	78.96	74.94	0.86
	22 to 27	1.39	12.20	-22.77	-23.42	-18.04	0.15	19.04	12.19	11.83	13.70	10.92	11.84	6.99	2184			3.62
Wash Coast 205	11 to 12	2.08	24.78	-22.55	-24.59	-16.35	0.19	21.65	8.20	7.55	10.53	12.67	12.16	14.50	5090			4.72
Wash. Coast 215	11 to 12	3.00	41.69	-22.68	-24.06	-20.75	0.27	39.11	9.83	10.22	9.21	12.75	12.20	13.59	15400			3.79
Wash. Coast 213	11 to 12	2.10	17.22	-23.52	-24.10	-20.75	0.28	29.04	9.17	8.40	11.06	8.72	10.18	5.17	4509			3.75
St-Lawrence 20	0 to 35	1.24	20.43	-22.75	-22.89	-22.23	0.13	22.17	6.62	6.47	7.15	11.24	11.49	10.36	4059			2.91
St-Lawrence Gulf	1.5 to 5	2.04	18.72	-22.56	-22.57	-22.52	0.36	14.93	9.80	10.37	6.60	6.63	6.33	8.31	5742			3.10
	470 to 500	0.83	27.25	-23.05	-23.72	-21.24	0.09	7.78	10.14	9.28	20.37	10.30	8.12	36.06	3605			2.92
Wash. Coast 202	11 to 12	1.27	28.05	-21.97	-22.09	-21.65	0.10	27.23	11.54	11.01	12.96	14.10	13.94	14.53	6230			2.66
Wash Coast 204	11 to 12	1.40	24.15	-24.13	-24.41	-23.27	0.10	23.56	7.88	8.45	6.05	16.30	16.17	16.71	6933			2.28
St-Lawrence 23	0 to 35	1.33	23.63	-24.60	-24.31	-25.54	0.11	19.56	5.34	4.87	7.30	13.72	13.02	16.58	7279	47.21	43.90	2.01
Wash Coast 206	11 to 12	1.50	24.97	-22.63	-23.29	-20.67	0.15	29.21	9.49	9.24	10.09	11.80	12.51	10.09	9178			1.91
Wash. Coast 203	11 to 12	1.96	14.03	-23.62	-23.90	-21.91	0.26	21.33	8.75	8.34	10.28	8.66	9.46	5.70	7091			1.81
St-Lawrence 25	0 to 35	1.03	25.13	-24.62	-24.64	-24.57	0.08	21.72	5.48	5.03	7.09	14.29	13.66	16.53	7053			1.71
Wash. Coast 201	11 to 12	1.03	19.94	-22.90	-23.99	-18.53	0.14	23.01	11.62	9.22	19.67	8.71	9.06	7.55	6235			1.54
Eel iver basin	0 to 1	1.02	12.90	-25.42	-26.03	-21.31	0.09	11.30	5.12	5.83	-0.52	13.30	13.06	15.18	5974			1.03
	15 to 20	0.98	16.05	-25.45	-26.23	-21.38	0.09	24.54	5.48	5.41	5.67	12.90	14.35	8.44	4655			1.58
MaKenzie river delta	0 to 1	1.11	7.64	-26.70	-25.91	-36.31	0.18	8.95	2.92	1.54	16.97	7.37	7.47	6.29	20259			0.20
Southern Ocean	8 to 12	0.45	29.00	-23.84	-23.80	-23.95									1380	20.94	18.76	4.40
Station M	0 to 1	1.33	17.13	-23.70	-24.33	-20.69	0.22	24.00	10.36	10.22	10.79	6.98	7.61	4.98	3669			2.89
	15 to 20	1.11	11.39	-23.92	-24.20	-21.77	0.16	12.47	10.94	10.76	12.26	8.21	8.31	7.50	2172			2.73
Equatorial Pacific 0°N	0 to 0.5	0.27	34.79	-22.60	-22.60	-22.60									1759			2.49
Equatorial Pacific 9°N	10 to 12	0.30	12.16	-22.80	-23.85	-15.15									4643	90.66	112.20	0.36

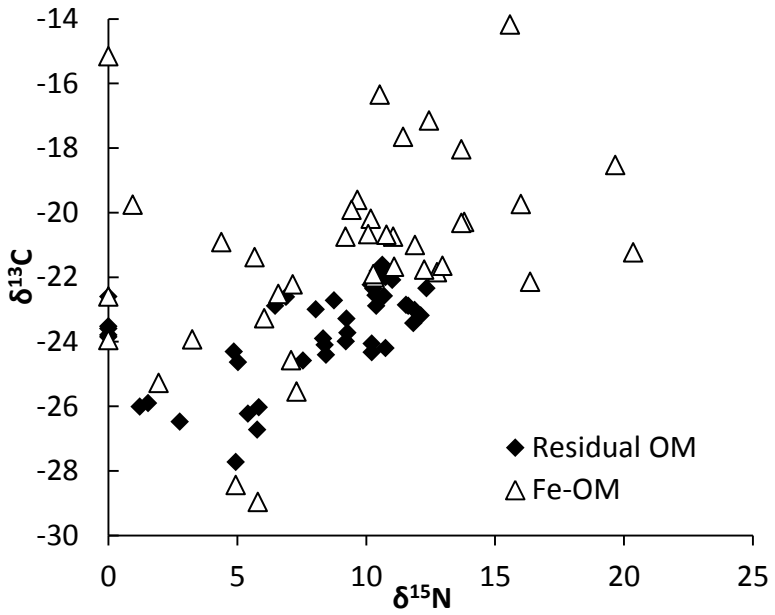

Figure 8-1: Stable C and N isotope compositions of the Fe-associated OC fraction (red diamonds) and the OM fraction not associated to iron (blue diamonds), showing a general enrichment in $\delta^{13}C$ for the Fe-OM fraction in most of the sediments.

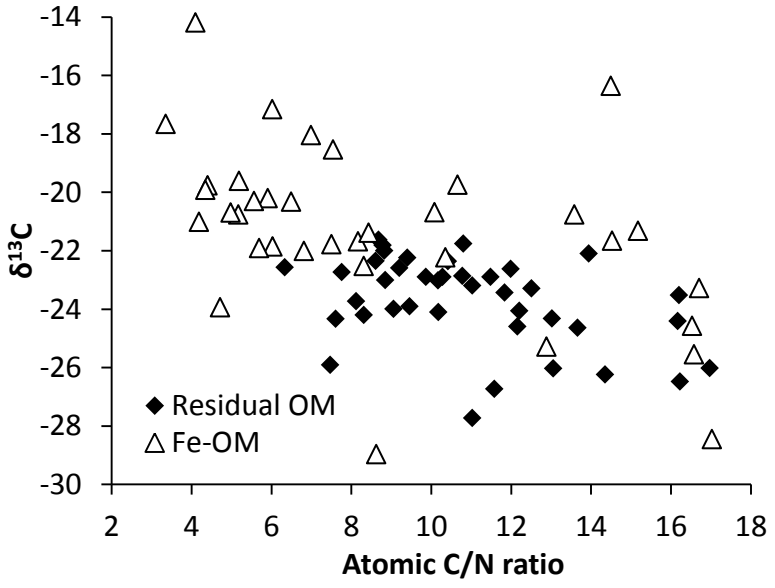

Figure 8-2: Stable carbon isotope signatures and atomic C/N ratios of the Fe-associated OM fraction (red diamonds) and the OM fraction not associated to iron (blue diamonds), showing a general enrichment in $\delta^{13}C$ and N (relative to C) for the Fe-OM fraction.

Appendix A3

This Appendix presents details and data that, due to space constraints, could not be included in the original manuscript (Chapter 3). It is separated into three sections: the first section shows $\delta^{13}C$ DOC time series for replicate vials of each redox and amendment condition, the second shows dissolved iron concentration in control vials for each redox condition and the third deals with thermodynamic calculations of feammox feasibility in marine sediments.

1. Time series of $\delta^{13}C$ of DOC

The concentration of the algal tracer in solution decreases throughout the incubation, following first order kinetics down to a relatively stable asymptotic value, attained within 30 to 150 days of the start of the incubation, depending on redox condition. Final DOC concentrations are given in Table 3-1 of the manuscript. Table 3-2 of the manuscript also shows the degradation rate and half-life of the DOC, the latter being 2 to 3 times shorter under oxic rather than anaerobic conditions. These rate constants are calculated from the decrease in DOC concentrations between sampling days, as discussed in the manuscript.

This section of the supplementary information shows time series of DOC concentrations, concomitantly to its $\delta^{13}C$ signature. Profiles of replicate vials are arranged firstly by amendment condition and secondly by redox condition. Timepoint values for each of the duplicate vials are shown as either triangles for the first vials (V1) or squares for the second vials (V2) of each condition. For the iron-amended condition, only one vial was measured for each of the three redox conditions. All concentrations (in $\mu g\ mL^{-1}$) are represented by white symbols whereas $\delta^{13}C$ (in ‰) values are shown in black. Background plot colors were modified to indicate the redox condition during sampling, either oxic or anoxic, and to highlight trends observed in DOC concentration or $\delta^{13}C$ upon changes in redox condition. A white background was used for

samples taken under oxic conditions, whereas a grey background was used for samples taken under anoxic conditions. We outline important trends observed for each amendment condition within the corresponding sub-section below. Note that errors on $\delta^{13}C$ measurements are slightly higher for amendment conditions in which the organic tracer was not added, due to lower DOC concentrations.

OM amended vials

For all redox conditions of this amendment scenario, $\delta^{13}C$ drifts from the depleted signature of the tracer (-41.34‰ ± 0.12‰) to a more enriched signature (between -30 and -36‰), demonstrating partial degradation, release and desorption of soluble material from the native sediment organic matter ($\delta^{13}C$ = -24.29 ± 0.10‰) into solution.

Because of higher DOC degradation rates under oxic conditions, we see a steeper decrease in DOC concentrations in oxic vials relative to anoxic vials. Under mixed redox conditions, the decomposition of DOC follows a segmented decrease, with slower DOC losses during the initial anoxic segment, followed by a sharper drop during oxic subsampling. We do not observe any clear trend in DOC concentrations during subsequent shifts in redox condition.

Oxic condition

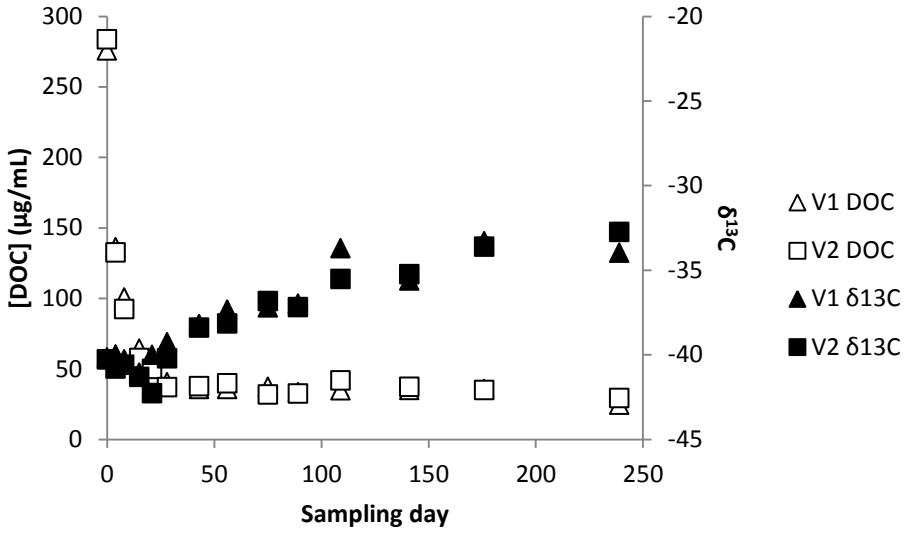

Figure 9-1: The temporal evolution of the DOC concentration (white) and $\delta^{13}C$ signature (black) for the oxic, OM amended scenario. V1 and V2 each represent duplicate vials.

Mixed redox condition

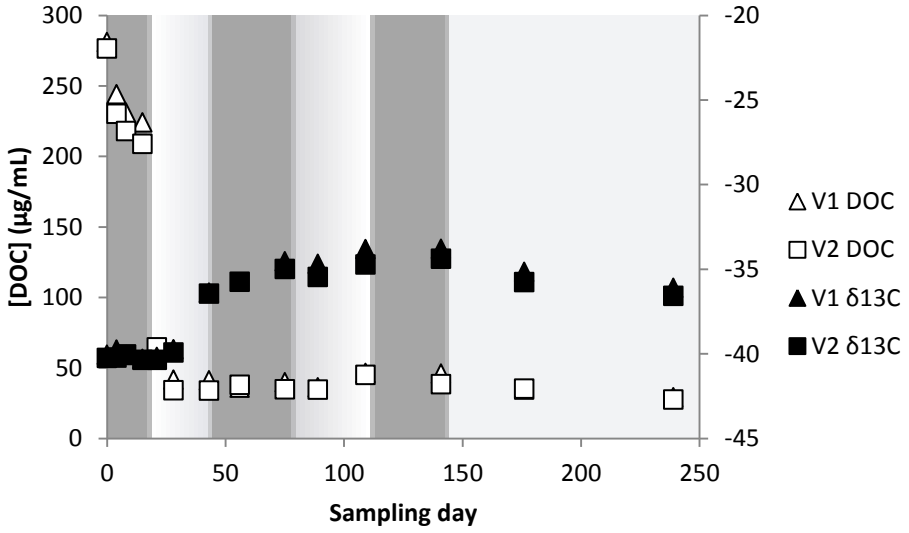

Figure 9-2: The temporal evolution of the DOC concentration (white) and $\delta^{13}C$ signature (black) for the mixed redox, OM amended scenario. Periods appearing with a grey background were anoxic at the time of subsampling while those appearing on a white background were subsampled while the vials were maintained under oxic conditions. V1 and V2 each represent duplicate vials.

Anoxic condition

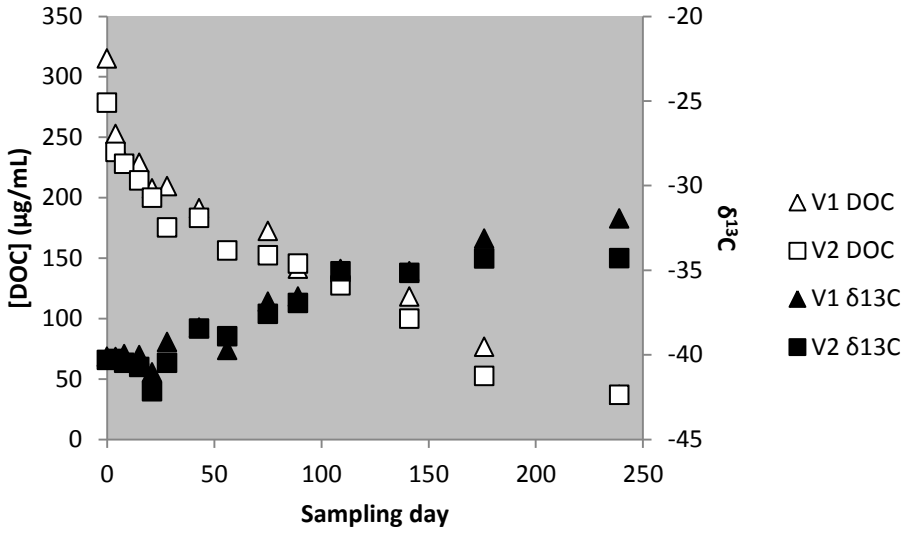

Figure 9-3: The temporal evolution of the DOC concentration (white) and $\delta^{13}C$ signature (black) for the anoxic, OM amended scenario. V1 and V2 each represent duplicate vials.

Fe and OM amendment scenario

DOC concentrations and $\delta^{13}C$ profiles are similar for vials that were both iron- & OM-amended and those amended only with OM. We see similar degradation profiles, with accentuated decomposition upon exposure to oxygen. As discussed in the manuscript, the precipitation of iron oxides in the oxic and mixed redox vials of this amendment condition, increases the partitioning of DOC from solution onto solid particles, therefore reducing the DOC concentrations compared to vials amended with OM only (see Table 3-1 of manuscript). Note that there is an initial DOC concentration discrepancy between duplicate vials of the anoxic condition of Fe and OM amendment scenario, which is carried over to the following time points. The slope of the DOC concentration decrease is however not affected, therefore both plots were used to calculate the rate of DOC decomposition (Table 3-2 of manuscript).

A noteworthy feature of these $\delta^{13}C$-DOC plots is the initial drop in $\delta^{13}C$ observed in oxic vials. This feature is not observed in vials amended with OM only. We postulate that the decrease in

$\delta^{13}C$ reflects the preferential absorption and/or coagulation of $\delta^{13}C$-enriched DOC with iron oxides, leaving in solution $\delta^{13}C$-depleted DOC. This is consistent with the comparison of solid-state $\delta^{13}C$ signatures of iron-associated versus non-iron-associated OC in marine sediments, reported previously (Lalonde et al., 2012). A similar $\delta^{13}C$ drop (though not as important) is observed upon transitioning between anoxic and oxic conditions in the mixed redox scenario, also likely caused by the adsorption and/or coagulation of $\delta^{13}C$-enriched molecules upon precipitation of iron oxides.

Oxic condition

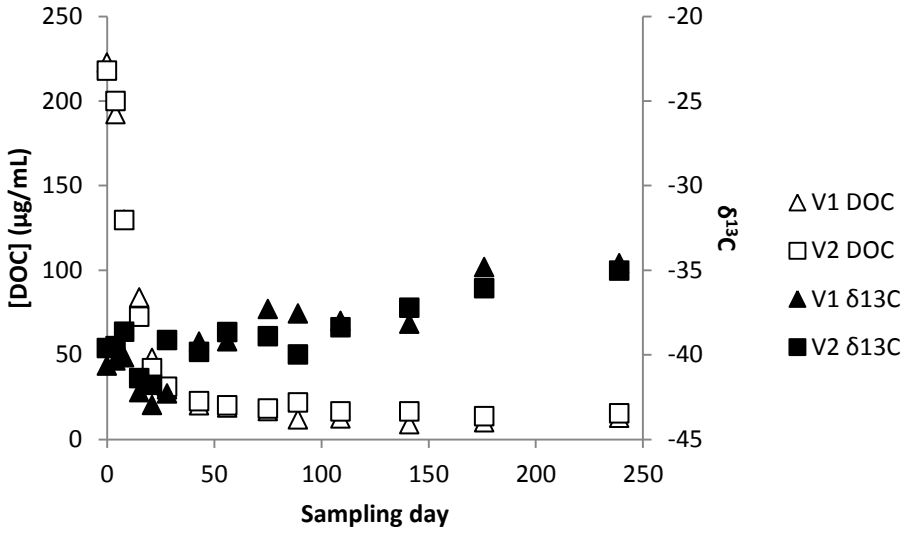

Figure 9-4: The temporal evolution of the DOC concentration (white) and $\delta^{13}C$ signature (black) for the oxic, Fe and OM amended scenario. V1 and V2 each represent duplicate vials.

Mixed redox condition

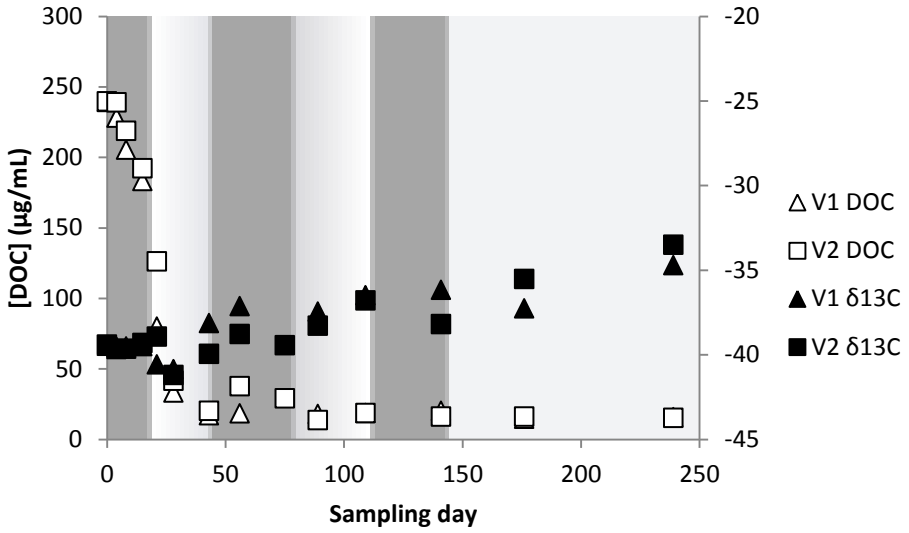

Figure 9-5: The temporal evolution of the DOC concentration (white) and $\delta^{13}C$ signature (black) for the mixed redox, Fe and OM amended scenario. Periods appearing with a grey background were anoxic at the time of subsampling while those appearing on a white background were subsampled while the vials were maintained under oxic conditions. V1 and V2 each represent duplicate vials.

Anoxic condition

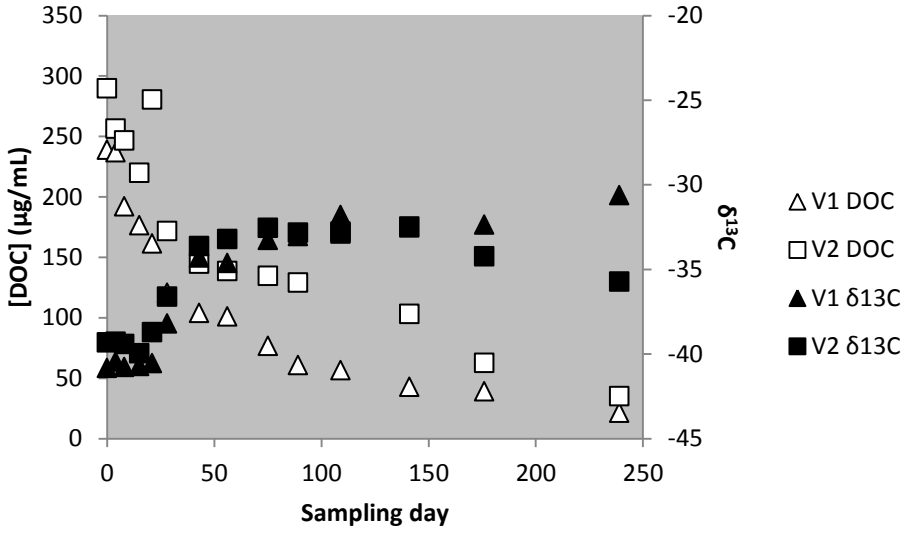

Figure 9-6: The temporal evolution of the DOC concentration (white) and $\delta^{13}C$ signature (black) for the anoxic, Fe and OM amended scenario. V1 and V2 each represent duplicate vials.

Control scenario

DOC concentrations measured in the control scenario are much lower than for the OM-amended scenarios. Concentrations start at 2 to 4 µg mL^{-1}, increasing progressively during the course of the experiment. $\delta^{13}C$ values do not seem to follow any obvious pattern in mixed redox and anoxic incubations, but become progressively more depleted in oxic vials.

Oxic condition

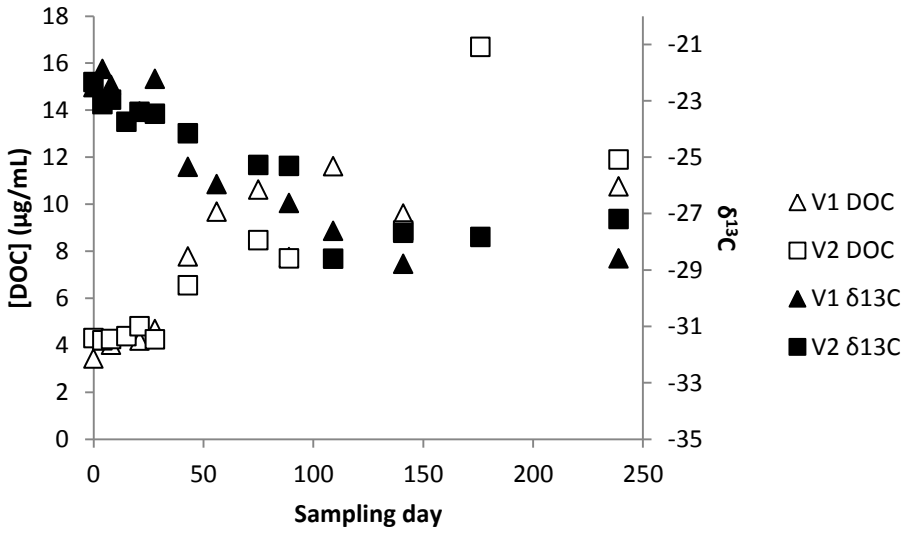

Figure 9-7: The temporal evolution of the DOC concentration (white) and $\delta^{13}C$ signature (black) for the oxic, control scenario. V1 and V2 each represent duplicate vials.

Mixed Redox condition

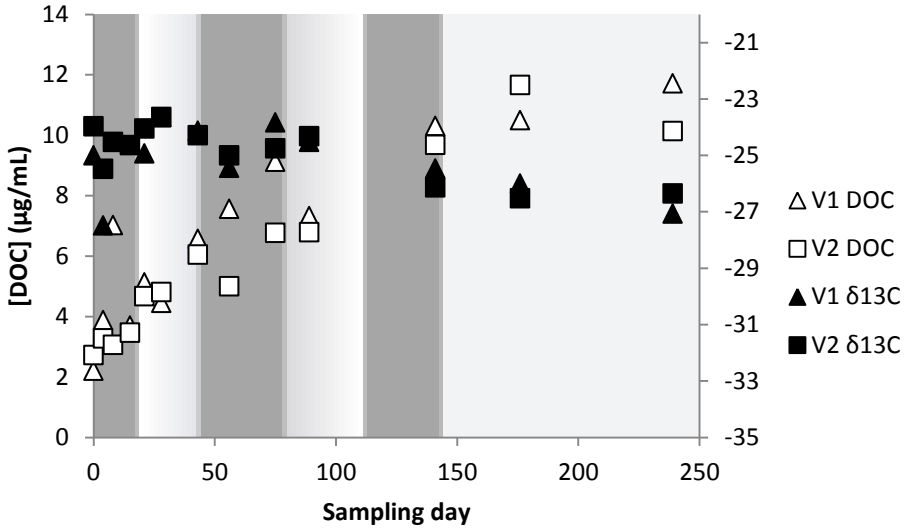

Figure 9-8: The temporal evolution of the DOC concentration (white) and $\delta^{13}C$ signature (black) for the mixed redox, control scenario. Periods appearing with a grey background were anoxic at the time of subsampling while those appearing on a white background were subsampled while the vials were maintained under oxic conditions. V1 and V2 each represent duplicate vials.

Anoxic Condition

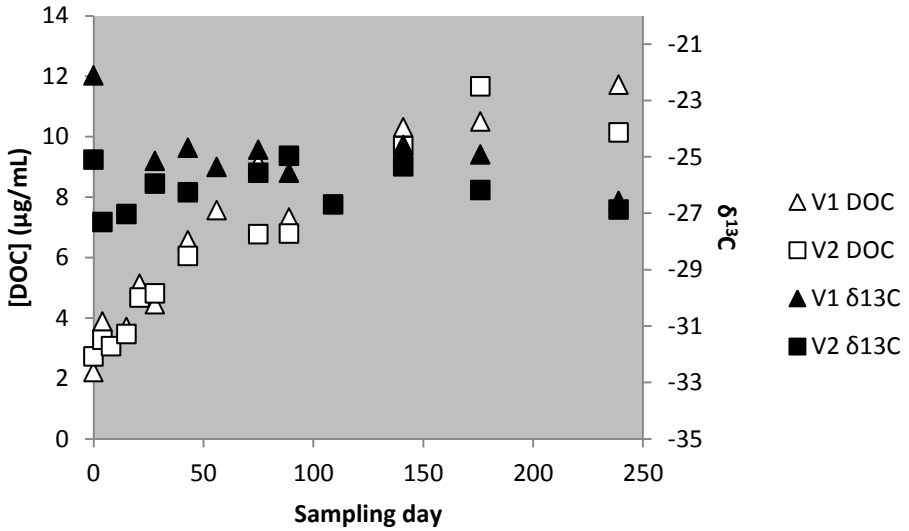

Figure 9-9: The temporal evolution of the DOC concentration (white) and $\delta^{13}C$ signature (black) for the anoxic, control scenario. V1 and V2 each represent duplicate vials.

Fe amended scenario

DOC concentration and $\delta^{13}C$ profiles are similar for control and iron-amended scenarios. Increased partitioning of DOC onto solid particles decreases DOC concentrations, as shown in Table 3-1 of the manuscript.

Oxic condition

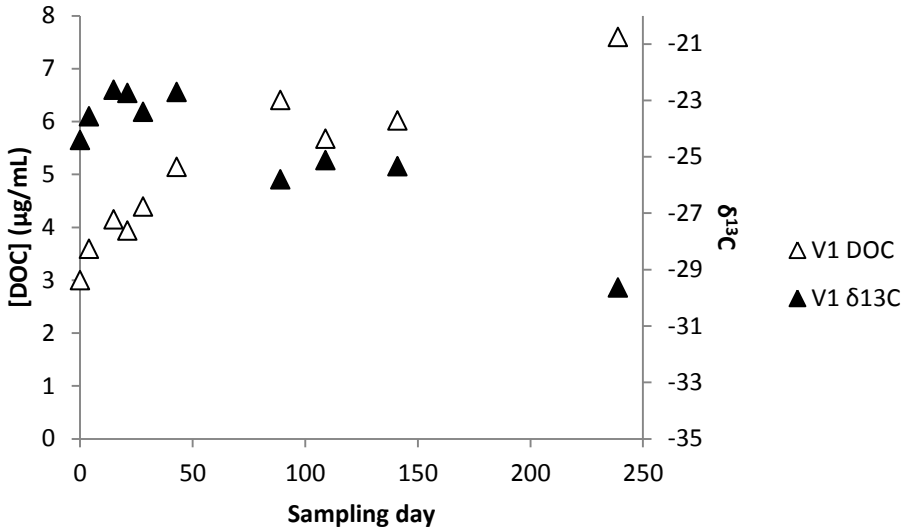

Figure 9-10: The temporal evolution of the DOC concentration (white) and $\delta^{13}C$ signature (black) for the oxic, Fe amended scenario. V1 and V2 each represent duplicate vials.

Mixed redox condition

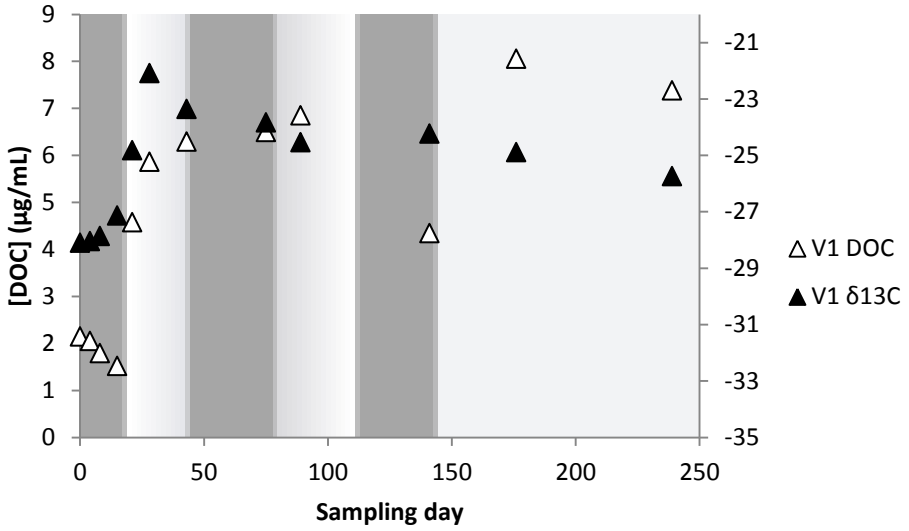

Figure 9-11: The temporal evolution of the DOC concentration (white) and $\delta^{13}C$ signature (black) for the mixed redox, Fe amended scenario. Periods appearing with a grey background were anoxic at the time of subsampling while those appearing on a white background were subsampled while the vials were maintained under oxic conditions. V1 and V2 each represent duplicate vials.

Anoxic Condition

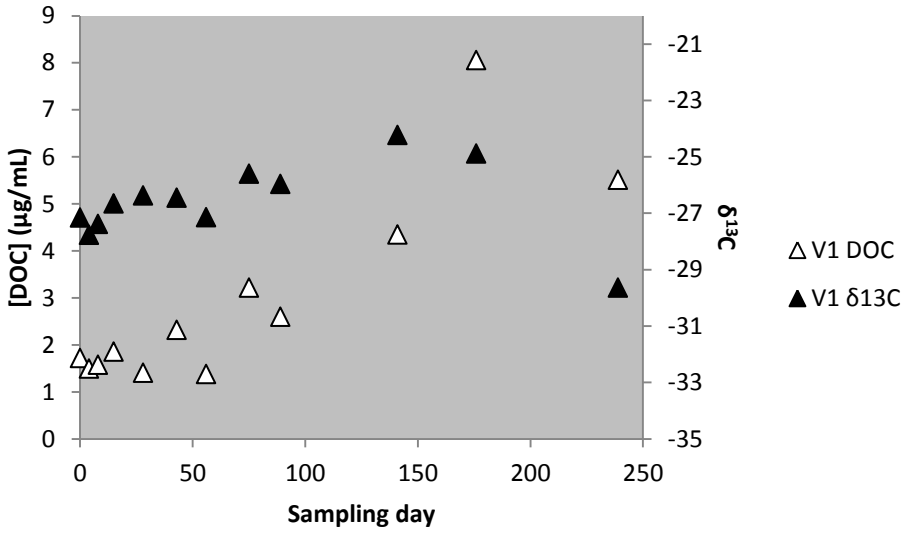

Figure 9-12: The temporal evolution of the DOC concentration (white) and $\delta^{13}C$ signature (black) for the anoxic, Fe scenario. V1 and V2 each represent duplicate vials.

2. Iron concentration profiles

Dissolved iron concentrations were measured in the anoxic control scenarios, in part to verify that the anoxic redox conditions were properly maintained throughout the incubation and during sampling. Control incubations were connected downstream of all other vials (Figure 1 of manuscript). Given the experimental design, these vials would be the first to become oxic due to a break in the flow of nitrogen gas used to maintain anoxic conditions. In the aerobic scenarios, soluble iron(II) concentrations were below detection limit within one week of the start of the incubations (except for one point in the mixed redox condition, which we believe to be a method or sampling artifact). In contrast, under the anoxic scenario, there was progressive release of dissolved iron from the unamended, natural sediment, to a concentration slightly above 1 µg mL^{-1}. Time series of dissolved iron concentrations in the control vials are shown below (only the most downstream of the duplicate vials was sampled for this analysis).

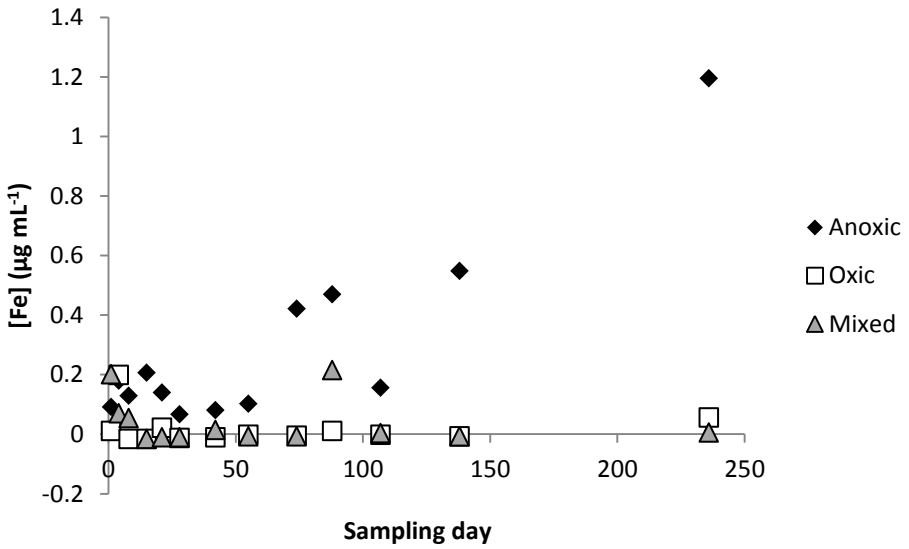

Figure 9-13: Soluble Fe^{2+} concentration with time for the unamended control vials in the anoxic, oxic and mixed redox scenarios.

Dissolved iron(II) concentrations in vials amended with iron(II) chloride were below detection within one week following its addition. In reactors maintained under anoxic conditions, iron(II) concentrations decreased from 250 µg mL^{-1} to about 20 µg mL^{-1} upon the addition of iron(II) chloride (Fe and Fe-OM scenarios), most likely in response to the strong affinity of iron(II) for sedimentary mineral surfaces (Burdige, 1993), its precipitation as sulfides throughout the incubation, as well as its oxidation to iron(III) by electron acceptors other than oxygen, such as manganese oxides and nitrate, at the start of the incubation (Magen et al., 2011). Iron(II) profiles of iron amended scenarios are shown here:

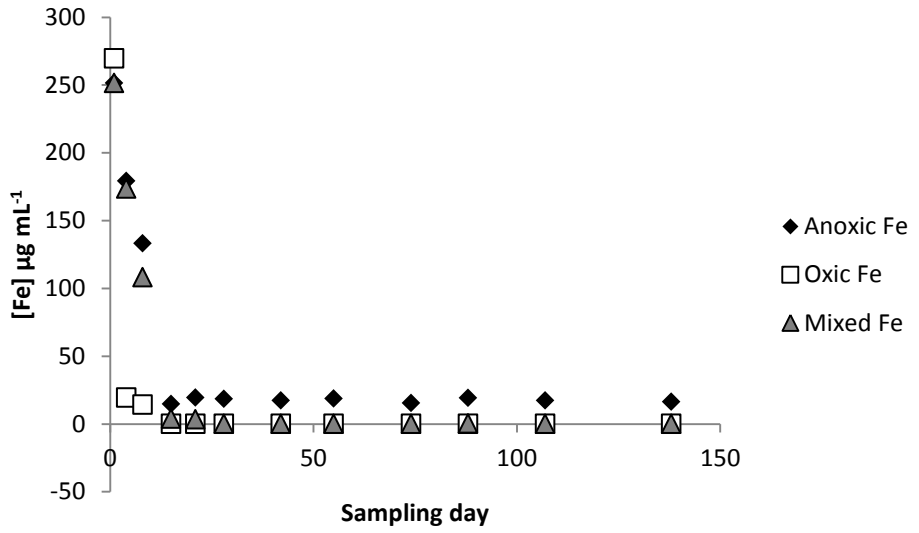

Figure 9-14: Soluble Fe^{2+} concentration with time for the Fe(II) amended vials in the anoxic, oxic and mixed redox scenarios.

It should be noted that dissolved iron was not measured in the OM-amended incubations as high DOM concentrations interfere with the complexation iron(II) to ferrozine and the generation of the chromophoric product.

3. Calculations for thermodynamic feasibility of feammox in marine sediments

Luther III et al. (1997) were first to propose the possible coupling of ammonium oxidation to N_2 through iron oxide reduction, though they state that Fe^{3+} catalysis of N_2 formation can only occur at pH < 6.8 based on pE-pH calculations. Above this pH, (Luther III et al., 1997) state that "the reaction between Fe^{3+} species and NH_4^+ to form N_2 is thermodynamically unfavorable". In contrast, Yang et al. (2012) note that "… Feammox to N_2 using ferrihydrite, a poorly crystalline Fe oxide … remains energetically favorable over a wide pH range". The thermodynamic feasibility of this reaction in soil systems is outlined in the supplementary information of Yang et al. (2012).

In the following section, we repeat these calculations, using reaction conditions typically found in marine sediments.

Firstly, we reproduced the electrochemical half-reactions D and G featured in Luther (1997) and associated log(K) and ΔG^o values. We also show the reduction of nitrite to ammonium using log(K) values from Stumm and Morgan (1970) (labelled below as equation H):

Table 9-1: Log(K) and ΔG^o values for selected electrochemical half-reactions

Half reactions:	Log (K)	ΔG^o (kJ/mol)
D) $1/6N_2 + 4/3H^+ + e^- \rightarrow 1/3NH_4^+$	+ 4.65	-91.12
G) $FeOOH + 3H^+ + e^- \rightarrow Fe^{2+} + 2H_20$	+ 15.99	-20.50
H) $1/6\ NO_2^- + 4/3\ H^+ + e^- \rightarrow 1/6\ NH_4^+ + 1/3\ H_2O$	+ 15.14	-86.27

The reduction reaction of iron oxide (equation G) can be coupled to the oxidation of ammonium (reverse of equation D and H) by reversing equations D and H and adding them to equation G to

yield electrochemical reactions A and B (table below). Log(K) values for the complete electrochemical reactions can then be calculated by subtracting Log(K) of D or H from the Log(K) of G (as carried out in Luther 1997):

Table 9-2: Log(K) and ΔG^{o} values for selected electrochemical reactions

Reactions:	Log (K)	ΔG^{o} (kJ/mol)
A) $FeOOH + 1/3NH_4^+ + 5/3H^+ \rightarrow 1/6N_2 + Fe^{2+} + 2H_2O$	+ 11.34	-64.62
B) $FeOOH + 1/6NH_4^+ + 5/3H^+ \rightarrow 1/6NO_2^- + Fe^{2+} + 5/3H_2O$	+ 0.85	-4.84

Positive Log(K) and negative ΔG^{o} indicate that these reactions are thermodynamically feasible when the system is under standard conditions, i.e. at a temperature of 298 K, total pressure of 1 atmosphere when all solutes are assigned a unit activity. We can calculate ΔG values for the reactions under conditions that are more typical of marine sediments using the following equation for process A.

$$\Delta G = \Delta G^{\circ} + RT \ln \frac{[N_2]^{1/6}[Fe^{2+}]^{1}[H_2O]^{2}}{[FeOOH]^{1}[NH_4^+]^{1/3}[H^+]^{5/3}}$$

where R is the gas constant (0.008314 kJ/mol*K) and T is the temperature in K (277 K). An activity of 1 is assigned to the solid-phase iron oxide minerals (FeOOH) and water as activities of pure solids and liquids are assumed to be equal to unity (Laidler and Meiser, 1999). The concentration of N_2 was at 0.001 mol/L (as used by Yang et al. 2012), based its aqueous solubility. Fe^{2+} concentrations in oxic sediment porewaters are extremely low since Fe^{2+} is quickly oxidized to Fe^{3+} and precipitated as iron oxides. We used 0.06nM, the solubility of freshly precipitated ferrihydrite in oxic seawater (Raiswell and Canfield, 2012a), for our Fe^{2+} concentration. The equation therefore becomes:

$$\Delta G = -64.62 + 0.008314 * 277 * \ln \frac{[0.001]^{1/6}[0.6 * 10^{-9}]^1[1]^2}{[1]^1[NH_4^+]^{1/3}[H^+]^{5/3}}$$

We can isolate the NH_4^+ and H^+ concentrations from the equation to determine the pH and ammonium concentration dependency of the Gibb's free energy for the oxidation of ammonium and iron oxide reduction:

$$\Delta G = -64.62 + 0.008314 * 277 * \left(\ln(1.9 * 10^{-10}) - \frac{1}{3}\ln NH_4^+ - 2.3\frac{5}{3}\log[H^+]\right)$$

$$\Delta G = -64.62 + 0.008314 * 277 * \left(\ln(1.9 * 10^{-10}) - \frac{1}{3}\ln NH_4^+ + 3.83pH\right)$$

We chose to determine ΔG as a function of both NH_4^+ (from 5µM to 300µM) and pH (0 to 14) for equation A. Values are displayed in the matrix below:

Table 9-3: ΔG values as a function of both NH_4^+ concentration and pH for equation A

pH ↓	NH_4^+ (µM)	5E-6 →	10E-6	20E-6	30E-6	50E-6	150E-6	200E-06	300E-06
0		-106.8	-107.3	-107.9	-108.2	-108.6	-109.4	-109.6	-109.9
1		-98.0	-98.5	-99.0	-99.3	-99.7	-100.6	-100.8	-101.1
2		-89.1	-89.7	-90.2	-90.5	-90.9	-91.7	-92.0	-92.3
3		-80.3	-80.8	-81.4	-81.7	-82.1	-82.9	-83.1	-83.4
4		-71.5	-72.0	-72.5	-72.8	-73.2	-74.1	-74.3	-74.6
5		-62.6	-63.1	-63.7	-64.0	-64.4	-65.2	-65.4	-65.8
6		-53.8	-54.3	-54.8	-55.2	-55.5	-56.4	-56.6	-56.9
7		-44.9	-45.5	-46.0	-46.3	-46.7	-47.5	-47.8	-48.1
8		-36.1	-36.6	-37.2	-37.5	-37.9	-38.7	-38.9	-39.2
9		-27.3	-27.8	-28.3	-28.6	-29.0	-29.9	-30.1	-30.4
10		-18.4	-19.0	-19.5	-19.8	-20.2	-21.0	-21.3	-21.6
11		-9.6	-10.1	-10.6	-11.0	-11.4	-12.2	-12.4	-12.7
12		-0.7	-1.3	-1.8	-2.1	-2.5	-3.4	-3.6	-3.9
13		8.1	7.6	7.0	6.7	6.3	5.5	5.3	4.9
14		16.9	16.4	15.9	15.6	15.2	14.3	14.1	13.8

ΔG values highlighted in yellow are not thermodynamically feasible (positive) under conditions typically found in sediments. Feammox can theoretically occur under conditions typically observed in marine sediment porewaters as the upper pH limit for feammox to N_2 using ferrihydrite is 13, a value that is well above that of seawater (pH ≈ 8).

Likewise, we can calculate ΔG for equation B (feammox to NO_2^-). Values are displayed in the matrix below:

Table 9-4: ΔG values as a function of both NH_4^+ concentration and pH for equation B

pH ↓	NH_4^+ (μM) →	5E-6	10E-6	20E-6	30E-6	50E-6	150E-6	200E-06	300E-06
0		-52.3	-52.6	-52.9	-53.0	-53.2	-53.6	-53.7	-53.9
1		-43.5	-43.8	-44.0	-44.2	-44.4	-44.8	-44.9	-45.1
2		-34.6	-34.9	-35.2	-35.3	-35.5	-36.0	-36.1	-36.2
3		-25.8	-26.1	-26.3	-26.5	-26.7	-27.1	-27.2	-27.4
4		-17.0	-17.2	-17.5	-17.7	-17.9	-18.3	-18.4	-18.5
5		-8.1	-8.4	-8.7	-8.8	-9.0	-9.4	-9.6	-9.7
6		0.7	0.4	0.2	0.0	-0.2	-0.6	-0.7	-0.9
7		9.5	9.3	9.0	8.9	8.7	8.2	8.1	8.0
8		18.4	18.1	17.8	17.7	17.5	17.1	17.0	16.8
9		27.2	27.0	26.7	26.5	26.3	25.9	25.8	25.6
10		36.1	35.8	35.5	35.4	35.2	34.7	34.6	34.5
11		44.9	44.6	44.4	44.2	44.0	43.6	43.5	43.3
12		53.7	53.5	53.2	53.0	52.8	52.4	52.3	52.2
13		62.6	62.3	62.0	61.9	61.7	61.3	61.2	61.0
14		71.4	71.1	70.9	70.7	70.5	70.1	70.0	69.8

This process is not thermodynamically favorable at seawater pH (pH ≈ 8) when ferrihydrite is used as a substrate. Nevertheless, it is interesting to consider how the ΔG^o of feammox to either N_2 or NO_2^- are affected by the choice of iron oxide substrate. ΔG^o for a chemical reaction can be calculated from the Gibb's free energy of formation (ΔG^o_f) of all the species involved. For example, ΔG^o for feammox to N_2 (process A) can be calculated from:

$$\Delta G^\circ = \frac{1}{6}\Delta G^\circ_{f(N_2)} + \Delta G^\circ_{f(Fe^{2+})} + 2\Delta G^\circ_{f(H_2O)} - \Delta G^\circ_{f(FeOOH)} - \frac{1}{3}\Delta G^\circ_{f(NH_4^+)} - \frac{5}{3}\Delta G^\circ_{f(H^+)}$$

ΔG^o for feammox to NO_2^- (process B) can be calculated from:

$$\Delta G^\circ = \frac{1}{6}\Delta G^\circ_{f(NO_2^-)} + \Delta G^\circ_{f(Fe^{2+})} + \frac{5}{3}\Delta G^\circ_{f(H_2O)} - \Delta G^\circ_{f(FeOOH)} - \frac{1}{6}\Delta G^\circ_{f(NH_4^+)} - \frac{5}{3}\Delta G^\circ_{f(H^+)}$$

The ΔG^o_f of the iron oxide substrate used by Luther (1997) was -699 kJ/mol; a value that is associated to ferrihydrite formation (Stumm and Morgan, 1970). Oxyhydroxides (nominally FeOOH), such as ferrihydrite, are generally thought to precipitate first from sediment porewaters, and are likely ammonium substrates in feammox. On the other hand, oxyhydroxides come in a variety of polymorphs (e.g. ferrihydrite, goethite, lepidocrocite), each having different morphologies, particle sizes as well as surface properties (e.g. level of hydration, isoelectric point, charge, reactivity.. etc.) (Navrotsky et al., 2008). Each of these factors greatly affects the oxyhydroxide's ΔG^o_f which, in turn, influences the thermodynamic feasibility of the reaction of interest. For example, the ΔG^o_f of goethite and lepidocrocite (-490.6 and -482.7 kJ/mol respectively; Navrotsky et al., 2008) are significantly different from the ΔG^o_f of ferrihydrite (-699 kJ/mol). Using the ΔG^o_f of goethite instead of ferrihydrite changes the ΔG^o of equation A from -64.62 kJ/mol to -273.02 kJ/mol and ΔG^o of equation B from -4.84 kJ/mol to -213.24 kJ/mol, which makes both reactions thermodynamically feasible at *all* pH conditions and ammonium concentrations encountered in marine sediments. Since nanophases of goethite have been identified as the dominant oxyhydroxide phase in lake and marine sediments (Van der Zee et al., 2003), it is not unreasonable to use these newly calculated ΔG^o values to assess the thermodynamic feasibility of feammox in marine sediments. We therefore feel justified in stating that it is *possible* that feammox takes place during our incubation experiments.